(2)

NAVAL POSTGRADUATE SCHOOL

Monterey, California

THESIS

EXPERIMENTAL AND ANALYTICAL INVESTIGATION
OF THE VIBRATION CHARACTERISTICS OF A
REMOTELY PILOTED HELICOPTER

by

William T. Trainer

June 1992

Thesis Advisor: E. Roberts Wood

Approved for public release; distribution is unlimited

REPORT DOCUMENTATION PAGE

1a. REPORT SECURITY CLASSIFICATION UNCLASSIFIED		1b. RESTRICTIVE MARKINGS	
2a. SECURITY CLASSIFICATION AUTHORITY		3. DISTRIBUTION/AVAILABILITY OF REPORT Approved for public release; distribution is unlimited.	
2b. DECLASSIFICATION/DOWNGRADING SCHEDULE			
4. PERFORMING ORGANIZATION REPORT NUMBER(S)		5. MONITORING ORGANIZATION REPORT NUMBER(S)	
6a. NAME OF PERFORMING ORGANIZATION Naval Postgraduate School	6b. OFFICE SYMBOL *(If applicable)* AA	7a. NAME OF MONITORING ORGANIZATION Naval Postgraduate School	
6c. ADDRESS *(City, State, and ZIP Code)* Monterey, CA 93943-5000		7b. ADDRESS *(City, State, and ZIP Code)* Monterey, CA 93943-5000	
8a. NAME OF FUNDING/SPONSORING ORGANIZATION	8b. OFFICE SYMBOL *(If applicable)*	9. PROCUREMENT INSTRUMENT IDENTIFICATION NUMBER	
8c. ADDRESS *(City, State, and ZIP Code)*		10. SOURCE OF FUNDING NUMBERS	
		Program Element No.	Project No. / Task No. / Work Unit Accession Number

11. TITLE *(Include Security Classification)*
Experimental and Analytical Investigation of the Vibration Characteristics of a Remotely Piloted Helicopter (U)

12. PERSONAL AUTHOR(S) Trainer, William T.

13a. TYPE OF REPORT	13b. TIME COVERED	14. DATE OF REPORT *(year, month, day)*	15. PAGE COUNT
Master's Thesis	From To	June 1992	145

16. SUPPLEMENTARY NOTATION
The views expressed in this thesis are those of the author and do not reflect the official policy or position of the Department of Defense or the U.S. Government.

17. COSATI CODES			18. SUBJECT TERMS *(continue on reverse if necessary and identify by block number)*
FIELD	GROUP	SUBGROUP	HHC, Modal Testing, Vibration, Finite Element Analysis, RPH, Shake Testing

19. ABSTRACT *(continue on reverse if necessary and identify by block number)*

The Department of Aeronautics and Astronautics at the Naval Postgraduate School is involved in an ongoing program of Higher Harmonic Control (HHC) research using Remotely Piloted Helicopters (RPH). To date a host RPH has been acquired and a preliminary HHC design study completed. This thesis reports the results of free vibration shake tests conducted on the host RPH as well as efforts to construct a representative finite element model of the vehicle. Broadband noise was used to excite the structure both laterally and vertically from 10-200 Hz in and attempt to accurately document the airframe and rotor system dynamics. Primary airframe structural modes were identified in the tail boom and at frequencies well below the characteristic 4/rev (78.3 Hz) main rotor induced vibration frequency. These modes should not be of concern at normal operating rpm. Main rotor blade modes were documented under non-rotating conditions then extended to predict the modes at operating rpm. Finally, a finite element model of the structure was constructed. Difficulties in matching finite element predictions with experimental results, however, will require refinements to the computer model before is can become a useful design tool.

20. DISTRIBUTION/AVAILABILITY OF ABSTRACT	21. ABSTRACT SECURITY CLASSIFICATION	
☒ UNCLASSIFIED/UNLIMITED ☐ SAME AS REPORT ☐ DTIC USERS	Unclassified	
22a. NAME OF RESPONSIBLE INDIVIDUAL Professor E. Roberts Wood	22b. TELEPHONE *(Include Area code)* (408) 646-2897	22c. OFFICE SYMBOL AA/Wd

DD FORM 1473, 84 MAR — 83 APR edition may be used until exhausted; All other editions are obsolete

Approved for public release; distribution is unlimited.

EXPERIMENTAL AND ANALYTICAL INVESTIGATION OF THE VIBRATION CHARCTERISTICS OF A REMOTELY PILOTED HELICOPTER

by

William T. Trainer
Lieutenant Commander, United States Navy
B.S., Marquette University, 1979

Submitted in partial fulfillment
of the requirements for the degree of

MASTER OF SCIENCE IN AERONAUTICAL ENGINEERING

from the

NAVAL POSTGRADUATE SCHOOL
June 1992

Author: _____
William T. Trainer

Approved by: _____
E. Roberts Wood, Thesis Advisor

_____
Ramesh Kolar, Second Reader

_____
for Daniel J. Collins, Chairman
Department of Aeronautics and Astronautics

ABSTRACT

The Department of Aeronautics and Astronautics at the Naval Postgraduate School is involved in an ongoing program of Higher Harmonic Control (HHC) research using Remotely Piloted Helicopters (RPH). To date a host RPH has been acquired and a preliminary HHC system design study completed. This thesis reports the results of free vibration shake tests conducted on the host RPH as well as efforts to construct a representative finite element model of the vehicle. Broadband noise was used to excite the structure both laterally and vertically from 10-200 Hz in an attempt to accurately document the airframe and rotor system dynamics. Primary airframe structural modes were identified in the tail boom and at frequencies well below the characteristic 4/rev (78.3 Hz) main rotor induced vibration frequency. These modes should not be of concern at normal operating rpm. Main rotor blade modes were documented under non-rotating conditions then extended to predict the modes at operating rpm. Finally, a finite element model of the structure was constructed. Difficulties in matching finite element predictions with experimental results, however, will require further refinements to the computer model before it can become a useful design tool.

TABLE OF CONTENTS

I. INTRODUCTION

Helicopter vibration reduction represents a major challenge to the helicopter designer and is an area of great interest to the helicopter industry. Expanding helicopter mission requirements including high dash speeds, nap of the earth flight, and night operations combined with an increased emphasis on improving systems reliability, reducing operating costs and increasing airframe structural life demand a significant reduction over current helicopter vibration levels. High vibration levels have been found to have a direct impact on crew fatigue and passenger comfort [Ref. 1] as well as the cost effectiveness of the helicopter, especially with respect to engine and avionic systems [Ref. 2].

Vibration reduction has long been the goal of the helicopter industry with an ultimate goal of attaining a "jet-smooth" ride. Figure 1 documents the improvements made in reducing vibration levels over the past 25 years. It is apparent however, that an asymptote has been reached in the level of vibration reduction which can be achieved through current conventional means [Ref. 3]. In fact the specified vibration levels for the U.S. Army AAH/UTTAS programs had to be revised upward from the original target of 0.05 g's to a more realistic value of 0.10 g's.

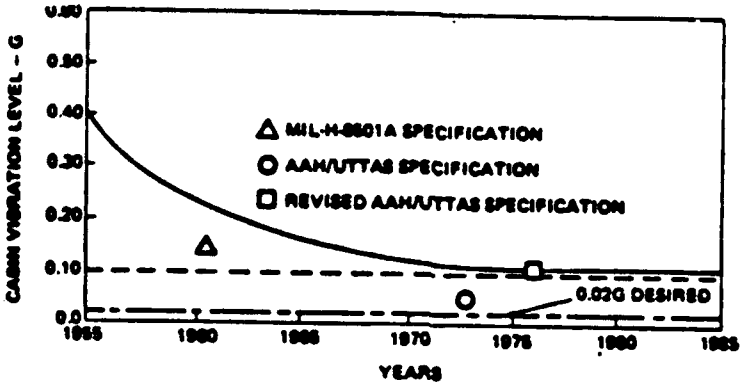

Figure 1. Trend in Helicopter Vibration Levels Since 1955

This was a reflection of the vibration suppression technology available at the time.

The large potential benefits to be gained from reducing vibration levels in helicopters have not been lost on potential customers. The adoption of Aeronautical Design Standard 27 (ADS-27) [Ref. 4] by the U.S. Army sets stringent requirements for allowable vibration levels in all future helicopter procurement. ADS-27 specifies a maximum vibration level of 0.05 g's at frequencies below the blade passing frequency (number of blades x main rotor speed). Additionally, the industry's ultimate goal of a "jet smooth ride" as represented by the lower dashed line in Figure 1 remains 0.02 g's. It has become apparent that such large vibration reductions will not be attainable through the use of current passive vibration suppression systems alone [Ref. 5]. The challenging requirements of ADS-27 have

stimulated renewed interest in all types of helicopter vibration suppression systems including both passive and active systems.

The Department of Aeronautics and Astronautics at the Naval Postgraduate School is actively pursing research in the area of helicopter dynamics and vibration control. A major facet of this research effort includes the use of Remotely Piloted Helicopters (RPH) to obtain low cost flight test verification and quantification of theoretically derived techniques. The school is currently embarked on a program to install Higher Harmonic Control (HHC) in it's ***Bruiser*** RPH manufactured by the Pacific RPV Co. Successful implementation of HHC or any vibration reduction system however, depends in large part on the designers' knowledge of the airframe and control system structural dynamics. ***Bruiser*** control system dynamics have been documented previously [Ref. 6]. This Thesis describes the results of detailed shake tests conducted on the ***Bruiser***, as well as efforts to model the airframe's structural dynamics through the use of finite element techniques using the CASA/GIFTS finite element program [Ref. 7].

II. BACKGROUND

A. SOURCES OF HELICOPTER VIBRATION

The primary source of helicopter airframe vibratory loads is the main rotor system. These loads are a natural consequence of flying the rotor system edgewise through the air. The main rotor operating in this non-uniform flow field produces oscillatory aerodynamic forces at the rotor blades. These loads occur at multiples of the following frequencies: n-1/rev, n/rev and n+1/rev where n is the total number of blades. The rotor hub then acts as a filter allowing only the transmission of n/rev vibratory loads to the airframe structure [Ref. 8]. Additional vibratory loads can result from the rotor being out-of-balance or out-of-track. These conditions produce airframe vibrations at multiples of the main rotor frequency (1/rev).

Secondary vibration sources include the tail rotor, engines and other rotating components (i.e. transmissions, generators, etc). These are of lesser concern however, as they typically occur at significantly higher frequencies where specification requirements are less stringent. Figure 2 shows the UTTAS/AAH specification requirement of 0.05 g's at frequencies below 20 Hz [Ref. 9].

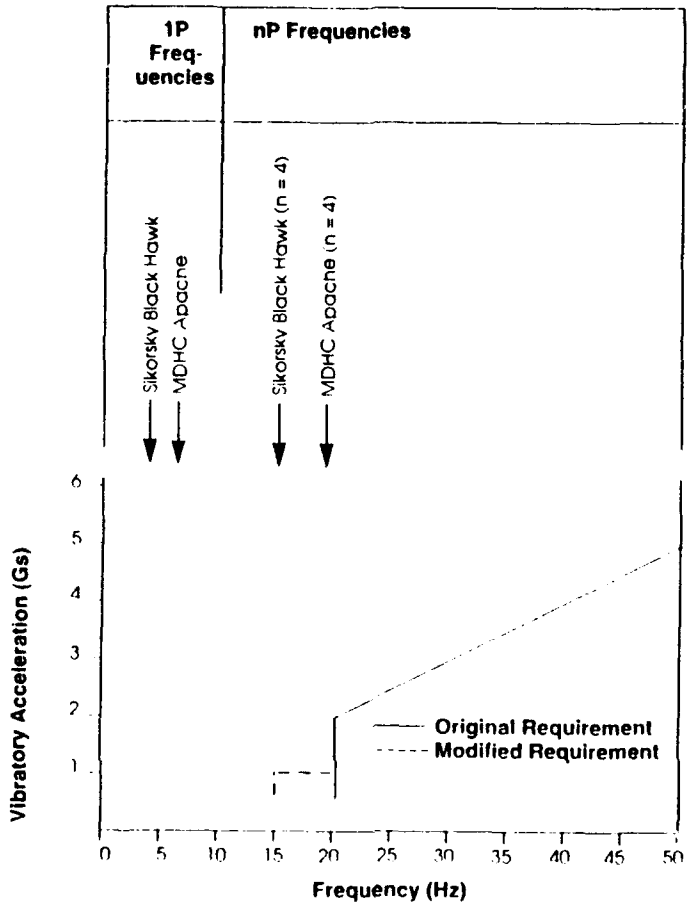

Figure 2. UTTAS/AAH Vibration Criteria

Twenty hertz represents the maximum typical blade passing frequency (n/rev). At frequencies above n/rev the specification requirements are significantly relaxed. The dashed line between 15 Hz and 20 Hz indicates the specification modification allowed after it became apparent that the original requirement could not be met.

B. VIBRATION REDUCTION TECHNIQUES

Helicopter vibration reduction can be accomplished by one of two means; passive systems or active systems. Historically the helicopter industry has used passive systems to maintain vibration levels within desired tolerances. With the more stringent requirements of ADS-27 the industry has looked to active means of reducing vibration levels. The following is a brief description of each technique.

1. Passive Systems

Passive systems consist of mechanical vibration absorbers and isolation mounts. Isolation mounts perform exactly as their name implies. They isolate helicopter components from airframe vibrations. They do not however, reduce airframe vibration levels. Typically referred to as shock or soft mounts they are used to mount individual components such as avionics boxes, transmissions and engines to the vibrating airframe. As an extreme example, the Boeing 360 technology demonstrator helicopter used isolation mounts to isolate the entire cabin deck from the airframe structure.

Mechanical vibration absorbers are the second type of passive system. These systems can be further subdivided into two types; spring mass systems and pendulum type absorbers. Spring mass systems are fixed tuned to a desired frequency, typically n/rev, where the vibration of the spring mass system is such that it exactly cancels the driving force (the

airframe vibration). This results in zero vibration at the absorber location (i.e. the absorber drives a node at its location). Pendulum absorbers or bi-filars are used on rotating systems such as rotor systems. The advantage of the bi-filar is that it can accommodate large variations in frequency.

While passive vibration absorber systems reflect the industry's current technology they have several limitations which are listed here.

1. Passive absorbers must be tuned to a specific frequency (typically n/rev). Small variations in rotor speed can result in severely degraded performance. Vibration levels can actually be amplified by the fixed tuned absorber at off design frequencies.

2. The weight penalties associated with passive systems can be significant, well in excess of 1% of the aircraft gross weight [Ref. 5].

3. Substantial parasite drag penalties are associated with rotor mounted absorbers such as bi-filar systems.

4. As seen in Figure 1 passive absorber systems have not demonstrated the capability to reduce airframe vibrations to desired levels.

2. Active Systems

Unlike passive vibration control systems, which simply respond to vibratory loads after they have been generated, an active system measures vibration levels then seeks to minimize those vibrations by imparting control inputs to the system. The advantage of active systems is that they are not subject to the limited frequency response of the passive systems and

because they seek to minimize vibration loads at their source they hold the potential for providing major reductions in overall helicopter vibration levels. The vast improvements in computing power and actuator technology have allowed for the practical implementation of these active systems. Two types of active vibration suppression systems are discussed below.

a. Higher Harmonic Control (HHC)

HHC has long been recognized as a means of reducing helicopter airframe vibrations. HHC involves high frequency feathering of rotor blade pitch to reduce vibrations at their source; before they can be transmitted to the airframe. Several methods of blade pitch control have been proposed including actuators in either the fixed airframe or rotating rotor system frame of reference. Individual blade control (IBC) has also been proposed by which blade pitch is individually controlled eliminating the requirement for a swashplate.

A joint NASA/U.S. Army flight test program [Ref. 3] documents the viability of the HHC technique. The HHC system was an electronic, computer-controlled system capable of collectively and/or cyclically imparting small (< 1 degree) feathering inputs to the main rotor blades at a frequency of n/rev and at selectable blade azimuths. Located in the fixed airframe system the HHC actuators allowed for the generation of any combination of (n-1)/rev, n/rev or (n+1)/rev feathering

motions in the rotating system. This allowed for direct access to the aerodynamic loads responsible for main rotor induced airframe vibrations. The system was operated in both open loop and closed loop modes. In the closed loop mode airframe vibration measurements were fed to a controller which varied the magnitude and phase of the HHC actuator output to minimize the measured vibration. The program produced very favorable results and demonstrated the viability of HHC technology and the need for further research in this area.

b. Active Control of Structural Response (ACSR)

Westland Helicopters Limited has recently investigated the feasibility of reducing airframe vibrations through the use of high frequency force actuators located throughout the airframe [Ref. 2]. In an ACSR system force actuators are mounted at or across locations in the structure which possess relative motion in the dominant vibratory modes. Sensors at key location in the airframe measure the vibration response and feed that information to an adaptive controller. The controller then generates a signal to the force actuators to produce forces which minimize the measured vibrations. Unlike HHC, ACSR does not attempt to reduce vibration loads at their source.

The attractiveness of ACSR is that it is not restricted to reducing only the rotor induced n/rev vibrations. Systems such as ACSR could be employed throughout

the aircraft to dampen areas of high vibration. In effect ACSR becomes an actively controllable vibration absorber similar to the fixed tuned spring mass type systems but capable of handling a large range of excitation frequencies. Because ACSR does not seek to effect the source of the vibration however, it is not felt that it offers the potential for overall airframe vibration reduction that the HHC approach does.

C. STATUS OF HHC RESEARCH PROGRAM AT NPS

The Department of Aeronautics and Astronautics at the Naval Postgraduate School (NPS) established a Remotely Piloted Helicopter (RPH) flight research program at its Unmanned Air Vehicle (UAV) Flight Research Facility in 1985. Efforts to establish an HHC research program including both analytical and RPH flight tests began in 1990. Table I presents a chronological listing of NPS HHC research efforts.

It is apparent that the primary focus at NPS has been on developing an HHC flight test program. The prohibitive costs and constraints associated with a full scale helicopter flight test program necessitate a more realistic approach to the problem. The RPH's at the UAV lab provide an ideal, cost effective platform for testing new theories, as well as providing the means for obtaining actual flight test data.

TABLE I. Chronological List of HHC Research at NPS

Year	Researcher/ Author	Subject of Research
1985	Hintze	Construction and Use of Radio Controlled Model Helicopter for Research [Ref. 10].
1986	Cotten	Hover performance of a Remotely Piloted Helicopter [Ref. 11]
1990	Sarigul-Klijn Kolar Wood Straub	Chaos Methods Applied to Higher Harmonic Control [Ref. 12]
1990	Scott	Establishment of a Remotely Piloted Helicopter Flight Test Program for HHC Research [Ref. 13]
1990	Webb	Initial Design study of Existing RPH Flight Control system and Feasibility Study of Implementing HHC on the SH-60B [Ref. 6]
1991	McGovern	Flight Operations for Higher Harmonic Control [Ref. 14]
1991	Wood Higman Kolar	Promise of Improved Dynamic Interface Operations through the use of HHC [Ref. 15]
1991	Ransford	Baseline Vibration Measurements of RPH for HHC Research [Ref. 16]

While the primary thrust of the RPH program has been to investigate HHC, future plans include the testing of NOTAR systems as well as new technology rotor systems. Additionally, research is being conducted at NPS into the design of an RPH specifically tailored to the research needs of the school.

III. SCOPE

The successful and timely implementation of any vibration reduction system depends in large part on an understanding of the airframe's structural dynamics. Incorporation of HHC technology in an RPH at the NPS UAV Flight Research Facility has been an evolutionary process. The initial "sport" RPH's used by the Department did not have the requisite payload capability to lift an HHC system. The acquisition of the Pacific RPV ***Bruiser*** in 1990 however, provided a flight vehicle capable of lifting HHC hardware including actuators and electronics. Initial investigation of HHC design requirements, as well as a static analysis of the ***Bruiser's*** flight control system, and baseline unaugmented flight vibrations measurements have been completed [Refs. 6 and 16].

This paper reports on the results of ***Bruiser*** shake tests and documents the structural modes of the airframe. Ground shake tests were performed using external excitation to document the airframe's response. The tests were conducted with full fuel tanks, rotor blades installed and with the aircraft suspended from a bungee at the rotor head. Airframe dynamic response was measured using accelerometers and recorded using a spectrum analyzer. A tabulation of the tests and test conditions is presented in Table II.

TABLE II. Tests and Test Conditions

Test	Shaker Orientation	Frequency Range (Hz)	Excitation Input Location
Vertical Shake Tests	Vertical	0-200	Nose of A/C
Lateral Shake Tests	Horizontal	0-200	Engine Comp.
Main Rotor Blade Flapwise Shake Tests	Vertical	0-200	Nose of A/C

Note: All tests conducted with fuel tanks ballasted with water, rotor blades, battery and ballast installed. The aircraft was flight configured with the exception of the radio transceiver unit which was removed to preclude possible damage during testing.

A finite element model of the airframe was generated using the Computer Aided Structural Analysis/Graphical Interactive Finite Element Total System (CASA/GIFTS) computer software program [Ref 7]. This finite element model was used to investigate and predict airframe free-free response characteristics and is meant to serve as a design tool for any future modification to the ***Bruiser's*** structure. Results of the structural shake test were used for subsequent correlation, improvement and validation of the CASA/GIFTS finite element model.

IV. DESCRIPTION OF TEST AIRCRAFT

The Pacific RPV *Bruiser*, Figure 3, is a four bladed remotely piloted helicopter manufactured by the Pacific RPV Co. of Startup, Washington.

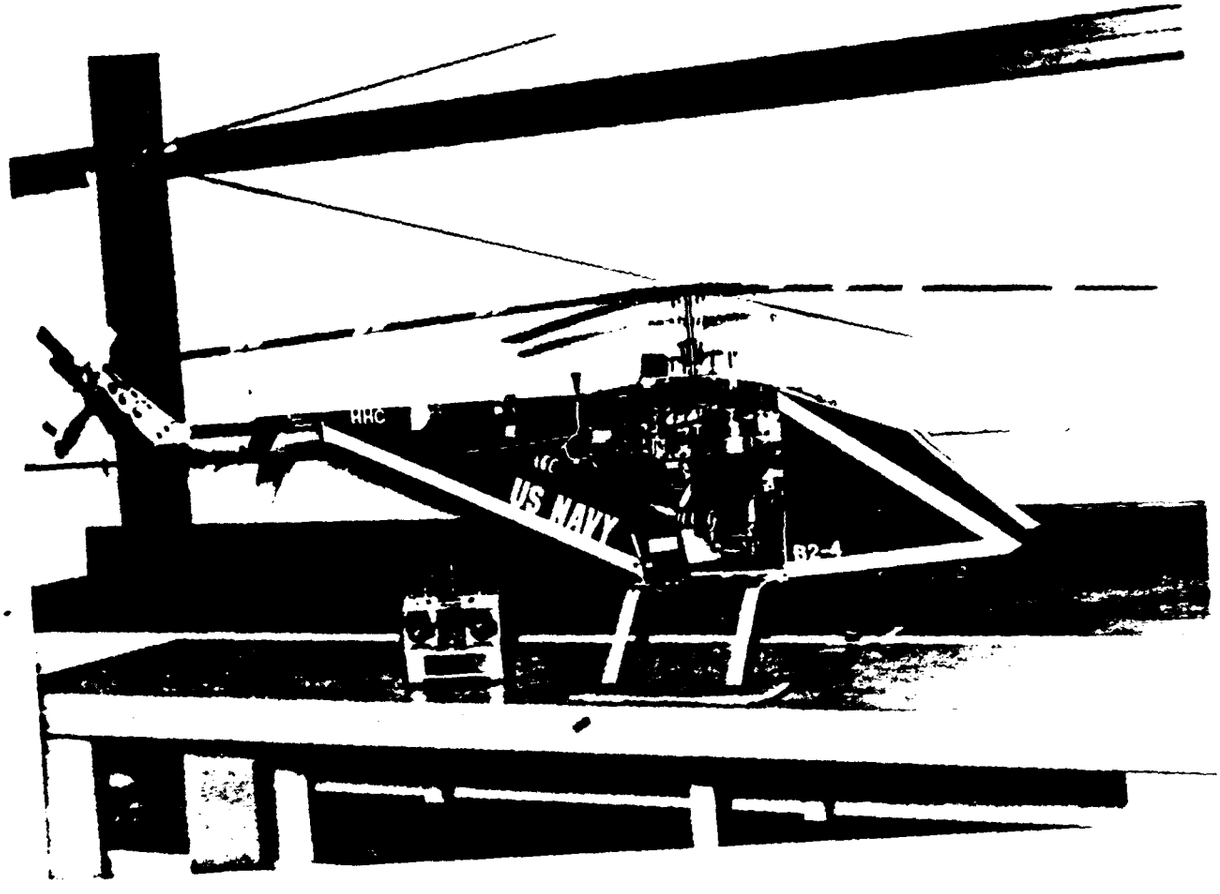

Figure 3. The Pacific RPV *Bruiser*

Originally designed to perform aerial spraying, photographic survey, and electronic countermeasures the *Bruiser* provides the requisite payload capability for the

incorporation of an HHC system. It is equipped with a four bladed, fully articulated, main rotor system, a four bladed tail rotor and is powered by a two-cylinder, two-cycle, air cooled Super Tartan T77i engine. General ***Bruiser*** technical specifications are given in Table III.

TABLE III. *Bruiser* Technical Specifications

Maximum Gross Weight	40 lbs
Empty Weight	20 lbs
Payload	20 lbs
Overall Length	77 in
Overall Height	26.5 in
Main Rotor Diameter	79.5 in
Flapping Hinge Offset (e)	0.8 in (2.0%)
Tail Rotor Diameter	13 in
Main Rotor Normal Operating RPM	1175 RPM
Tail Rotor Normal Operation RPM	4700 RPM
Gearing Ratio's	
Engine to Main Rotor	8:1
Main Rotor to Tail Rotor	6:1
Engine	
Type	Super Tartan T77i
Weight	5 lbs
Peak Output	3.95 BHP @ 8800 RPM
Maximum Torque	30 in-lb @ 7000 RPM

Airframe construction is fairly simple. The main structural member is the engine compartment, which consists of an aluminum deck, two side frames and a front frame. Structural rigidity of the assembly is maintained by several aluminum cross braces. A schematic representation of the engine compartment is presented in Figure 4.

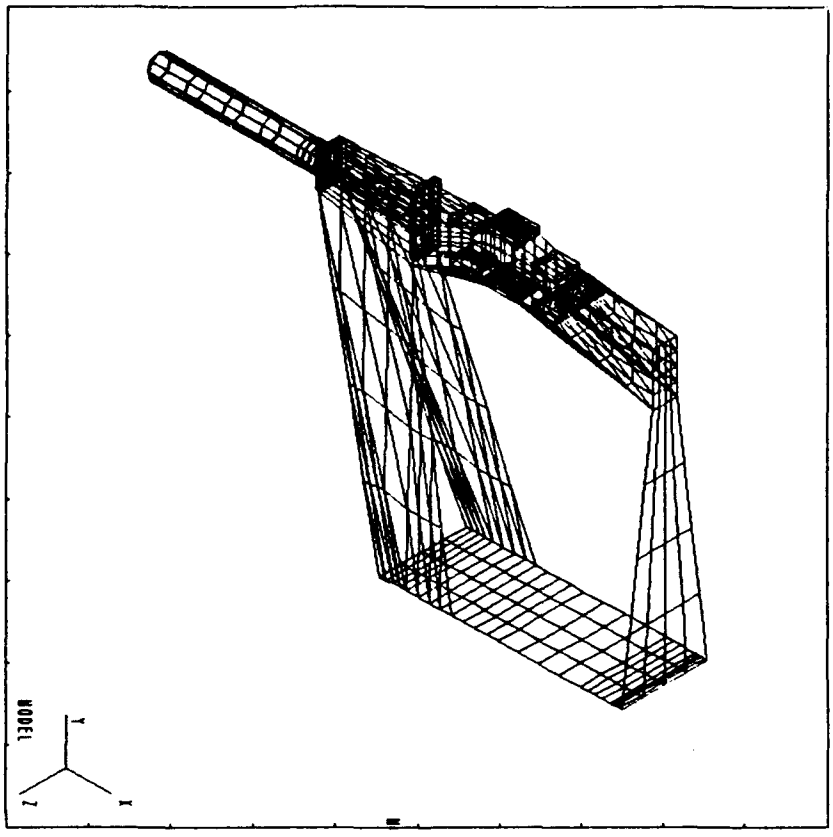

Figure 4. Schematic Drawing of the *Bruiser's* Engine Compartment

The engine compartment supports the main rotor system above and the skids below. A cantilevered composite nose deck is attached to the front of the engine frame and is supported by Lexan skin panels. This nose compartment houses the battery and ballast, as well as providing an enclosed volume for payloads. Attached to the rear of the engine compartment frame is the tail boom assembly. The tail boom (seen in Figure 4) is a circular hollow aluminum beam attached to the engine frame by two cross brackets. The tail boom is

supported at approximately two thirds of its length by two aluminum tie rods which emanate from either side of the engine compartment assembly's aft end. Two Lexan skin panels also provide some tail boom support. Attached to the end of the tail boom is the tail rotor support assembly. Its construction is similar to that of the engine compartment using two aluminum plates connected by rectangular and circular cross braces. A schematic drawing of the tail rotor frame is presented in Figure 5.

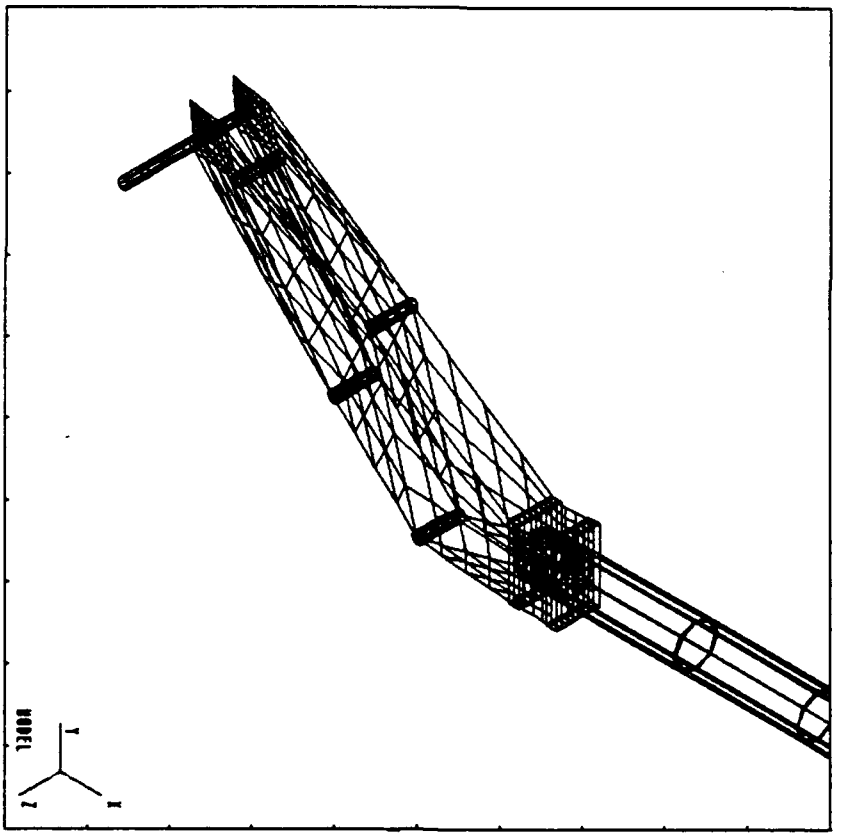

Figure 5. Schematic Drawing of the *Bruiser* Tail Rotor Assembly

The material types used in the construction of the ***Bruiser's*** primary structural components are given in Table IV.

TABLE IV. Major *Bruiser* Structural Components and Material Type

Component	Material Type
Engine Compartment	
Deck Plate	6061T6 Aluminum
Side Frames	7075T6 Aluminum
Front Frame	6061T6 Aluminum
Cross Braces	6061T6 Aluminum
Nose Compartment	
Deck Plate	Delrin
Side Panel Skin	Lexan
Tail Boom Assembly	
Tail Boom	6061T6 Aluminum
Tie Rods	6061T6 Aluminum
Side Panels	Lexan
Tail Rotor Assembly	
Side Frames	7075T6 Aluminum
Cross Braces	6061T6 Aluminum
Tail Rotor Shaft	Stainless Steel
Main Rotor System	
Main Rotor Shaft	Stainless Steel
Rotor Hub and Blade Grips	7075T6 Aluminum
Rotor Blades	Maple Spar with Balsa trailing edge

As discussed earlier the primary frequencies of concern in helicopter airframe vibration are the main rotor n/rev and the 1/rev and 2/rev vibrations resulting from an out-of-track or out-of-balance conditions. The n/rev airframe vibration results from the (n-1)/rev, n/rev and (n+1)/rev blade loads. In the case of the 4 bladed ***Bruiser*** (n=4) these correspond to the 3/rev, 4/rev and 5/rev, as well as their harmonic

multiples. Other vibration sources include the tail rotor and engine. Table V summarizes the characteristic *Bruiser* frequencies when operating at its normal main rotor operating speed of 1175 RPM.

TABLE V. *Bruiser* Characteristic Frequencies at Normal Operating RPM: 1175 RPM

Main Rotor n/rev	**Frequency**	
1/rev (track/balance)	19.6 Hz	1175 rpm
2/rev (1st harmonic of 1/rev)	39.2 Hz	2350 rpm
3/rev (n-1/rev)	58.7 Hz	3525 rpm
4/rev (n/rev, primary vib freq.)	78.3 Hz	4700 rpm
5/rev (n+1/rev)	97.9 Hz	5875 rpm
8/rev (1st harmonic of 4/rev)	156.7 Hz	9400 rpm
Tail Rotor n/rev	**Frequency**	
1/rev (track/balance)	117.5 Hz	7050 rpm
2/rev (1st harmonic of 1/rev)	235.0 Hz	14100 rpm
4/rev (tail rotor n/rev)	470.0 Hz	28200 rpm
Engine n/rev	**Frequency**	
1/rev	156.7 Hz	9400 rpm
2/rev	313.3 Hz	18800 rpm

V. EXPERIMENTAL SETUP

The ***Bruiser*** shake tests were conducted in the basement of Halligan Hall at NPS. A schematic representation of the experimental setup is presented in Figure 6.

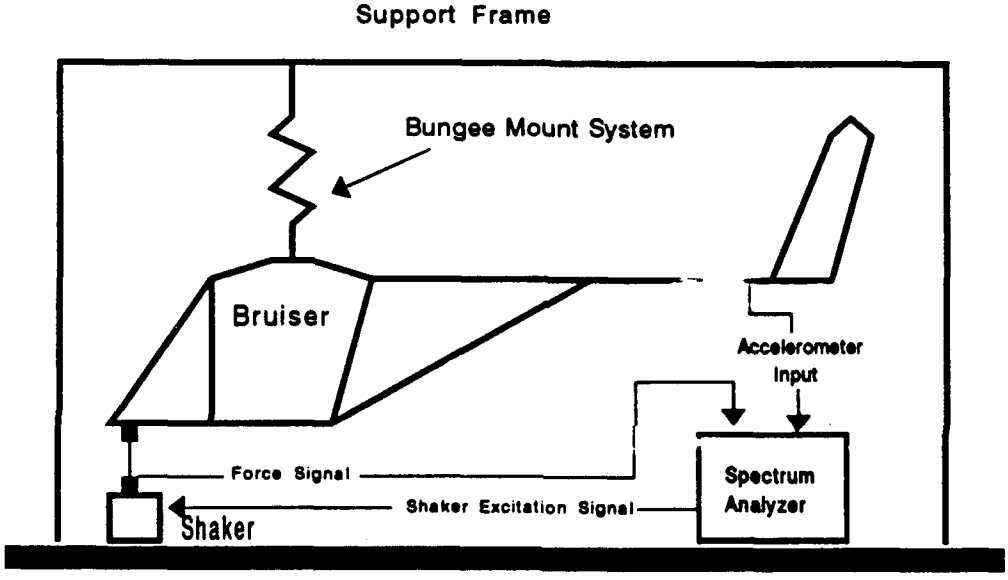

Figure 6. Schematic of Shake Test Setup

The airframe was suspended from an overhead frame assembly where an electromagnetic shaker was used to impart both vertical and lateral vibratory loads to the airframe structure. Input force and response acceleration measurements were obtained and recorded using a spectrum analyzer. The following is a detailed description of the experimental setup.

A. SUSPENSION SYSTEM

The *Bruiser* airframe was suspended at the main rotor head by a bungee chord system attached to an overhead frame. The bungee chord suspension system consisted of a loop of surgical tubing around each blade grip arm (total of four loops) These loops were then attached to an eye bolt in the overhead frame. The entire experimental setup is shown in Figure 7 and Figure 8 shows a close up of the bungee suspension system.

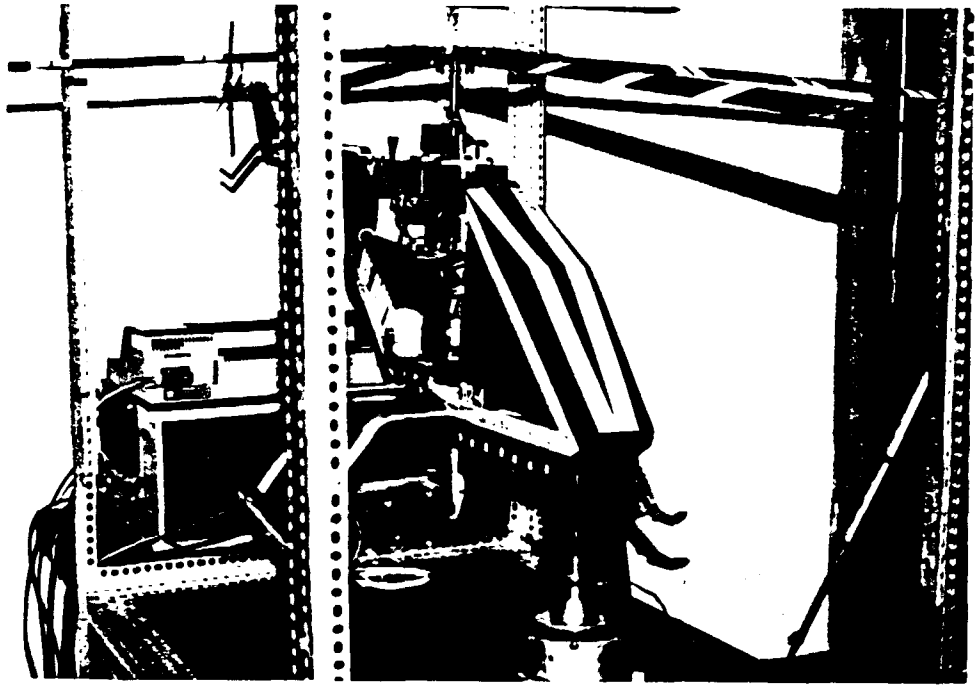

Figure 7. Experimental Setup

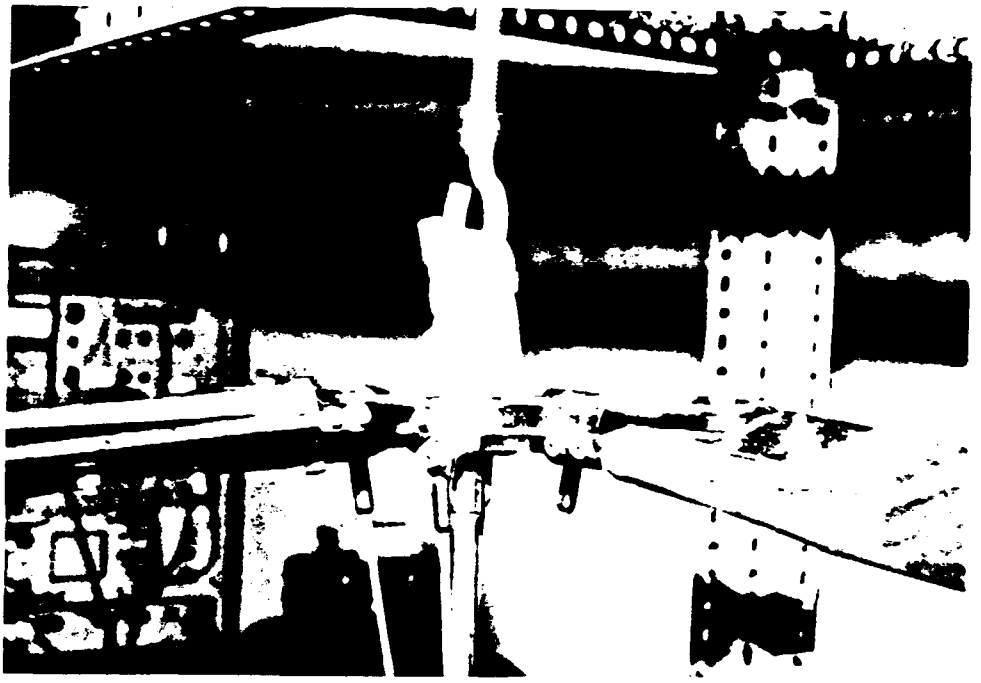

Figure 8. Bungee Chord Suspension System

The suspension system was designed to isolate the ***Bruiser*** from the overhead frame and provide for rigid body modes of less than 2 Hz. This provided sufficient separation from the lowest ***Bruiser*** elastic modes to prevent significant influence on their response. The suspension system was designed to approximate actual flight conditions and to match the CASA/GIFTS free-free analysis as closely as possible.

B. EXCITATION SYSTEM

Airframe excitation was provided by the Wilcoxon Research Model F7/F4 shaker. The shaker was a dual component electromagnetic/piezoelectric type. The F4 (electromagnetic)

component provided low frequency excitation from 10-7,500 Hz while the F7 (piezoelectric) component provided high frequency excitation from 500-20,000 Hz. A photograph of the F7/F4 shaker is presented in Figure 9.

MODEL F7/F4 WITH Z7 TRANSDUCER BASE

Figure 9. Wilcoxon Model F7/F4 shaker

The frequency range of interest during the shake tests was less than 500 Hz hence only the F4 portion of the shaker was required. A piezoelectric accelerometer transducer and a piezoelectric force transducer incorporated in the head of the shaker were used to document the vibratory excitation inputs. The shaker was driven by the Wilcoxon Research model PA7C two channel power amplifier utilizing the Model N7C Matching Network. Detailed descriptions of the F7/F4 shaker, and the PA7C amplifier can be found in References 17 and 18.

The shaker body was mounted in a support frame provided by the manufacturer. For vertical excitation the support frame was secured to the test bench by three aluminum brackets, Figure 10.

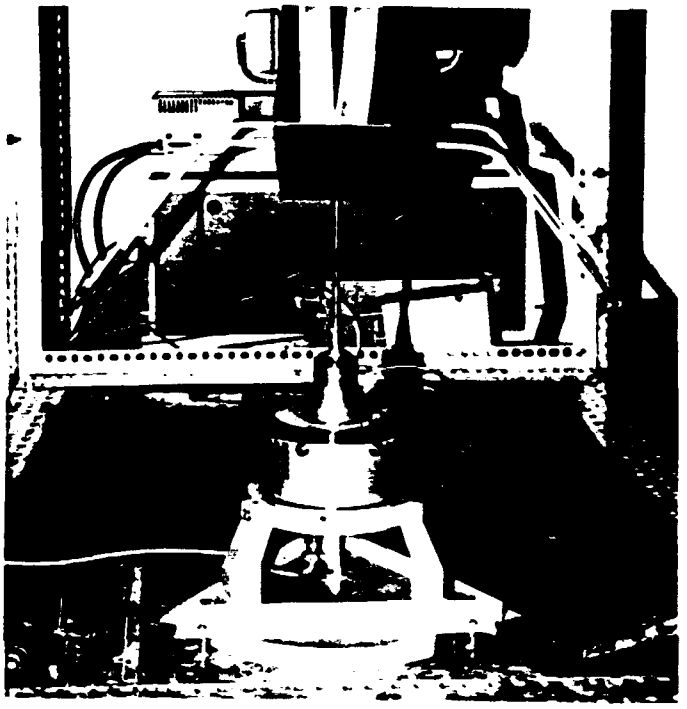

Figure 10. Vertical Shaker Arrangement

For lateral excitation the shaker support frame was secured horizontally to an aluminum plate clamped to an aluminum I-beam which was ultimately secured to the test bench by clamps. In the lateral arrangement bending of the I-beam and vertical mounting plate resulted in a reduced excitation input to the airframe. This may explain the lower response levels obtained during the lateral shake tests. The lateral shaker mounting arrangement is shown in Figure 11.

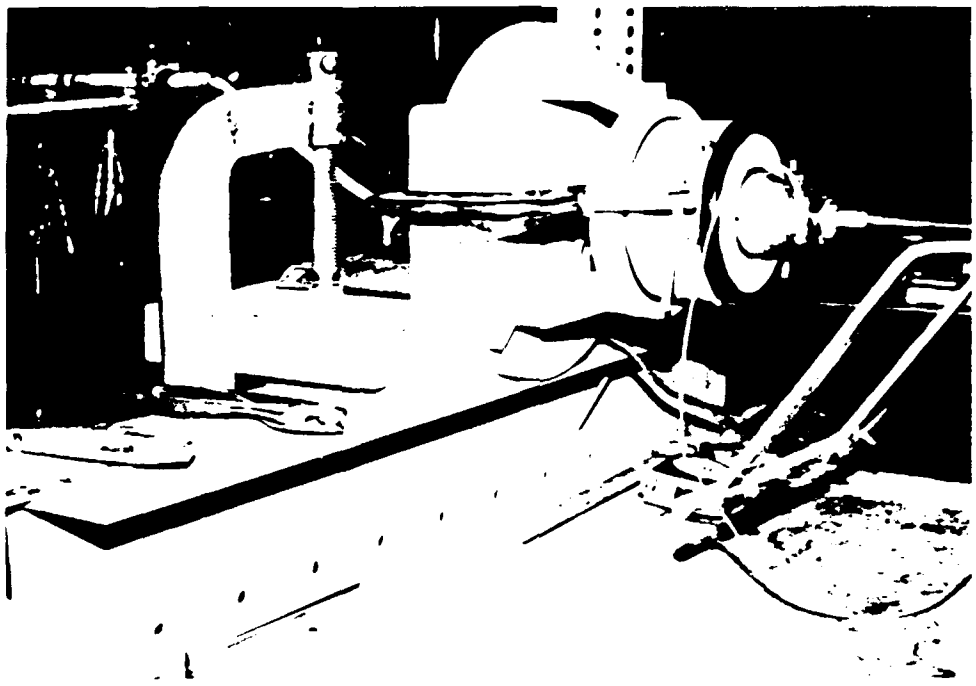

Figure 11. Lateral Shaker Arrangement

Shaker outputs were imparted to the ***Bruiser*** airframe through a flexible slender steel rod or stinger. The tapered stinger was used to reduce bending moments in an attempt to assure single point and direction excitation of the airframe. The airframe was excited vertically at the nose and laterally at the engine compartment. Locking bolts were incorporated on the excitation rod to eliminate any free play in the system. Figures 12 and 13 show the tapered stinger as well as the vertical and lateral excitation driving points on the airframe.

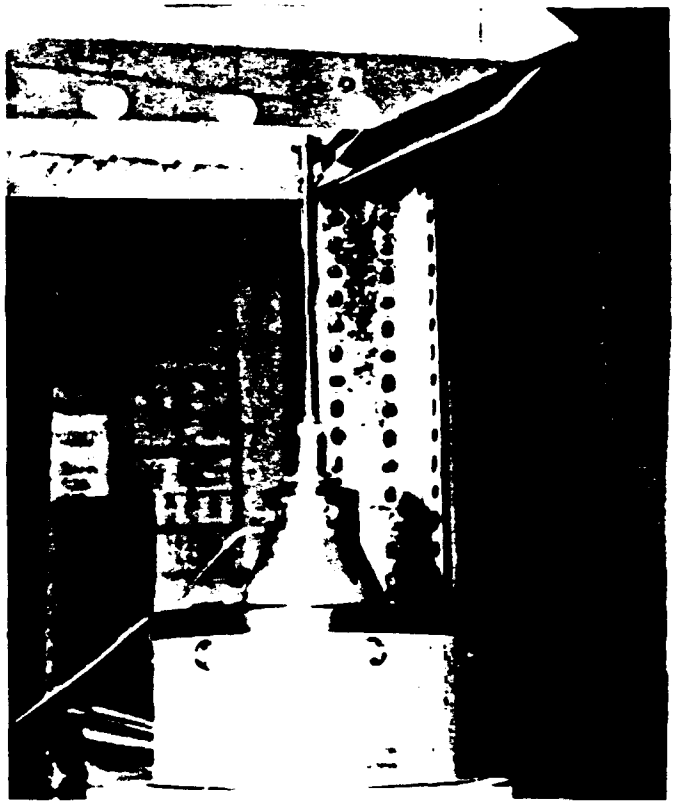

Figure 12. Vertical Excitation Driving Point

Figure 13. Lateral Excitation Driving Point

C. DATA ACQUISITION SYSTEM

1. Components

a. Scientific Atlanta SD380 Signal Analyzer

The Scientific Atlanta SD380 Signal Analyzer was the primary component in the data acquisition system. It was a four channel spectrum analyzer capable of providing single or multichannel display of spectrum and time domain data. Multi-channel capabilities included transfer function, phase shift and correlation measurement/display as well as waterfall displays. Scaling options included linear, logarithmic and decibel scales. An integral signal generator was capable of generating broad band and band limited noise signals, pseudo random signals and either stationary or sweeping sine signals. Frequency resolution was adjustable to a maximum of 800 lines per displayed range. A zoom feature allowed for more precise investigation of desired frequency ranges. Control of the SD380's many features was simple and accomplished via the keyboard to the right of the CRT display. A cursor was provided to mark points of interest on the display. A digital readout of cursor position and the value of the measured parameter at that position simplified data reduction. Data could be stored on 3.5 inch floppy disks via the SD380's integral disk drive. Plotting either the CRT display or stored data was accomplished via the installed IEEE 488 data bus and a suitable X-Y plotter. A more detailed description

of the Scientific Atlanta SD380 Signal Analyzer may be found in Reference 19. Figure 14 shows the SD380 CRT display and keyboard.

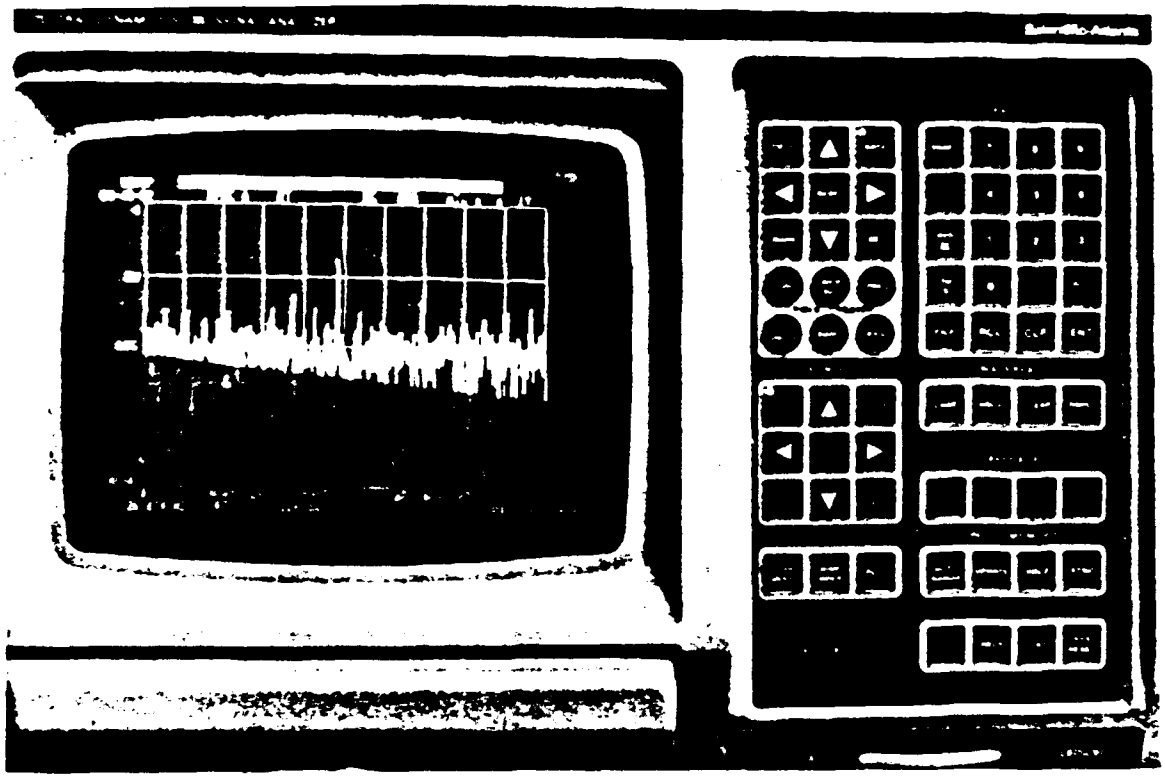

Figure 14. Scientific Atlanta SD380 Signal Analyzer

b. Hewlett Packard HP 54600A Oscilloscope

The HP 54600A was a 4-channel digital oscilloscope. Features included automatic scaling, x-y display of two signals and an automatic amplitude/frequency measurement capability. Other standard oscilloscope features were also available. Control of the of the HP 54600A was accomplished through the front panel soft keys or it could be controlled by computer through its installed IEEE data transfer bus. The digitization of the signals allowed for

easy storage and output of all signals and/or displays. The HP 54600A Oscilloscope is presented in Figure 15.

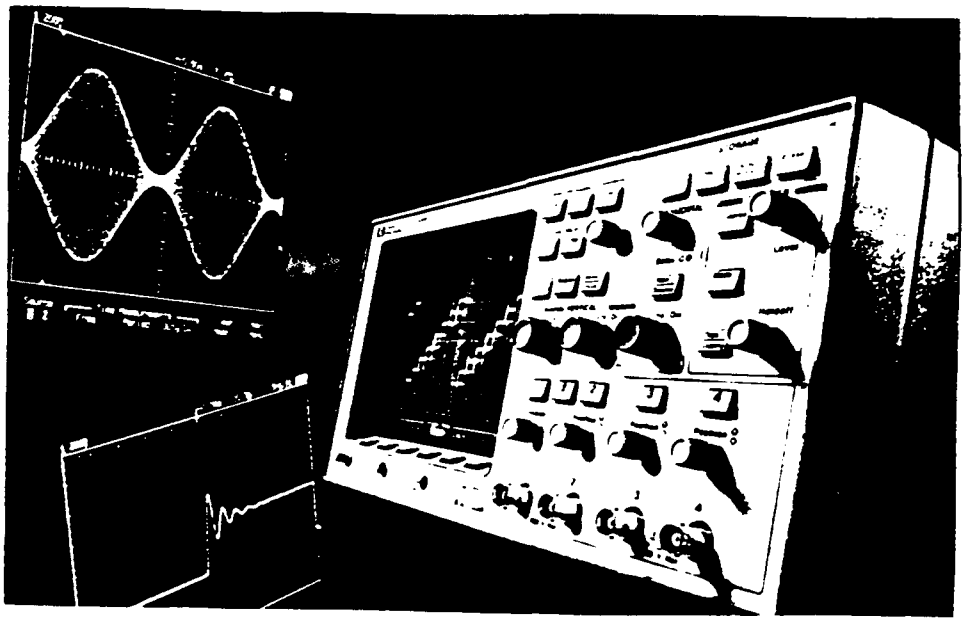

Figure 15. Hewlett Packard Digital Oscilloscope

c. PCB Piezotronics Inc. Series 336A Accelerometer

A PCB series 336A Flexcel accelerometer was used to record the airframe acceleration response to the vibratory input. The Series 336A accelerometer was lightweight and provided high output, low noise, matched phase and good low frequency response characteristics. Pertinent performance specification are given in Table VI.

TABLE VI. PCB Series 336A Accelerometer Specifications

Range (g pk)	5
Resolution (g pk)	0.0005
Sensitivity (mV/g)	1004
Diameter (inches)	0.625
Height (inches)	0.75
Weight (grams)	6.2

Calibration charts show an essentially flat response from 0 to 2,000 Hz. The accelerometer was affixed to the structure with Petro wax supplied by the manufacturer. This provided for flat response over the frequency range tested and the ability to quickly change accelerometer location. The PCB 336A accelerometer is presented in Figure 16.

Figure 16. PCB Series 336A Flexcell Accelerometer

d. PCB Model 464A Dual Mode Charge Amplifier

The PCB Piezotronics Model 464A Dual Mode charge Amplifier was a wide range amplifier designed to work with conventional charge generating transducers as well as with transducers containing built-in impedance converting amplifiers. Two charge amplifiers were used during testing, one for input force and the other for response acceleration signal conditioning. Output from the Model 464A charge amplifiers was provided to both the SD380 Signal Analyzer and the digital oscilloscope. The PCB Model 464A Dual-Mode Charge Amplifier is presented in Figure 17.

Figure 17. PCB Model 464A Dual-Mode Charge Amplifier

2. System Operation

The data acquisition system was designed around the SD380 Signal Analyzer with the digital oscilloscope being used primarily for system calibration and investigation of signal characteristics (i.e. amplitude, frequency, phase difference, signal noise content, etc.). The system included one PCB Series 366A accelerometer, two charge amplifiers and an X-Y plotter. Additional instrumentation included the electro-mechanical shaker and its associated electronics as described previously. Figure 18 provides a schematic representation of the experimental setup and data acquisition system.

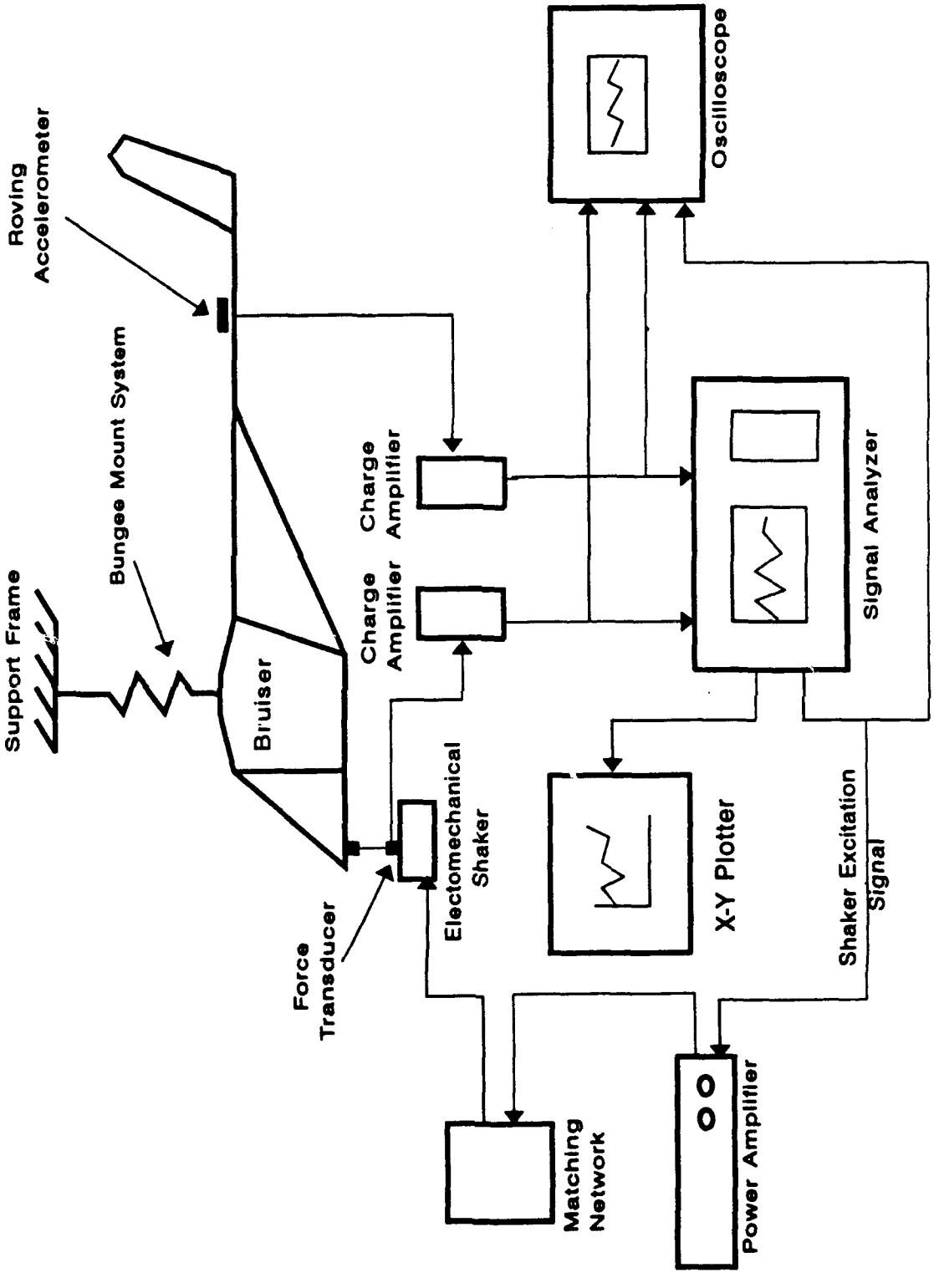

Figure 18. Experimental Setup and Data Acquisition System

The shaker driving signal was generated by the spectrum analyzer and sent to both the power amplifier for shaker control and to the digital oscilloscope for monitoring. The amplified driving signal was routed through the matching network and used to power the electro-mechanical shaker. Force measurements from the shaker's force transducer were amplified by a charge amplifier and sent to both the signal analyzer and the digital oscilloscope. The roving accelerometer was used to obtain the airframe response at various locations. The accelerometer output was amplified by a charge amplifier and sent to both the signal analyzer and the digital oscilloscope. The signal analyzer allowed for simultaneous measurement of both the excitation force and the airframe's acceleration response. Transfer function and phase calculations were performed in the signal analyzer and displayed on the CRT. Displayed and/or stored data was then plotted on the X-Y plotter.

VI. METHOD OF TEST

A. THEORY

Modal testing is performed by subjecting a structure to an input force and measuring its response. Input force types can include sinusoidal, sweeping sinusoidal, white noise, impact and broad band noise. The response per input or "Transfer Function" is typically plotted against frequency to produce "Frequency Response Function" curves. The classic frequency response function for a single degree of freedom system is presented in Figure 19 where $H(\omega)$ represents the magnitude of the transfer function, ζ is the system damping, ω is the excitation frequency and ω_0 is the natural frequency of the system.

For the lightly damped system, resonance is indicated by the peak in the response curve. Physically this means that the force required to excite the system goes to zero while the systems response is infinite. The phase difference or phase shift between the input and response also provides an indication of resonance. At resonance, a 90 degree phase shift occurs between input and response.

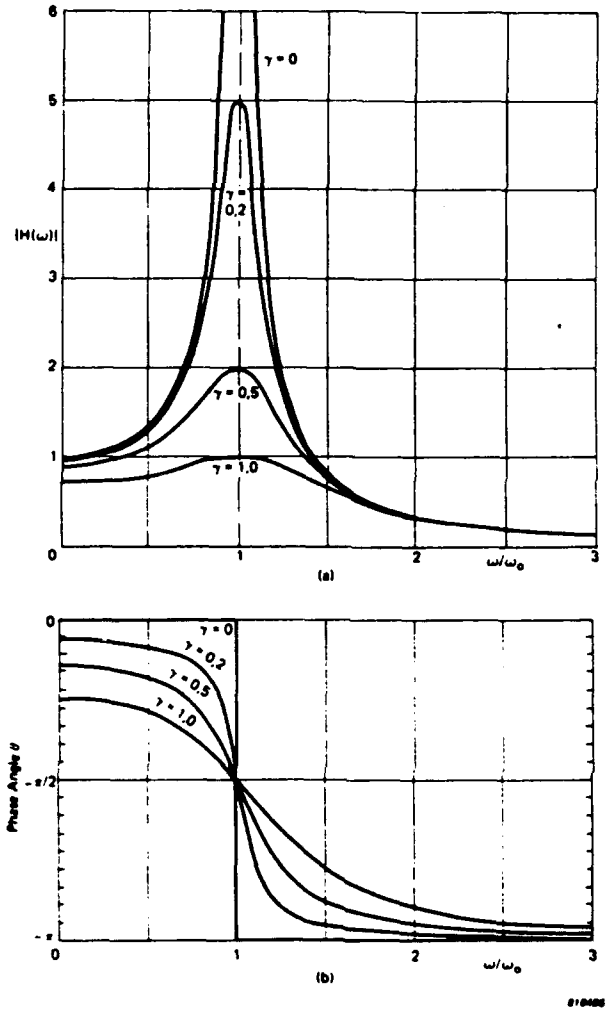

Figure 19. Single Degree of Freedom Frequency Response Function

This is sometimes used to provide a more accurate indication of the modal frequency than the peak value of the transfer function because the transfer function peaks at the resonance frequency only in the case of lightly damped systems.

Transfer function units can vary depending on the units by which the response is measured. The following is a list of common terminology used to define the transfer function [Ref. 20]:

- acceleration/force = Inertance
- velocity/force = Mobility
- displacement/force = Receptance, Compliance, Admittance
- force/displacement = Impedance

Discrete physical systems with multiple degrees of freedom have a discrete number of resonances, "natural" frequencies or what are sometimes called "eigen" values. In the case of continuous systems, it can be shown that an infinite number of natural frequencies exist. The significance of these natural frequencies is that when the structure is excited or driven at one of these frequencies the resulting structural motions, and hence stresses, can be magnified significantly. For the idealized situation of zero damping, the amplification can mathematically be shown to approach an infinite value. This can be seen in Figure 19 for the single degree of freedom system. Multiple degree of freedom systems react similarly near their resonance frequencies. A more in-depth discussion of modal theory and testing techniques can be found in [Ref. 21].

B. TEST OPERATION

The *Bruiser* was excited independently in both the vertical and lateral directions. Longitudinal excitation was not investigated due to the airframes structural rigidity along its longitudinal axis and the fact that the longitudinal vibrations associated with helicopters are typically very low.

Broadband noise was used to excite the structure. This provided a significant reduction in testing time as compared to the sinusoidal sweep method. The SD380 Signal Analyzer was used to generate the broad band noise signal to drive the F7/F4 shaker and to perform digital Fast Fourier Transforms (FFT) on the incoming force and acceleration data. Transfer function calculations were then performed on the digitized data and presented on the SD380 display along with phase information. The "averaging" feature of the SD380 was used to smooth out noise in the plots, and the "zoom" feature was used to investigate specific areas of interest. A roving accelerometer was used to obtain acceleration response at various points and orientations on the airframe. The various roving accelerometer locations are presented in Figure 20. Figure 21 shows the roving accelerometer attached laterally to the tail rotor assembly and vertically to the skids. Specific coordinate locations and orientations of the roving accelerometer attachment points are given in Table VII.

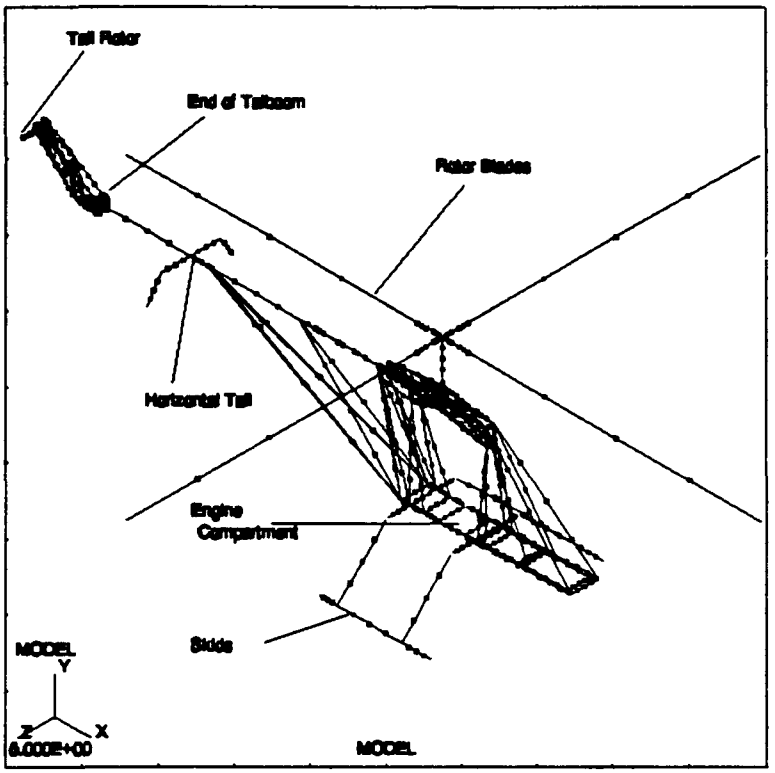

Figure 20. Roving Accelerometer Locations

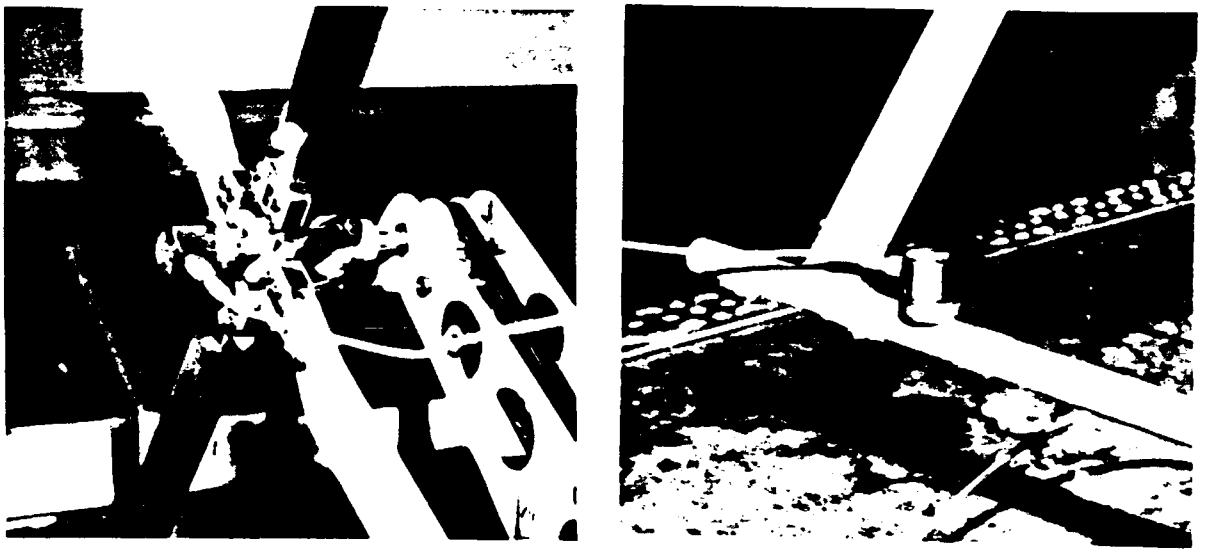

(a) Tail Rotor Lateral (b) Skid Vertical

Figure 21. Roving Accelerometer Attachments

TABLE VII. Accelerometer Locations and Orientations

Location	Position[1]			Orientation
	Long.	Lat.	Vert.	
Tail Rotor	-76.6	2.50	24.2	Lateral
	-76.6	1.75	24.4	Vertical
End of Tail Boom	-68.5	-0.50	19.0	Lateral
	-68.5	0.00	19.8	Vertical
Horizontal Tail	-57.0	-0.50	19.0	Lateral
	-57.0	0.00	19.5	Vertical
Engine Compartment	-20.0	-1.82	6.90	Lateral
	-20.0	-1.50	6.90	Vertical
Skid	-24.0	±11.5	0.00	Lateral
	-24.0	±11.5	0.00	Vertical
Rotor Blade	2 inches from blade attachment pin			Vertical Only

1. Indicates position relative to aircraft reference point. Reference point is at the nose of the aircraft, on centerline and at skid level. All measurement in inches.

A full spectrum of transfer function data was taken at each location, each orientation and for each excitation method (i.e. vertical and lateral excitation). Estimates of the structural mode shapes were obtained by sinusoidally exciting the airframe at each of the observed modal frequencies. Acceleration measurements were then taken at two inch increments down the airframe. Both the first lateral and

first vertical, as well as for the 2nd vertical bending mode, were documented in this way.

Main rotor blade flapwise modes were documented in a similar fashion. Flapwise blade natural frequencies were obtained from the frequency response functions generated while the roving accelerometer was mounted on a rotor blade. The airframe was then excited vertically at those discrete natural frequencies. Vertical acceleration measurements were then taken at three inch increments down the length of the rotor blade.

VII. GIFTS FINITE ELEMENT MODEL

A. GENERAL

A finite element model of the ***Bruiser*** was developed using the CASA/GIFTS computer program [Ref. 7] as installed on the Department of Aeronautics and Astronautics VAX computer system. Model generation was accomplished by first accurately defining the geometry of the ***Bruiser's*** structure. This was done by establishing a reference point at the nose of the aircraft on centerline and at skid level. All subsequent measurements used this reference point as their origin.

The ***Bruiser*** was flight configured and supported on its main landing gear (skids) for all measurements. A grease pencil grid was established on all exterior surfaces to aid in the measurement process and to also document roving accelerometer position during the shake tests. Major structural component dimensions, locations and attachment points were documented during the measurement phase. Beam shapes and sizes were measured and confirmed with the manufacturer as were the individual material types. Material types were given previously in Table II.

B. MODEL GENERATION

With the measurement phase complete, generation of the GIFTS finite element model could begin. In arriving at a

solution to the free-free dynamic response of a structure, the GIFTS program attempts to solve the following matrix equation

$$[K]^{-1}[m]\{\ddot{x}\}=0, \qquad (1)$$

where [K] is the stiffness matrix and [m] is the mass matrix. The eigenvalue solutions to equation (1) represent the modal frequencies, and the corresponding eigenvectors define the structures deflected mode shape. Table VIII lists the sequence of GIFTS modules used to arrive at a solution to equation (1).

TABLE VIII. GIFTS Module Sequence for Free-Free Dynamic Structural Analysis

Module	Description
BEAMCS	Define beam cross sections and plate thicknesses.
BULKM	Generate model.
BULKF	Determine basic freedom patterns.
LOADBC	Apply desired loadings and define mass matrix [m].
OPTIM	Optimize bandwidth.
ADSTIF/ELSTFF	Compute stiffness matrix [k].
SUBS	Subspace iteration routine to solve equation (1).
RESULT	Displays deflected mode shapes.

Model generation was accomplished by identifying "Key Nodes" in the structure and attaching beams and/or flat plate elements between them. BEAMCS and BULKM were the primary GIFTS modules used for model generation. BEAMCS was used to define all plate thicknesses and beam cross section dimensions. BULKM was used to define the key nodes and specific element properties of the structure. BULKM was then used to attach beams with cross sections as defined in BEAMCS between specified key nodes. Plates were generated in BULKM by defining three and/or four sided grids and assigning appropriate materials and thicknesses to them. Figure 22 shows the completed finite element model of the ***Bruiser***.

After the model was constructed and verified, its structural mass was generated. Masses corresponding to concentrated weights were lumped at appropriate nodes then a global stiffness/mass matrix was computed. A subspace iteration technique was then used for the simultaneous extraction of selected modal frequencies and corresponding mode shapes. The following section provides a brief description of each module and how it was tailored to meet the requirements of the ***Bruiser*** free-free analysis.

C. DESCRIPTION OF GIFTS MODULES

BULKF is a non-interactive module and intended to allow only those freedoms which the model can support, thereby relieving the user of the need to interactively suppress all

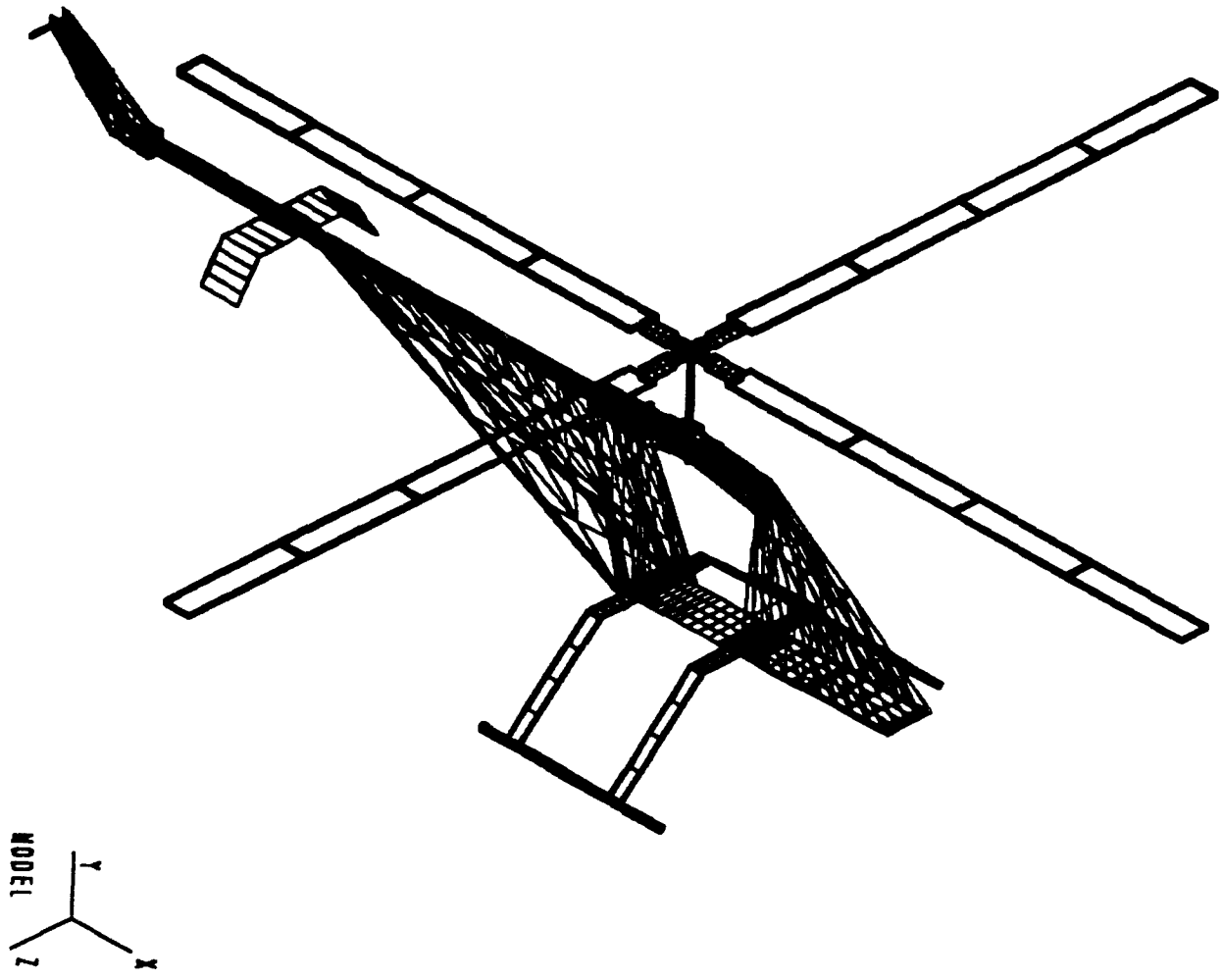

Figure 22. ***Bruiser*** **Finite Element Model**

superfluous freedoms. This also reduces the model's overall degrees of freedom.

LOADBC is an interactive module which allows for the application of boundary conditions, the suppression of freedoms, the application of point and distributed masses, and the application of point and distributed loads. Based on the

element properties defined in BULKM, and the user defined lumped masses and boundary conditions, LOADBC computes and stores the mass matrix [m] of the model. In the ***Bruiser*** free-free analysis no boundary conditions were specified. Distributed masses were used for the engine and transmission, the fuel tank, the ballast and the battery. A point mass was applied to the end of the tail rotor drive shaft to account for the mass of the tail rotor.

The OPTIM module is a bandwidth optimizer designed to reduce the spread of the stiffness matrix coefficients, thereby increasing the efficiency of the matrix solution scheme. From user defined starting nodes, OPTIM rearranges node numbers internally to minimize the model's half bandwidth. The user may input starting nodes in groups of up to ten to optimize the half bandwidth. OPTIM computes the bandwidth for each case; then automatically selects and stores the run with the minimum bandwidth. The computed bandwidth for the final ***Bruiser*** configuration was 581.25.

ADSTIF and ELSTFF are non-interactive modules used to compute the overall assembled stiffness matrix coefficients. ADSTIF assigns disk allocations for the stiffness matrix and partitions the stiffness matrix in small blocks of less than 18x18. ELSTFF computes the actual coefficients and stores the assembled stiffness matrix for use by subsequent GIFTS modules.

The SUBS module is an interactive module used for free vibration analysis. Using the previously determined mass and stiffness matrices, SUBS employs a subspace iteration technique to determine a user selected number of the model's natural modes of vibration. The method reduces the large eigenvalue problem to a smaller size by subspace transformation. The iterative process is continued until convergence is obtained. The convergence criteria is specified by the desired digits of accuracy required of the eigenvalue solutions. The default number of iterations (10) was used for all ***Bruiser*** runs. Finally, SUBS stores the computed eigenvalues and corresponding eigenvectors for display in the RESULT module. BEAMCS, BULKM and LOADBC files are given in Appendix A.

D. SUMMARY OF COMPUTATIONAL STATISTICS

The GIFTS dynamic analysis was computationally intensive with an average of 48 CPU hours for each run. The entire sequence with the exception of the RESULT module was run in "batch" mode on a VAX 3100 Work Station. The VAX batch file is given in Appendix C. A summary of model and computational statistics is presented in Table IX.

E. MODEL VERIFICATION

It is apparent from equation (1) that the only factors affecting the GIFTS results are the stiffness and mass

TABLE IX. GIFTS Model and Computational Statistics

Number of Structural Nodes	1225
Number of Active Elements	1556
Total Number of Unknowns	7350
Computational Bandwidth[1]	581.25134
Maximum Half Bandwidth[1]	767
Degrees of Freedom	7350
Double Degrees of Freedom	3675
Computational Time	
BULKF processor	12.2 sec
OPTIM processor	81.6 sec
ADSTIF processor	433.4 sec
SUBS processor[2]	89,192.5 sec
Charged CPU Time	25 Hrs 2 Min 26.8 sec
Total Elapsed Time	37 Hrs 59 Min 28.5 sec

Notes: 1. Bandwidths presented are the final optimal bandwidths calculated in the OPTIM processor.
2. SUBS computational time is time required to obtain convergence of the first 13 modes.

distributions. As a cross check on the accuracy of the GIFTS model, the ***Bruiser*** was disassembled to accurately determine the mass of major individual components. A comparison of the actual measured component masses to the masses as computed from the GIFTS model is presented in Table X. The component masses computed by GIFTS were consistent with actual values with an average component error of approximately 3%. The total GIFTS calculated ***Bruiser*** mass differed from the actual measured mass by 3.2%.

TABLE X. Comparison of Actual Component Masses to GIFTS Calculated Masses

Component	Actual Mass (lbm)	GIFTS Calculated Mass (lbm)
Engine Compartment and Rotor Mast	18.05	17.49
Nose Compartment	6.96	6.99
Tail Boom Assembly[1]	3.0	2.4
Skids	1.68	1.75
Tail Rotor Assembly	0.69	0.71
Main Rotor Blades (4)	2.09	2.10
Total A/C Mass	**32.47**	**31.44**

Notes: 1. Engine Mufflers not included in GIFTS model. Mass of both mufflers = 0.8 lbm.
2. Ballast, fuel, engine, battery and tail rotor masses are incorporated in all measurements.

VIII. EXPERIMENTAL RESULTS

A. AIRFRAME STRUCTURAL TESTS

Results of the airframe structural vibration tests are presented as frequency response functions generated by the SD380 signal analyzer. Frequency response functions were obtained for four 50 Hz intervals from 0 to 200 Hz at each of the roving accelerometer locations specified in Figure 20 and for each method of excitation (i.e. vertical and lateral).

1. Vertical Excitation

Figure 23 presents the 0-50 Hz frequency response function for vertical excitation of the airframe. It was obtained with the roving response accelerometer attached laterally at the tail rotor. Figure 24 gives the frequency response function obtained at the same location, but with the roving accelerometer oriented vertically. Frequency response functions for all roving accelerometer locations and orientations are presented in Appendix B.

Figure 23 shows modes at approximately 15, 20.4, 22.4, 25.7, and 35.7 Hz as indicated by the peaks in the frequency response function curves. Similarly, Figure 22 shows modes at 21.3, 25.5, 26.3 and 35.5 Hz.

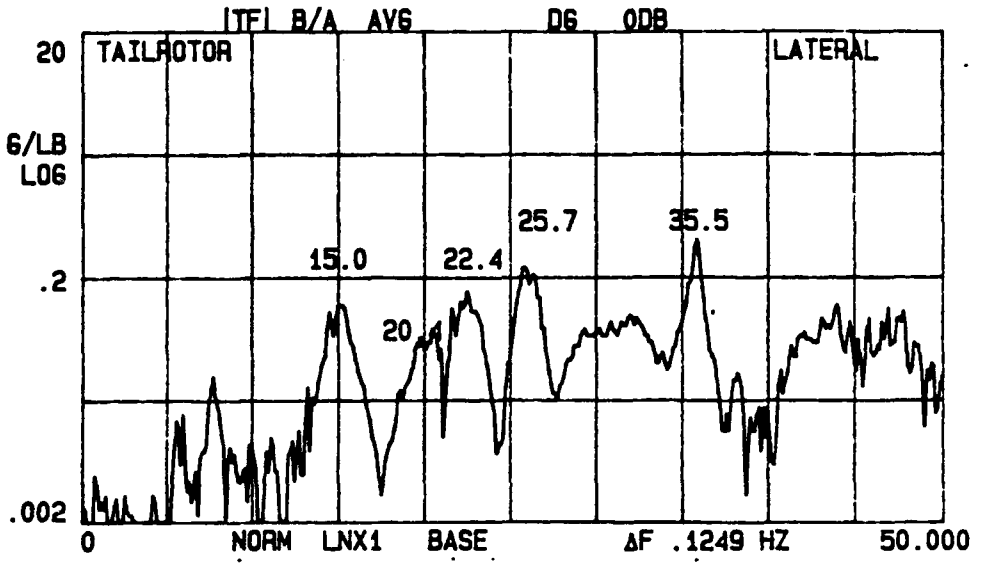

Figure 23. Tail Rotor Lateral Frequency Response Function (Vertical Excitation)

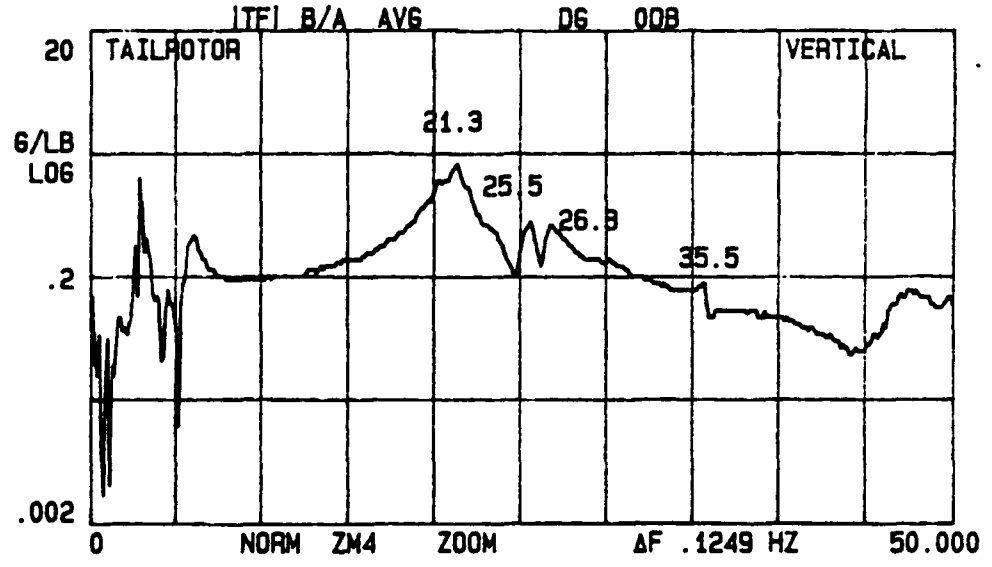

Figure 24. Tail Rotor Vertical Frequency Response Function (Vertical Excitation)

An additional indication of modal resonance is provide by the phase plots, given in Appendix B, which indicate 90 degree phase shifts at each modal frequency. Finally, the modal peaks apparent at frequencies below 10 Hz on both Figures 23 and 24 are felt to be unreliable based on the poor rated performance of the F7/F4 shaker and its integral force gauge at frequencies below 10 Hz.

The modes identified in Figures 23 and 24 are apparent at each roving accelerometer location. Only the magnitude of the response varies. Small shifts (less than 0.5 Hz) in the modal frequency however, were observed at the different locations and accelerometer orientations (i.e. lateral vs vertical). Some closely located modes tended to merge together at locations and/or orientations different their from points of maximum response. This can be seen in Figure 23 where modes are apparent at 20.4 and 22.4 Hz while Figure 24 shows only one mode in the 21-22 Hz range. Conversely, Figure 24 shows modes at 25.5 and 26.3 Hz while Figure 23 shows only one mode at 25.75 Hz. A distinction between the structural response at these closely located nodes was sometimes difficult and other times easy to determine.

For the above example, the two closely located modes at between 25 and 26.5 Hz were easily distinguishable since the lower frequency corresponded to an easily observable bending mode in the horizontal tail, while the mode at 26.4 Hz was determined to be a major tail boom bending mode.

Unfortunately it was impossible to separate the response between the other set of closely located modes between 20-22 Hz.

The highest significant mode visually observed during the vertical shake tests was the one at 35.5 Hz (the skid bending mode). Higher, less dramatic modes could be seen on the frequency response function plots but the energy associated with these higher modes was not considered significant. Additionally, it was impossible to determine the character or general mode shapes of these higher frequency modes. The lower modes were classified based on visual observation of the airframes response as well as by interpretation of the quantitative data. Table XI summarizes the modes identified during vertical excitation tests.

The relative response and direction of response at each location on the structure defines the mode shape of the structure at that modal frequency. Simultaneously recording multiple accelerometer readings at several locations on the structure would allow for the documentation of the structures complete mode shapes [Ref 20]. Unfortunately only one accelerometer was available for this experiment.

To obtain an indication of the response characteristics of the structure and an initial idea of the ***Bruiser*** mode shapes, lateral and vertical response values (inertance (g/lb)) were normalized and plotted against roving accelerometer position.

TABLE XI. Summary of *Bruiser* Modes Identified During Vertical Shake Tests

Mode	Frequency (Hz)	Comments
First Vertical Tail Boom Bending Mode	15	Mode Readily Apparent
Vertical Tail Boom Bending Mode	21-22	Limited Airframe Response. Difficult to Interpret
Horizontal Tail Bending Mode	25.5	Large Horizontal Tail Deflections Readily Apparent (Localized Mode)
Second Vertical Tail Bending Mode	26.5	Mode Readily Apparent
Tail Panel Skin Mode	32	Combination Tail Panel/Tail Boom Tie Rod Mode (Localized Mode)
Skid Bending Mode	35.5	Mode Readily Apparent

The data were normalized to the highest measured response for each mode. Vertical data only are presented at the skid location due to difficulties associated with attaching the accelerometer in a lateral orientation. Bar graph plots for the modes at 15, 21, 26.5 and 35.5 Hz are presented in Figures 25 through 28.

Figures 25 through 28 show the general nature of the major ***Bruiser*** modes. Variations in vertical and lateral response give an indication of possible torsional modes. The 15 and 26.5 Hz modes correspond to major tail boom bending modes as observed visually and as documented with the roving

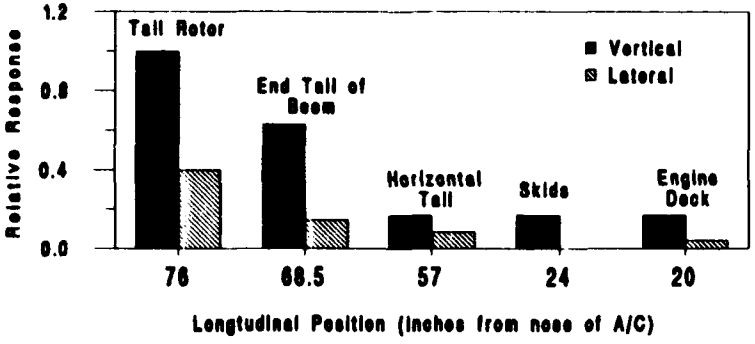

Figure 25. Relative Response to Vertical Excitation (15 Hz)

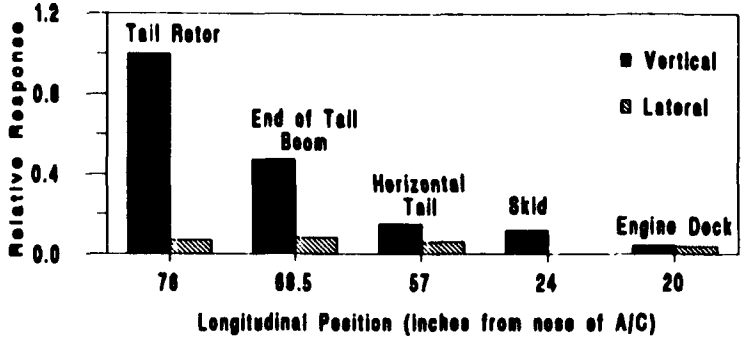

Figure 26. Relative Response to Vertical Excitation (21 Hz)

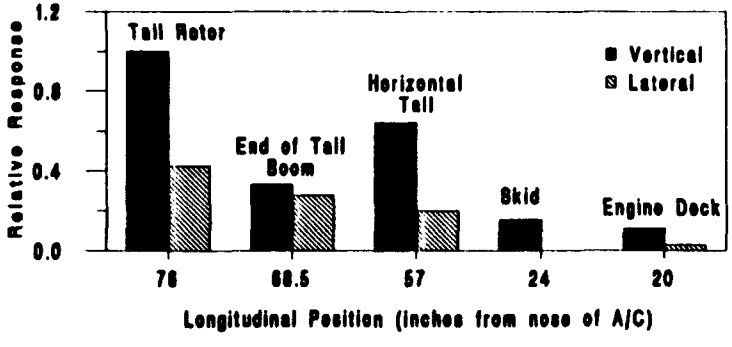

Figure 27. Relative Response to Vertical Excitation (25.5 Hz)

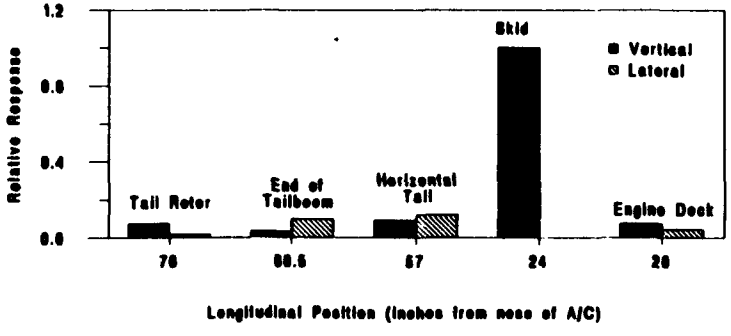

Figure 28. Relative Response to Vertical Excitation (35 Hz)

accelerometer. The large vertical response at the skid location in Figure 28 graphically illustrates the localized nature of this mode and its relative magnitude.

The roving accelerometer was used to more precisely document the ***Bruiser's*** major tail boom bending modes at 15 and 26.5 Hz. The structure was excited with a sinusoidal input at these frequencies, and acceleration measurements were taken at two inch longitudinal intervals along the airframe. The response at these modes was visually observed to be primarily vertical in nature and therefore only vertical acceleration measurements were taken. Acceleration measurements were normalized to the largest measured response and are plotted in Figures 29 and 30. Figure 29 is representative of a beam first bending mode while Figure 30 is representative of a beam second bending mode and hence these modes are referred to as the "First" and "Second Vertical Bending Modes" in Table XI.

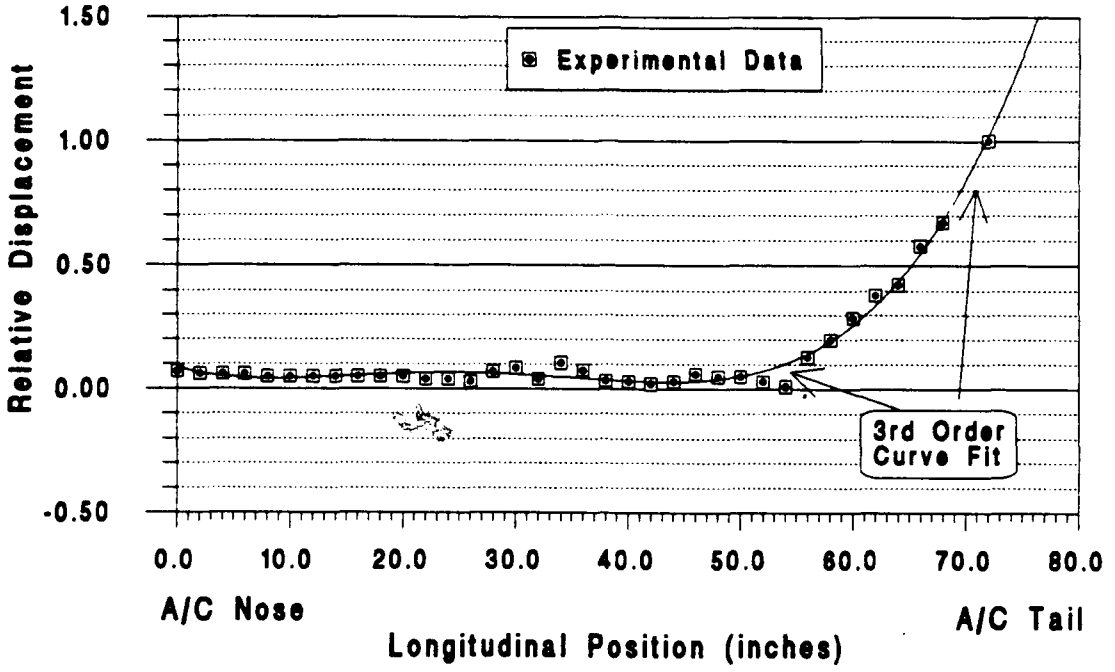

Figure 29. *Bruiser* First Vertical Bending Mode (15.0 Hz)

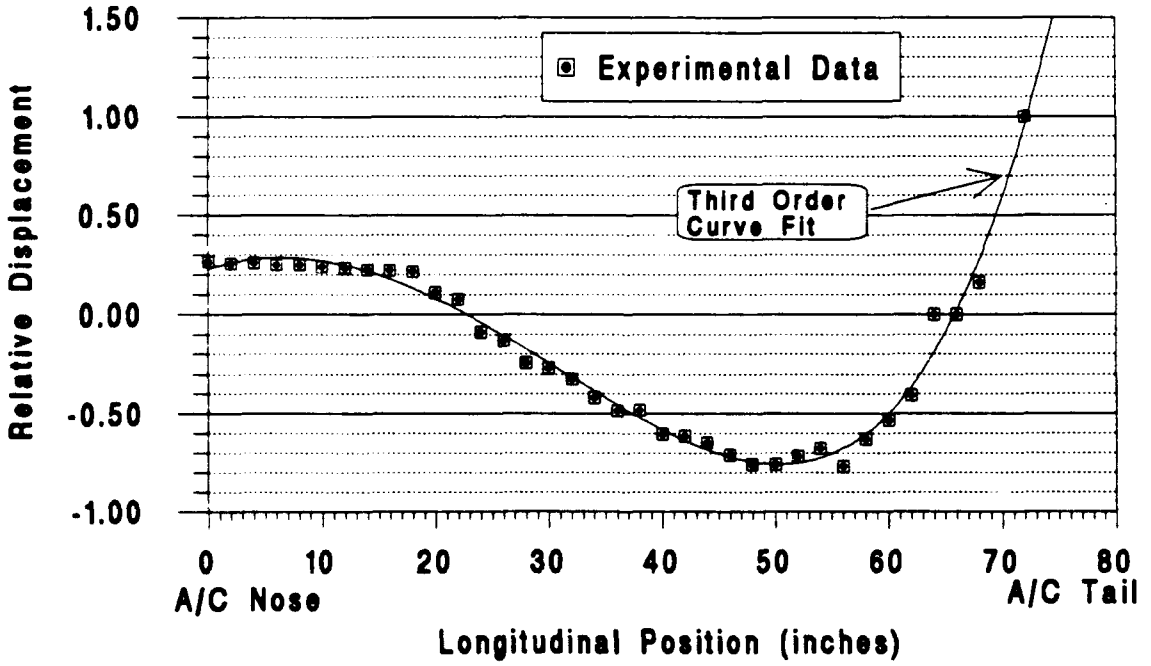

Figure 30. *Bruiser* Second Vertical Bending Mode (26.5 Hz)

2. Lateral Excitation

Lateral excitation data reduction and interpretation techniques were similar to those discussed for vertical excitations. Representative frequency response function curves are presented in Figures 31 and 32. These curves represent the lateral and vertical response as measured at the tail rotor. Lateral excitation frequency response curves from 0-200 Hz at each roving accelerometer position are presented in Appendix C.

The lateral excitation input location, Figure 13, was much closer to the structures center of gravity. This resulted in significantly lower response levels for the lateral excitation tests than for the vertical tests. As modal testing is concerned with structure's relative response only, this did not affect the accuracy of the lateral tests. The lower structural response levels did however, require increased accelerometer gains to obtain measurable responses. These increased gains, in conjunction with the larger amount of metal associated with the lateral shaker mounting arrangement, Figure 11, were felt to be responsible for the electromagnetic interference evident at 60 Hz and odd multiples of 60 Hz. This interference can be seen as spikes on the frequency response function plots in Appendix C. These spikes were extremely localized and did not affect the accuracy of the tests. The source of the interference was presumably the building's 60 Hz electrical service. Future

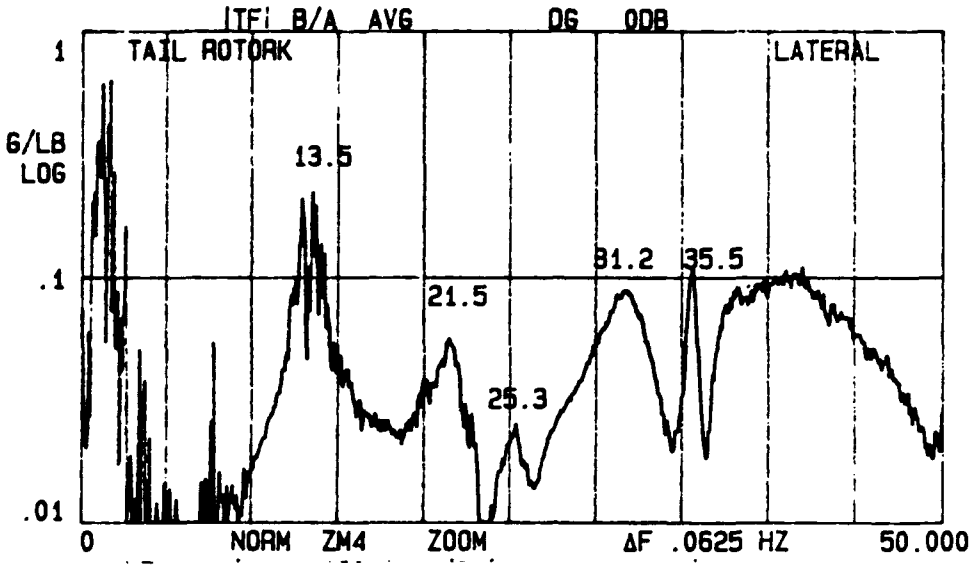

Figure 31. Tail Rotor Lateral Frequency Response Function (Lateral Excitation)

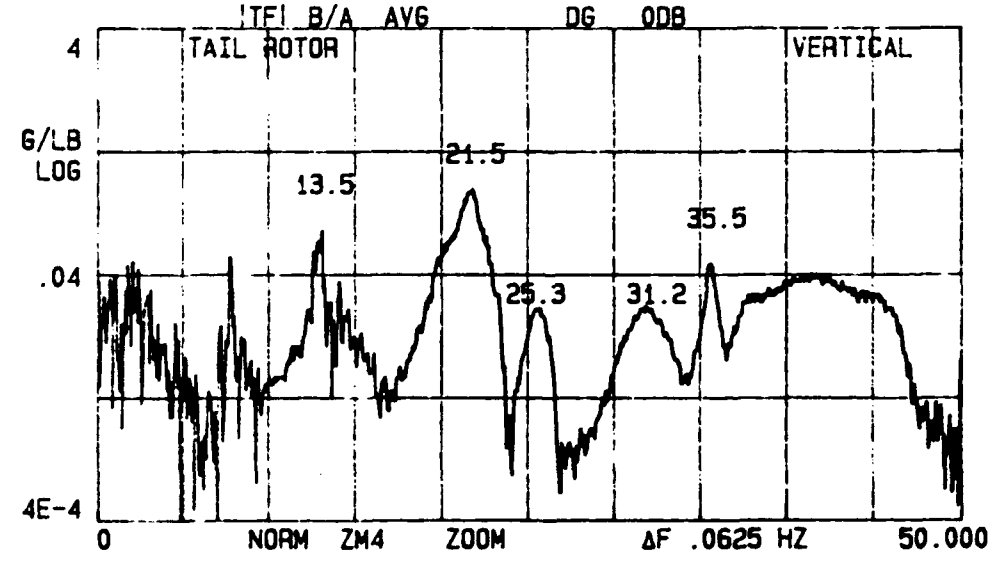

Figure 32. Tail Rotor Vertical Frequency Response Function (Lateral Excitation)

test set-ups should ensure proper shielding and grounding of equipment to eliminate this problem.

Figures 31 and 32 document the same modes observed during the vertical excitation tests with one notable exception. A major lateral-torsional tail boom mode is apparent at 13.5 Hz in the lateral test data, while no indication of this mode is observed in the vertical excitation plots. Conversely, Figure 23 shows a major tail boom vertical bending mode at 15.0 Hz while this mode does not appear in the lateral excitation test data. It is felt that because the mode at 13.5 Hz is primarily lateral-torsional in nature it is most responsive to lateral excitation and hence only apparent in the lateral excitation plots. Through similar reasoning the mode at 15.0 Hz is almost exclusively vertical in nature and hence only apparent when the structure is excited vertically. Due to the nature of the response at 13.5 Hz, this mode was called the "First Lateral Bending Mode" of the airframe.

An additional difference observed between the vertical and lateral shake test data was the relative prominence of the mode at approximately 31.5 Hz during the lateral excitation tests as opposed to what was observed during the vertical excitation tests. While the mode was apparent at some locations during the vertical tests, it was not nearly as distinct. The mode is primarily a tail boom skin panel and tie rod mode. These components are significantly stiffer

vertically than they are laterally; hence the higher response to the lateral excitation inputs.

As with the vertical shake tests, bar graph plots of the normalized response to lateral excitation were also constructed. They are presented for the four dominant modes identified during the lateral shake tests in an attempt to better describe the observed response. Bar graph plots are presented in Figures 33-36.

3. Summary

The structural vibration tests were used to accurately determine the dynamic response of the ***Bruiser*** between 10 and 200 Hz. While data was recorded for the entire range, the primary area of interest was less than 40 Hz where the major structural modes occurred and where modal analysis was possible. Higher frequency modes were apparent from the frequency response function curves but were not specifically investigated. Comparison of the ***Bruiser*** modal frequencies with the ***Bruiser*** characteristic frequencies (Table V) indicates that the majority of possible excitation frequencies occur at significantly higher frequencies than those of the primary ***Bruiser*** structural modes. The only exception to this is the 1/rev (19.6 Hz) vibration associated with an out-of-track or out-of-balance rotor system. This possible excitation frequency is 1.9 Hz less than the closest modal

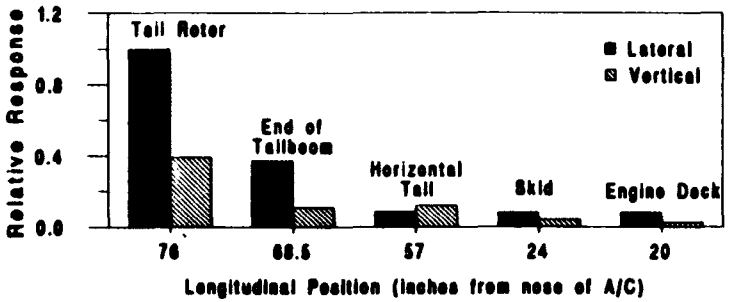

Figure 33. Relative Response to Lateral Excitation (13 Hz)

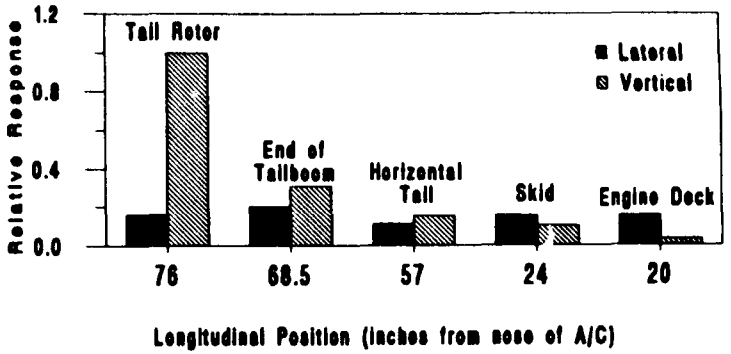

Figure 34. Relative Response to Lateral Excitation (22 Hz)

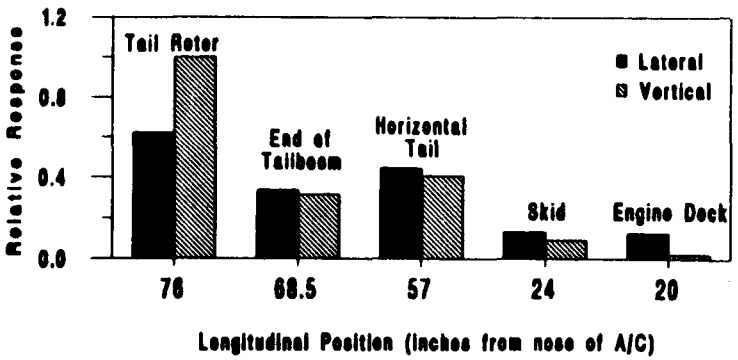

Figure 35. Response to Lateral Excitation (25.5 Hz)

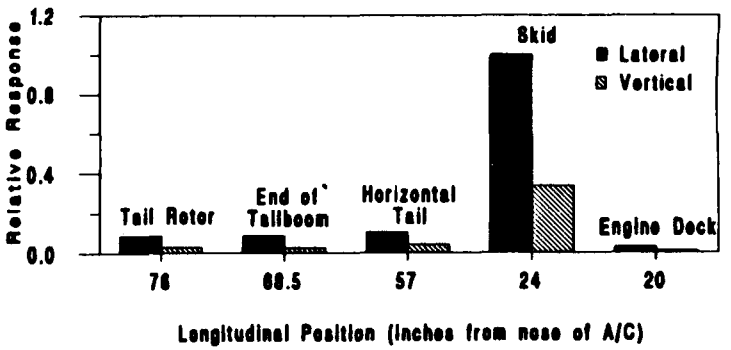

Figure 36. Response to Lateral Excitation (35 Hz)

frequency and should not cause concern. Additionally, this excitation source can be easily controlled by maintaining proper rotor track and balance.

B. MAIN ROTOR BLADE TESTS

1. Blade Natural Frequencies

The flapwise modes of the main rotor blades were experimentally determined during vertical shake tests. Frequency response function curves, Figures 37 and 38, document modes at 25.25 and 82.63 Hz.

Analytical validation of the experimental results was accomplished by treating the articulated rotor blade as a uniform beam, hinged at its root and free at the tip. Natural frequencies were analytically determined using equation (2) [Ref. 22]

$$\omega_n = a_n \sqrt{\frac{EI}{\mu_1 l^4}}, \qquad (2)$$

where EI is the bending stiffness of the section, l is the length of the beam, a_n is a constant, μ_1 is the mass density per unit length = W/gl, W is the total beam weight and g is the gravitational acceleration. The constants a_n are determined by the end boundary conditions. Values for the hinged free beam are given below:

$a_1 = 0.0$ $\quad$ $a_4 = 104.0$
$a_2 = 15.4$ $\quad$ $a_5 = 178.0$
$a_3 = 50.0$

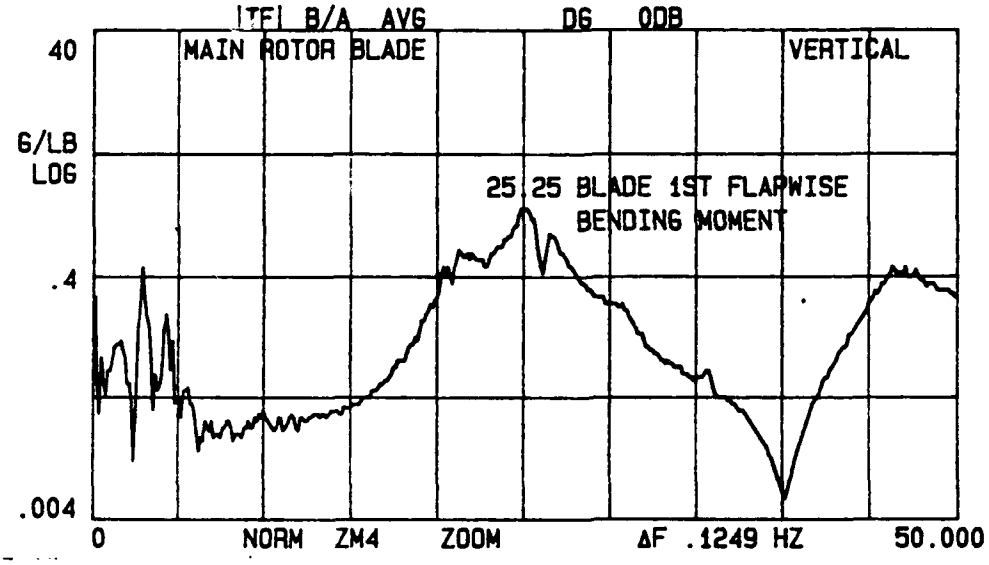

Figure 37. Rotor Blade Frequency Response Function

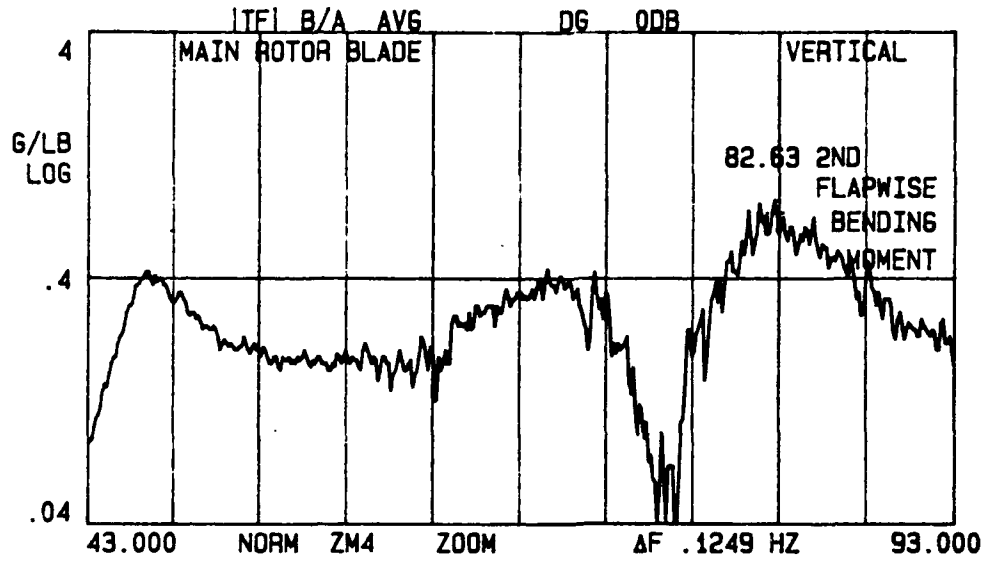

Figure 38. Rotor Blade Frequency Response Function

An equivalent EI was experimentally determined by clamping the root end of the blade and suspending a mass from the tip. The deflection was measured and EI calculated using equation (3) [Ref. 23]

$$EI = \frac{Pl^3}{3\delta}, \tag{3}$$

where P is the applied load, l is the length of unsupported beam and δ is the deflection at the tip. Measured and calculated values as well as the blade's modal frequencies are given in Table XII.

TABLE XII. Experimentally Determined Parameters

Measured Values	
P(applied load)	0.3395 lb
l(exposed blade length)[1]	2.75 ft
δ(deflection)	0.0625 ft
W(blade weight)	0.611 lb
l(actual blade length)[2]	3.08 ft
g(gravitation accel.)	32.174 ft/sec^2
Calculated Values	
E(stiffness)	37.66 lb-ft^2
μ_l(mass/unit length)	0.006159 slugs

Blade Modes

ω_1 = 0.0 Hz (rigid body mode)
ω_2 = 25.34 Hz (1st flapwise mode)
ω_3 = 82.28 Hz (2nd flapwise mode)
ω_4 = 171.2 Hz (3rd flapwise mode)
ω_5 = 292.9 Hz (4th flapwise mode)

Notes: 1. Exposed blade length used in equation (3).
2. Actual blade length used in equation (2).

The calculated values of the first two bending modes agree to within less than 1% of those determined during the experimental shake tests. This provides strong verification of the analytical techniques and justification for using the theoretical results in future ***Bruiser*** main rotor system dynamic studies and/or design modifications.

2. Blade Mode Shapes

Blade mode shapes were experimentally determined using the roving accelerometer technique described earlier. The airframe was sinusoidally excited at the previously documented blade modes at 25.25 and 82.63 Hz while acceleration measurements were taken at incremental distances along the blade.

An analytical investigation of the blade mode shapes was also conducted to determine the validity of using an analytical model to describe the response of the ***Bruiser's*** main rotor system. The Blade mode shapes were determined by solving the governing differential equation for the hinged-free boundary conditions associated with the ***Bruiser's*** articulated main rotor system. The method of approach is similar to that described in Reference 24.

For the case where the flexural rigidity EI remains constant along the length of the bar, or in this case the

rotor blade, the response is governed by the Bernoulli-Euler 4th order partial differential equation:

$$EI\frac{\partial^4 y}{\partial x^4} = -\frac{\gamma A}{g}\frac{\partial^2 y}{\partial t^2} \tag{4}$$

Where $\gamma A/g$ is the mass density per unit length (μ_1 as defined previously), y is the deflection, x is the distance along the beam and t is time.

Recognizing that the deflection (y) at any location varies harmonically with time allows y to be represented by,

$$y = X(A\cos pt + B\sin pt), \tag{5}$$

where X is a function of the coordinate x and defines the shape of the vibration mode. A and B are constants and p is the frequency of the mode. Substituting for y in equation (4) results in

$$\frac{\partial^4 X}{\partial x^4} = k^4 X, \tag{6}$$

where,

$$k^4 = \frac{p^2 A\gamma}{EIg}. \tag{7}$$

Homogeneous solutions to equation (6) include sin kx, cos kx, sinh kx, and cosh kx. A linear combination of these

particular solutions leads to the general solution of the form,

$$X=C_1\sin kx+C_2\cos kx+C_3\sinh kx+C_4\cosh kx, \tag{8}$$

where C_1, C_2, C_3, and C_4 are constants to be determined by applying the appropriate boundary conditions.

The boundary conditions associated with the hinged-free beam model are (a) zero displacement at the root, (b) zero moment at the root, (c) zero moment at the tip, and (d) zero shear at the tip. These correspond to the following equations:

$$\begin{aligned} &\text{(a)} \quad (X)_{x=0}=0, \qquad &&\text{(b)} \quad \left(\frac{d^2X}{dx^2}\right)_{x=0}=0, \\ &\text{(c)} \quad \left(\frac{d^2X}{dx^2}\right)_{x=l}=0, \qquad &&\text{(d)} \quad \left(\frac{d^3X}{dx^3}\right)_{x=l}=0. \end{aligned} \tag{9}$$

From the first two boundary conditions (equations 9(a) and 9(b)) it can be shown that $C_1 = C_2 = 0$. From the boundary conditions at the tip (equations 9(c) and 9(d)) the following "frequency" equation is obtained:

$$\tan kl=\tanh kl. \tag{10}$$

The roots of equation (10) define the frequencies of the corresponding modes. Explicit closed form solutions to equation (10) are not possible however, numerical solution techniques yield the following first four roots: $k_1l=0$, $k_2l=3.927$, $k_3l=7.069$ and $k_4l=10.210$.

Each root defines a C_3/C_4 ratio. Assuming a value for either constant defines the value of the other. Substituting the constant values (C_1, C_2, C_3, and C_4) for each mode into the original deflection equation yields

$$X=C_3(\sin k_n x+\sinh k_n x)+C_4(\sin k_n x-\sinh k_n x), \qquad (17)$$

where x is the position along the blade and k_n = n'th root ($k_n l$)/blade length (l).

Normalized experimental blade mode shape data as well as analytically determined blade mode shapes are presented in Figures 39 and 40. Figures 33 and 34 show general agreement between the theoretically determined mode shapes and the experimental shake test results. The variations are most probably due to the influence of the accelerometer mass. Unlike during the airframe vibration tests where the mass of the accelerometer was insignificant compared to the mass of the structure, the mass of the accelerometer and associated wiring (approximately 7 grams) represented a measurable percentage (2.7%) of the rotor blade system.

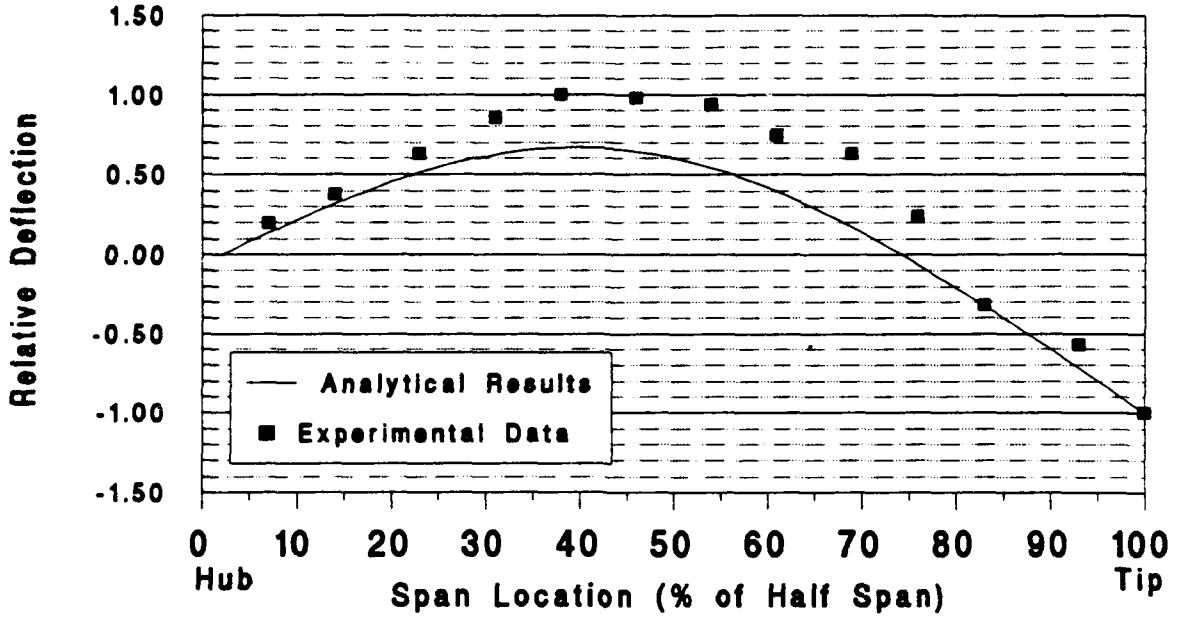

Figure 39. Main Rotor Blade 1st Flapwise Mode Shape (25.25 Hz)

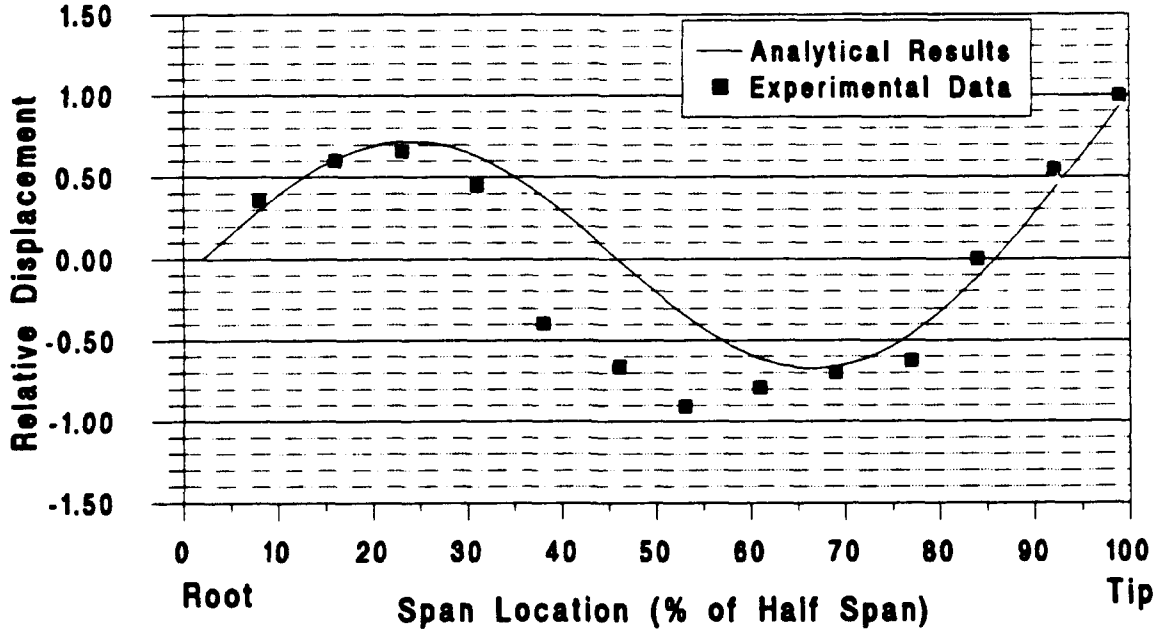

Figure 40. Main Rotor Blade 2nd Flapwise Mode Shape (82.63 Hz)

This influence was visually apparent during tests at the first blade mode where amplitudes could be easily observed.

3. Estimated Rotating Bending Frequencies

Main rotor blade natural frequencies were estimated using the results obtained from the non-rotating blade shake tests through a technique developed by Robert Yntema [Ref. 25]. The rotating bending modal frequencies were assumed to vary as a function of the non-rotating modal frequencies and the rotational speed of the rotor system. A simplified form of the relationship is

$$\omega^2_{Rn} = \omega^2_{NRn} + K_n \Omega^2, \tag{18}$$

where ω_{Rn} is the rotating bending frequency, ω_{NRn} is the non-rotating bending frequency and Ω is the speed of rotation. K_n is a constant which can be subdivided in two independent components as follows:

$$K_n = K_{0n} + K_{1n} e, \tag{19}$$

where e is the blade offset in percent, K_{0n} is referred to as the zero offset Southwell coefficient and K_{1n} is referred to as the offset correction factor for the Southwell coefficient. Values of K_{0n} and K_{1n} are tabularized in Reference 24. A Southwell plot was generating using equation (17) and the

first 4 non-rotating flapwise modal frequencies including the rigid body rotation mode at 0 Hz. This plot is presented in Figure 41.

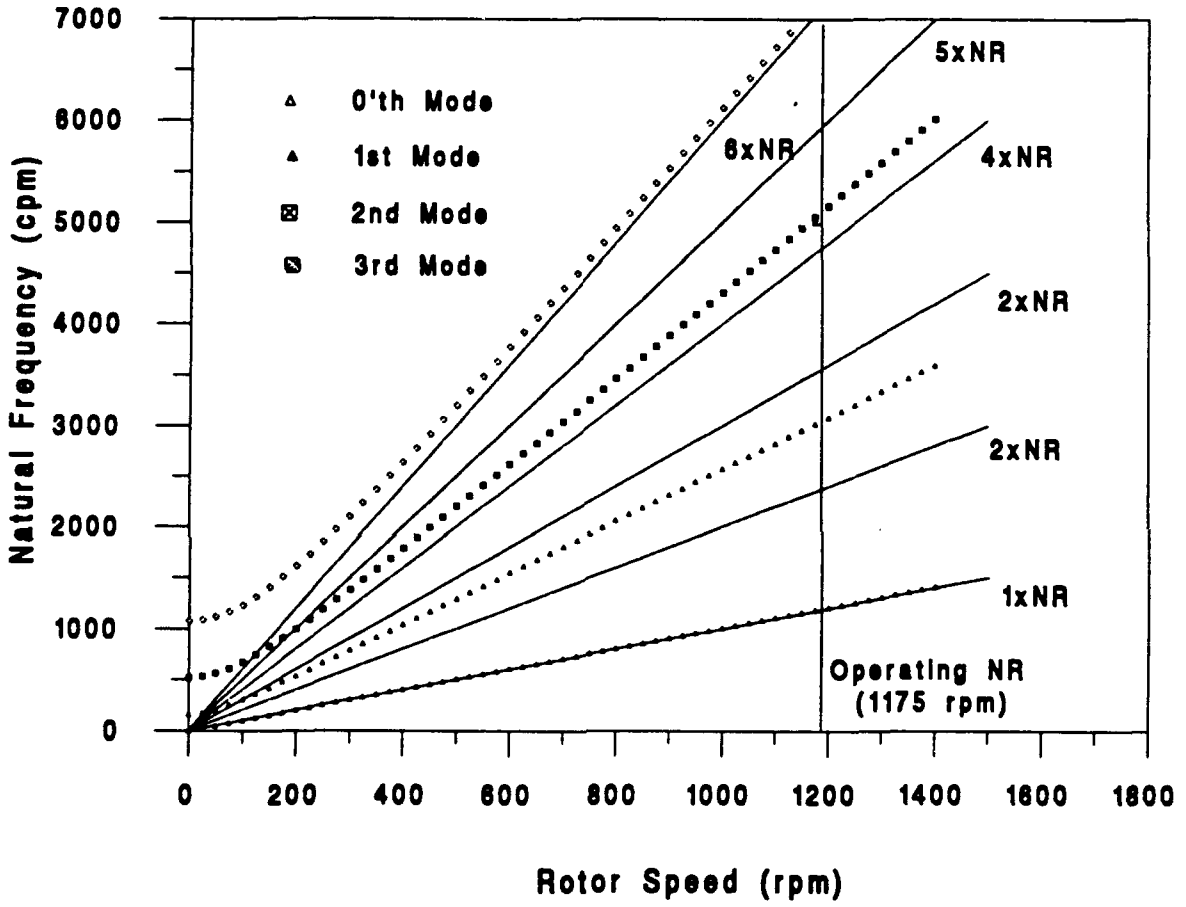

Figure 41. Southwell Plot of Blade Flapwise Bending

Figure 41 shows the effect of increasing centrifugal stiffness on the flapwise blade bending modes. The vertical line at 1175 rpm indicates the normal ***Bruiser*** operating rpm.

It is imperative that good separation be maintained between the blade modes and the harmonic multiples of the rotor speed. The exception to this is the rigid body (zeroth) flapping mode which should be close to the main rotor speed to minimize blade feathering control loads. It is apparent that the zeroth, first and second modes are well placed. The third flapwise mode however, is very close to the sixth harmonic of main rotor speed and may be cause for concern.

IX FINITE ELEMENT ANALYSIS

A. GENERAL

Experimental results determined during the airframe structural shake tests were used to verify, modify and optimize the GIFTS finite element model of the ***Bruiser***. Excessive run times associated with using the VAX 3100 workstation necessitated a reduction in the model's complexity. Figure 21 shows the initial model used. Simplifications included the removal of the rotor system and the horizontal tail. These components were selected due to their limited impact on the airframe's dynamic response as determined during the shake tests. Equivalent masses were lumped at their respective attachment points to maintain model accuracy.

B. RESULTS

Results from the initial running of the GIFTS free vibration analysis showed mode shapes similar to those observed during experimental testing but at significantly higher frequencies. As individual component masses had already been verified, it was decided that the material stiffness of the components should be adjusted in an attempt to match GIFTS results with experimental results. Both experimental and initial GIFTS runs showed the primary

structural response to be in the tail boom and tail rotor assemblies. Hence, it was decided to reduce the stiffness of the beam defining the circular aluminum tail boom. The stiffness (EI) of the tail boom was incrementally reduced by reducing E from 10 million psi (standard Modulus of Elasticity for 6061T6 Aluminum) to an eventual value of 1.5 million psi. This is almost an order of magnitude reduction and is considered excessive. This was required however, to obtain a match of the first two experimentally determined mode shapes. Figures 42 and 43 document the first two GIFTS computed mode shapes at this lower stiffness value.

These modes closely match the shape and frequency of the modes identified experimentally at 13.0 and 15.0 Hz. Higher modes, however, do not match experimental results and are dominated by the excessively soft tail boom. Additionally, many higher modes are characterized by local resonances of insignificant structural members such as the side panel and nose compartment skin.

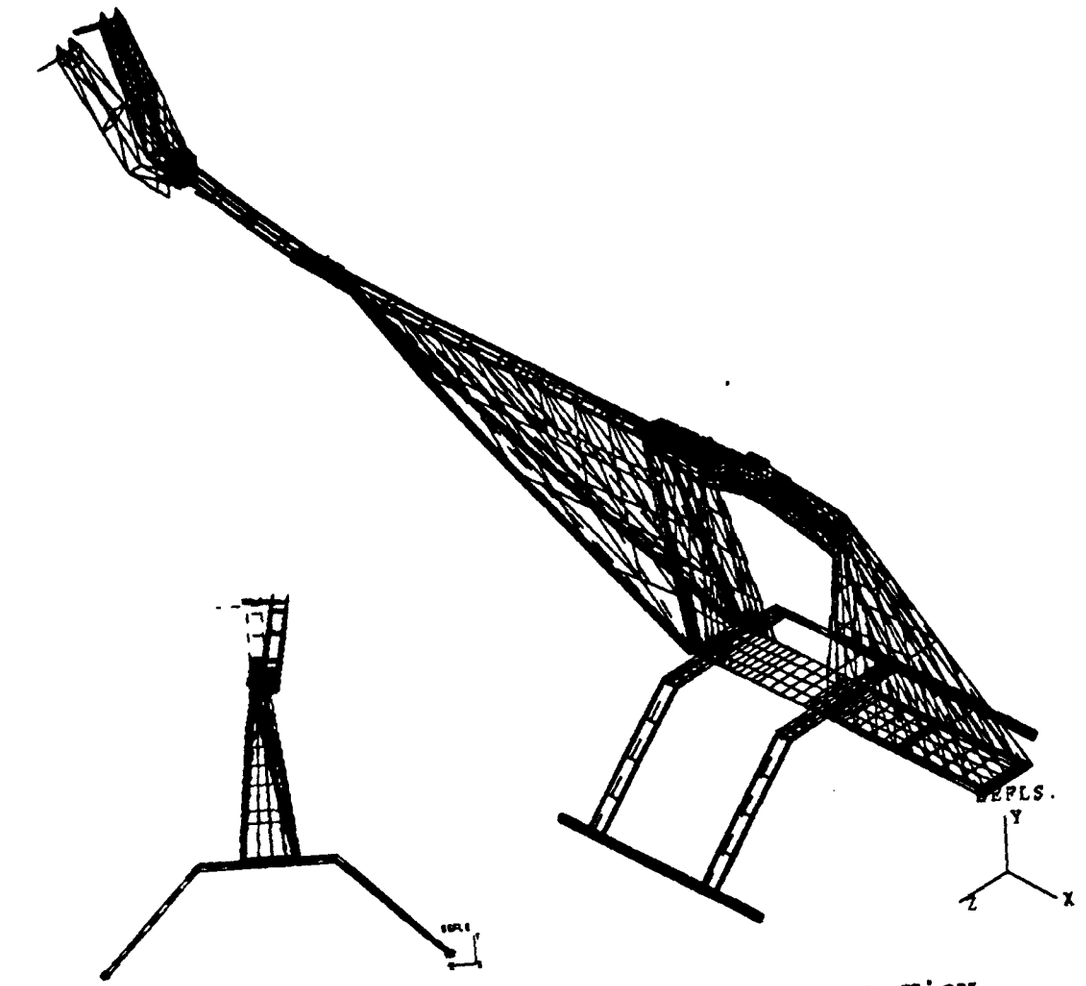

3-D View

Front View

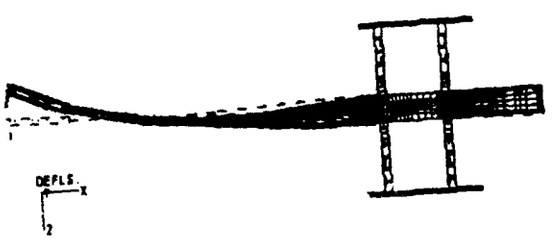

Top View

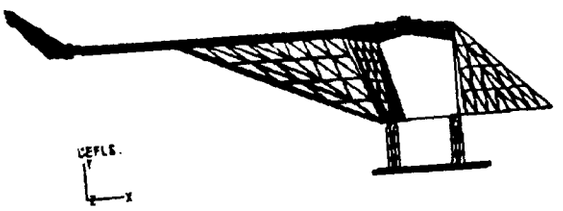

Side View

Figure 42. GIFTS Computed First Lateral-Torsional Bending Mode (14.0 Hz)

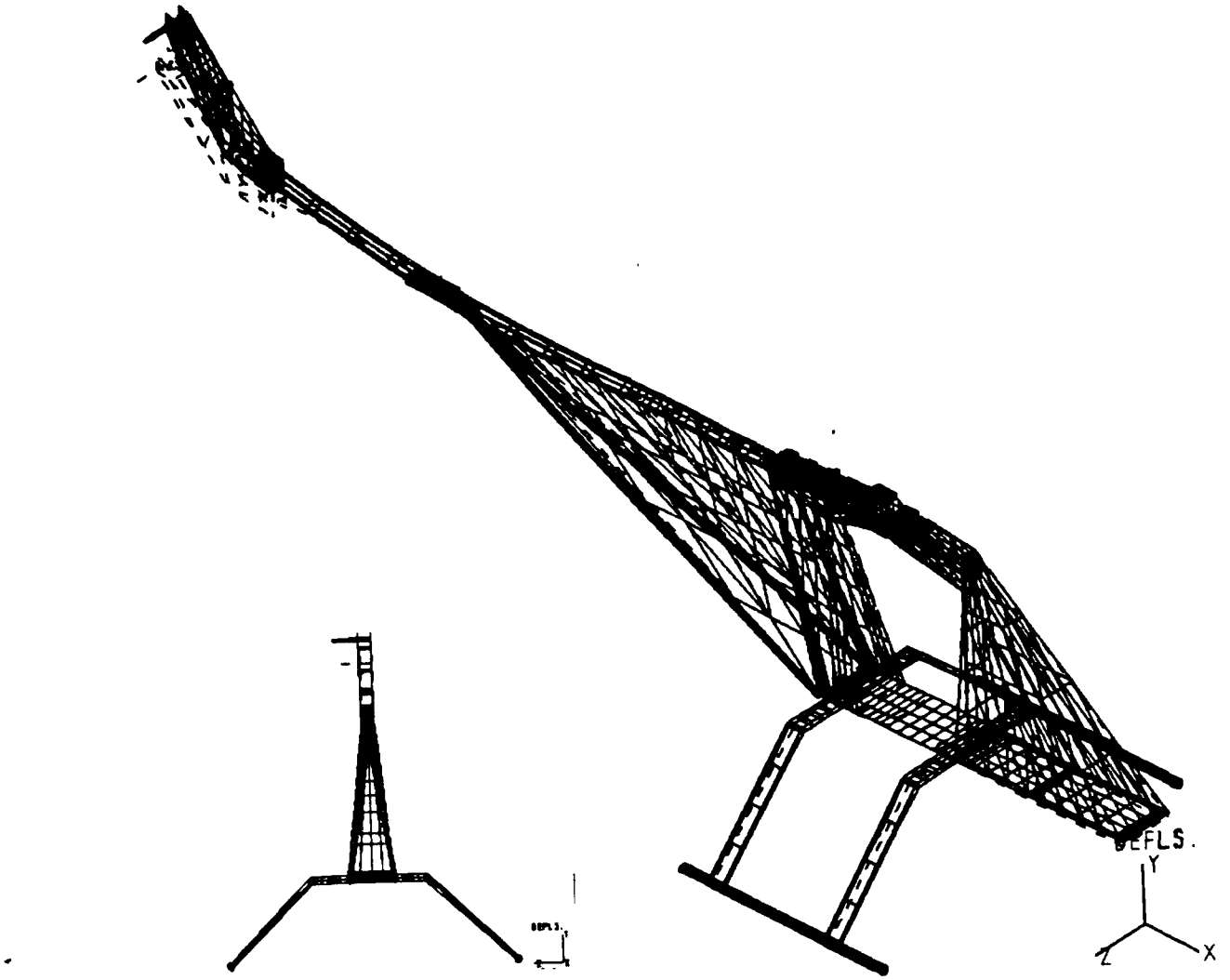

Front View

3-D View

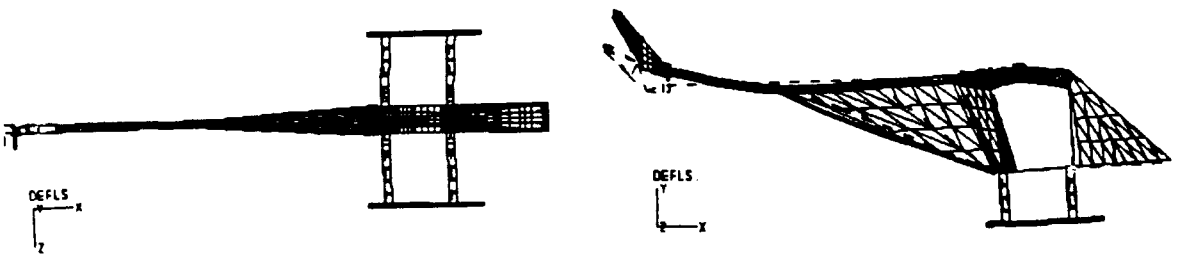

Top View

Side View

Figure 43. GIFTS computed First Vertical Bending Mode (14.5 Hz)

These highly localized modes were also observed during the shake tests but were difficult to define. Frequency correlation between the skin panel modes computed by GIFTS and those observed experimentally showed some similarities but no attempt was made to adjust the GIFTS model to minimize these differences. This was primarily due to the excessive run times associated with changes to the model and the limited effect of skin panel resonances on the overall structural response.

Of note in the GIFTS analysis is the lack of any skid mode below the maximum frequency investigated (approximately 75 Hz). This is surprising given the classic uniform beam cantilever construction of the landing gear. Experimentally, a dominant skid mode was documented at approximately 35 Hz for both lateral and vertical excitation methods. The mode was easily visible and characterized by a classic first bending mode shape. Given the dominant experimental response and simplistic construction of the landing gear it was felt that the landing gear would provide the first step in matching the GIFTS model to the actual airframe response. This was unfortunately not the case.

The lack of a response in the full GIFTS analysis prompted a simplified investigation of the landing gear only. The model consisted of the two landing gear cross beams and the two skid tubes. In an attempt to match the actual skid boundary conditions, the landing gear model was constrained at

the fuselage attachment points. The resultant fixed-free analysis showed a mode very similar to that observed experimentally but again it occurred at a significantly higher frequency (46 Hz vice the 35.5 Hz).

These discrepancies between the GIFTS model and the actual airframe response could not be rectified. Beam, plate and attachment point coordinates were double checked and numerous analyses run at varying material stiffness values in an attempt to correlate the GIFTS response to the actual response. The other area to be investigated is the stiffness distribution of the individual components. This would involve disassembly of the ***Bruiser*** and experimental measurement of component stiffnesses similar to what was done for the main rotor blades.

C. SUMMARY

Finite element methods provide a useful tool for investigating the static and dynamic responses of structures; however, they cannot be conducted in isolation. Total reliance on a finite element model without experimental verification could well result in disastrous consequences. In this investigation, numerous adjustments to the model had to be made just to match the first two vibration modes. One lesson learned from this investigation is to start the modeling using simple geometry then gradually increase the complexity. Simplicity allows for quicker computational run

easier interpretation of the results. As understanding is gained the complexity can be increased. This incremental approach allows one to evaluate model changes individually rather than trying to find a problem area among numerous possible sources. The current ***Bruiser*** finite element model is far from perfect. It requires further refinement and detailed verification of the geometric, elastic and mass distributions. However, the present finite element model could be used as a baseline model for subsequent investigations.

X. CONCLUSIONS AND RECOMMENDATIONS

A. CONCLUSIONS

The purpose of this research effort was to document the dynamic characteristic of the Pacific RPV ***Bruiser*** in preparation for the design and installation of an HHC system. In depth structural shake tests documented the primary structural modes of the airframe as well as providing the in-house capability to conduct subsequent RPV shake tests as needs arise.

The major airframe modes were confined to frequencies below 36 Hz and do not appear to be major factors with respect to the main rotor induced 4/rev vibrations or the higher frequency excitations associated with the tail rotor and engine. As had been expected the primary airframe structural modes were associated with both lateral and vertical tail boom bending. Secondary modes in the skin panels and local resonances in control linkages were also identified but these were localized and not considered significant. The only remaining mode was a major landing gear (skid) resonance at 35.5 Hz.

Although not initially planned for, main rotor blade shake testing produced very credible results and verification of theoretical principles. The use of experimental data in

conjunction with analytical techniques provided a wealth of information on the structural response of the main rotor system. Rotating blade modes were well spaced between the primary blade excitation frequencies of 3/rev, 4/rev and 5/rev at the ***Bruiser's*** operating rpm of 1175. The only possible problem area occurred in the close proximity of the blades third flapwise bending mode to the sixth harmonic of main rotor speed. This, as well as other blade data, will prove invaluable in the ultimate design of an HHC system, especially with respect to required HHC control loads.

A major side benefit associated with this research effort was the expertise gained in conducting shake tests to document the structural dynamics of remotely piloted flight vehicles. These techniques and test equipment can be readily modified to conduct dynamic investigations on any of the RPV's at the Department's UAV laboratory. One problem noted however, was the Department's lack of proper equipment for conducting shake tests. This includes the lack of a shaker as well as a limited amount of accelerometers and associated signal conditioning. Modern dynamic testing techniques require simultaneous recording from multiple accelerometers to accurately define structural mode shapes. This not withstanding, surprisingly good results were obtained using the roving accelerometer technique and it is recommend as a low cost alternative to more expensive modern techniques.

A final goal of this research effort was to establish a useable finite element model of the ***Bruiser*** for subsequent use in the design of structural modifications associated with the installation of an HHC system and possible NOTAR modifications to the tail boom. While a workable GIFTS finite element model of the ***Bruiser*** was developed a detailed verification of the model needs to be performed.

B. RECOMMENDATIONS

Investigation of flight vehicle structural dynamics will continue to play a major role in future aircraft design and development. This is true of unmanned flight vehicles as well. The growth and expansion of the Departments UAV flight facility and the prospect of producing a locally designed and manufactured RPH point to the need for establishing and maintaining a viable in-house dynamic shake test capability. To that end it is recommend that the Department procure the following items:

- Electro-Mechanical Shaker with associated power amplifier.
- High response light weight accelerometers. A minimum of two, preferably four.
- Charge Amplifiers. One per accelerometer.
- Micro-computer with compatible IEEE bus for recording and storing digitized data.

Not listed above is the Signal analyzer which is essential to any modal testing (the Department has three of these).

With regards to the scope of this investigation, it is recommended that the GIFTS finite element model be refined. This includes matching the GIFTS response to the experimentally documented response. Also included in this refinement effort would be the disassembly of ***Bruiser*** for the measurement of individual component stiffnesses.

Other areas of interest and possible research topics include the determination of the ***Bruiser's*** structural response due to excitation at its primary rotor induced vibration frequency (4/rev). This could be accomplished by experimental methods, by using the GIFTS finite element model, or by using the transfer functions determined during the experimental shake tests. This would allow one to predict the ***Bruiser's*** inflight vibration characteristics and ultimately allow for applying HHC excitation loads to the model in an attempt to analytically predict the airframes HHC response.

Finally, dynamic (rotors turning) shake tests should be conducted to verify the results of the static tests reported in this thesis. An ultimate goal would be to install a miniature shaker in the airframe to obtain inflight vibration spectrum and modal analysis data. To the author's knowledge, this has never been done and would serve to validate or invalidate the helicopter industry's reliance on static (rotors stopped) shake tests alone.

APPENDIX A: GIFTS MODEL PROGRAMS

A. BEAMCS "SRC" FILE

```
ETH,1
1/0.28
2/0.25
3/0.15
4/0.1
5/0.5
6/0.065
7/0.075

CIRCH
8/0.5,0.45
9/0.175,0.170
10/0.25,0.20

CIRCS
11/0.118
12/0.125
13/0.19
14/4.0

RECTS
15/0.275,1.0
16/0.05,3.0
17/1.4,0.25
18/2.5,0.25
19/0.25,1.0
20/0.3125,1.375
21/1.7,0.25
22/0.6,0.6
23/0.8,0.8
24/0.35,1.0
25/0.5,3.0

END
```

B. BULKM "SRC" FILE

```
ELMAT,4
1/10000,8.0E6,0.4,1.814E-4
2/68000,10.4E6,0.368,2.620E-4
3/40000,10.0E6,0.316,2.538E-4
4/10000,6E6,0.4,3.367E-4
5/40000,29.5E6,0.29,7.339E-4
6/70000,28.0E6,0.28,7.252E-4
7/10000,1.5E6,0.3,6.251E-5
8/40000,5.0E6,0.316,3.0E-6
9/40000,8E6,0.316,3.0E-6

KPOINT
$  STARBOARD SIDE AND CENTERLINE OF AIRCRAFT
1/0.00,0.00,0.00
2/-4.39,7.25,1.82
3/-10.00,7.11,1.82
4/-15.88,6.97,1.82
5/-16.88,6.95,1.82
6/-17.38,6.94,1.82
7/-24.13,6.77,1.82
8/-26.00,6.73,1.82
9/-27.13,6.70,1.82
10/-13.38,0.00,11.50
11/-17.38,0.00,11.50
12/-26.00,0.00,11.50
13/-28.50,0.00,11.50
15/-16.88,19.50,0.50
16/-16.88,17.25,0.50
17/-23.32,20.50,0.50
18/-23.32,20.50,0.00
19/-31.06,19.75,0.50
20/-31.06,18.25,0.50
21/-27.06,17.52,0.50
22/-23.32,18.50,0.50
23/-23.32,18.50,0.00
24/-20.44,19.63,0.00
25/-20.44,19.63,0.50
26/-21.50,20.00,0.50
27/-21.50,18.50,0.50
28/-17.38,6.94,4.82
29/-26.00,6.73,4.82
30/-23.32,21.50,0.00
31/-23.32,26.50,0.00
32/-23.32,17.75,0.00
33/-25.00,20.00,0.50
34/-25.00,18.50,0.50
35/-27.06,19.00,0.50
36/-31.06,19.00,0.50
```

```
37/-32.05,19.00,0.00
38/-38.25,19.00,0.00
39/-42.50,19.00,0.00
40/-54.00,19.00,0.00
41/-55.00,19.00,0.00
42/-57.00,19.00,0.00
43/-57.00,19.00,4.00
44/-57.00,16.00,5.80
45/-68.50,19.00,0.50
46/-68.50,19.80,0.50
47/-69.38,19.80,0.50
48/-68.50,18.20,0.50
49/-69.38,18.20,0.50
50/-69.38,19.00,0.50
51/-71.63,18.40,0.50
52/-73.63,20.30,0.50
53/-72.75,22.15,0.50
54/-75.90,23.60,0.50
55/-76.20,24.55,0.50
56/-77.00,24.70,0.50
57/-76.90,23.70,0.50
$    TAIL ROTOR SHAFT
58/-76.60,24.20,0.50
59/-76.60,24.20,2.50
$    ENGINE MOUNT PAD
60/-18.63,6.91,1.82
61/-22.13,6.82,1.82
$    TAIL ROTOR HUB
62/-76.6,24.20,2.50
$    TAIL BOOM ATTACH POINTS
63/-68.50,19.00,0.00
64/-69.38,19.00,0.00
65/-27.06,19.00,0.00
66/-31.06,19.00,0.00
$    BATT MOUNT PAD
67/-5.13,7.23,1.5
68/-5.13,7.23,-1.5
69/-11.13,7.08,-1.5
70/-11.13,7.08,1.5
71/-11.68,7.07,1.5
72/-11.68,7.07,-1.5
73/-15.68,6.98,-1.5
74/-15.68,6.98,1.5
$    ROTOR HEAD
75/-24.92,26.50,0.00
76/-27.32,26.50,0.00
77/-65.70,26.50,0.00
78/-23.32,26.50,1.60
79/-23.32,26.50,4.00
80/-23.32,26.50,42.38
81/-21.72,26.50,0.00
```

```
82/-19.32,26.50,0.00
83/+19.26,26.50,0.00
84/-23.32,26.50,-1.60
85/-23.32,26.50,-4.00
86/-23.32,26.50,-42.38
87/-57.00,19.00,0.50
$    PORT SIDE OF AIRCRAFT
102/-4.39,7.25,-1.82
103/-10.00,7.11,-1.82
104/-15.88,6.97,-1.82
105/-16.88,6.95,-1.82
106/-17.38,6.94,-1.82
107/-24.13,6.77,-1.82
108/-26.00,6.73,-1.82
109/-27.13,6.70,-1.82
110/-13.38,0.00,-11.50
111/-17.38,0.00,-11.50
112/-26.00,0.00,-11.50
113/-28.50,0.00,-11.50
115/-16.88,19.50,-0.50
116/-16.88,17.25,-0.50
117/-23.32,20.50,-0.50
119/-31.06,19.75,-0.50
120/-31.06,18.25,-0.50
121/-27.06,17.52,-0.50
122/-23.32,18.50,-0.50
125/-20.44,19.63,-0.50
126/-21.50,20.00,-0.50
127/-21.50,18.50,-0.50
128/-17.38,6.94,-4.32
129/-26.00,6.73,-4.32
133/-25.00,20.00,-0.50
134/-25.00,18.50,-0.50
135/-27.06,19.00,-0.50
136/-31.06,19.00,-0.50
143/-57.00,19.00,-4.00
144/-57.00,16.00,-5.80
145/-68.50,19.00,-0.50
146/-68.50,19.80,-0.50
147/-69.38,19.80,-0.50
148/-68.50,18.20,-0.50
149/-69.38,18.20,-0.50
150/-69.38,19.00,-0.50
151/-71.63,18.40,-0.50
152/-73.63,20.30,-0.50
153/-72.75,22.15,-0.50
154/-75.90,23.60,-0.50
155/-76.20,24.55,-0.50
156/-77.00,24.70,-0.50
157/-76.90,23.70,-0.50
158/-76.60,24.20,-0.50
```

```
160/-18.63,6.91,-1.82
161/-22.13,6.82,-1.82
187/-57.00,19.00,-0.50
200/0.00,19.63,0.00
201/0.00,20.00,0.00
202/0.00,18.50,0.00
203/0.00,20.50,0.00
204/0.00,19.00,0.00
206/0.00,16.00,5.80
207/0.00,16.00,-5.80
208/0.00,26.50,1.00
209/-57.00,0.00,0.00

SLINE
$    NOSE DECK
L2102/2,102,5
L23/2,3,5
L102103/102,103,5
L34/3,4,5
L103104/103,104,5
L45/4,5,5
L104105/104,105,5
L267/2,67,5
L68102/68,102,5
L6768/67,68,5
L6869/68,69,5
L69103/69,103,5
L6970/69,70,5
L370/3,70,5
L6770/67,70,5
L7172/71,72,5
L7273/72,73,5
L73104/73,104,5
L73105/73,105,5
L7374/73,74,5
L574/5,74,5
L474/4,74,5
L7174/71,74,5
L5105/5,105,5
L7071,/70,71,5
L6972/69,72,5
L471/4,71,5
L72104/72,104,5
$    ENGINE DECK
L56/5,6,5
L105106/105.106,5
L5105/5,105,5
L7107/7,107,5
L78/7,8,5
L8108/8,108,5
L107108/107,108,5
```

```
L89/8,9,5
L108109/108,109,5
L9109/9,109,5
L660/6,60,5
L6061/60,61,5
L761/7,61,5
L106160/106,160,5
L60160/60,160,5
L61161/61,161,5
L160161/160,161,5
L107161/107,161,5
L6106/6,106,5
$    RIGHT MAIN FRAME
L920/9,20,5
L2036/20,36,5
L1936/19,36,5
L1719/17,19,5
L1627/16,27,5
L1516/15,16,5
L1622/16,22,5
L2122/21,22,5
L721/7,21,5
L2021/20,21,5
L3536/35,36,5
L2134/21,34,5
L1935/19,35,5
L3334/33,34,5
L1733/17,33,5
L2135/21,35,5
L3335/33,35,5
L2234/22,34,5
L1722/17,22,5
L2627/26,27,5
L2526/25,26,5
L2227/22,27,5
L1726/17,26,5
L2527/25,27,5
L1525/15,25,5
L1526/15,26,5
L1625/16,25,5
L1933/19,33,5
L820/8,20,5
L821/8,21,5
$    LEFT MAIN FRAME
L109120/109,120,5
L120136/120,136,5
L119136/119,136,5
L117119/117,119,5
L116127/116,127,5
L115116/115,116,5
L116122/116,122,5
```

```
L121122/121,122,5
L107121/107,121,5
L120121/120,121,5
L135136/135,136,5
L121134/121,134,5
L119135/119,135,5
L133134/133,134,5
L117133/117,133,5
L121135/121,135,5
L133135/133,135,5
L122134/122,134,5
L117122/117,122,5
L126127/126,127,5
L125126/125,126,5
L122127/122,127,5
L117126/117,126,5
L125127/125,127,5
L115125/115,125,5
L115126/115,126,5
L116125/116,125,5
L119133/119,133,5
L108120/108,120,5
L108121/108,121,5
$    FORWARD FRAME
L516/5,16,5
L16116/16,116,5
L105116/105,116,5
L1516/15,16,5
L15115/15,115,5
L115116/115,116,5
$    RIGHT SIDE NOSE SKIN
L215/2,15,5
L315/3,15,5
L415/4,15,5
$    LEFT SIDE NOSE SKIN
L102115/102,115,5
L103115/103,115,5
L104115/104,115,5
$    RIGHT TAIL SKIN
L937/9,37,5
L3739/37,39,5
L3940/39,40,5
L940/9,40,5
L939/9,39,5
$    LEFT TAIL SKIN
L37109/109,37,5
L40109/109,40,5
L39109/109,39,5
$    RIGHT TAIL ROTOR FRAME
L4546/45,46,5
L1548/45,48,5
```

```
L4647/46,47,5
L4750/47,50,5
L4550/45,50,5
L4950/49,50,5
L4849/48,49,5
L4951/49,51,5
L5152/51,52,5
L5253/52,53,5
L5153/51,53,5
L4753/47,53,5
L5354/53,54,5
L5355/53,55,5
L5254/52,54,5
L5457/54,57,5
L5455/54,55,5
L5556/55,56,5
L5657/56,57,5
L5257/52,57,5
L5458/54,58,5
L5558/55,58,5
L5658/56,58,5
L5758/57,58,5
L5051/50,51,5
$     LEFT TAIL ROTOR FRAME
L145146/145,146,5
L145148/145,148,5
L146147/146,147,5
L147150/147,150,5
L145150/145,150,5
L149150/149,150,5
L148149/148,149,5
L149151/149,151,5
L151152/151,152,5
L152153/152,153,5
L151153/151,153,5
L147153/147,153,5
L153154/153,154,5
L153155/153,155,5
L152154/152,154,5
L154157/154,157,5
L154155/154,155,5
L155156/155,156,5
L156157/156,157,5
L152157/152,157,5
L154158/154,158,5
L155158/155,158,5
L156158/156,158,5
L157158/157,158,5
L150151/150,151,5
```

```
$     NOSE DECK
GETY/QB4/1,1

GRID4
NDECK1/L267,L6768,L68102,L2102
NDECK2/L6869,L69103,L102103,L68102
NDECK3/L6770,L6970,L6869,L6768
NDECK4/L23,L370,L6770,L267
NDECK5/L370,L34,L471,L7071
NDECK6/L7071,L7172,L6972,L6970
NDECK7/L6972,L72104,L103104,L69103
NDECK8/L7174,L7374,L7273,L7172
NDECK9/L574,L5105,L73105,L7374

GETY/TB3/1,1

GRID3
NDECK10/L471,L474,L7174
NDECK11/L45,L574,L474
NDECK12/L7273,L73104,L72104
NDECK13/L73105,L104105,L73104

$     ENGINE DECK
GETY/QB4/3,2

GRID4
EDECK1/L56,L6106,L105106,L5105
EDECK2/L660,L60160,L106160,L6106
EDECK3/L6061,L61161,L160161,L60160
EDECK4/L761,L7107,L107161,L61161
EDECK5/L78,L8108,L107108,L7107
EDECK6/L89,L9109,L108109,L8108

$     MAIN FRAMES
GETY/QB4/2,3

GRID4
$     RIGHT FRAME
RFRAME2/L2021,L2036,L3536,L2135
RFRAME3/L2134,L2135,L3335,L3334
RFRAME4/L2234,L3334,L1733,L1722
RFRAME5/L2227,L1722,L1726,L2627
$     LEFT FRAME
LFRAME2/L120121,L120136,L135136,L121135
LFRAME3/L121134,L121135,L133135,L133134
LFRAME4/L122134,L133134,L117133,L117122
LFRAME5/L122127,L117122,L117126,L126127
```

```
GETY/TB3/2,3

GRID3
$     RIGHT FRAME
RFRAME6/L1935,L1933,L3335
RFRAME7/L3536,L1936,L1935
RFRAME8/L2122,L2134,L2234
RFRAME9/L2627,L2526,L2527
RFRAME10/L1625,L1525,L1516
RFRAME11/L2526,L1526,L1525
RFRAME12/L1622,L2227,L1627
RFRAME13/L1627,L2527,L1625
RFRAME14/L89,L920,L820
RFRAME15/L820,L2021,L821
RFRAME16/L78,L821,L721
$     LEFT FRAME
LFRAME6/L119135,L119133,L133135
LFRAME7/L135136,L119136,L119135
LFRAME8/L121122,L121134,L122134
LFRAME9/L126127,L125126,L125127
LFRAME10/L116125,L115125,L115116
LFRAME11/L125126,L115126,L115125
LFRAME12/L116122,L122127,L116127
LFRAME13/L116127,L125127,L116125
LFRAME14/L108109,L109120,L108120
LFRAME15/L108120,L120121,L108121
LFRAME16/L107108,L108121,L107121

$     FRONT FRAME
GETY/QB4/2,4;  LOWER FRONT FRAME

GRID4
FFRAME1/L5105,L516,L16116,L105116

GETY/QB4/2,5
$     UPPER FRONT FRAME

GRID4
FFRAME2/L16116,L1516,L15115,L115116

$     FORWARD NOSE PANEL
GETY/QB4/4,6

GRID4
NPANEL/L2102,L215,L15115,L102115

$     SIDE PANEL SKIN
GETY/TB3/4,6

GRID3
$     RIGHT NOSE SIDE PANEL
```

```
RNPANEL1/L23,L315,L215
RNPANEL2/L34,L415,L315
$     LEFT NOSE SIDE PANEL
LNPANEL1/L102103,L103115,L102115
LNPANEL2/L103104,L104115,L103115
$     RIGHT TAIL BOOM PANEL
RTPANEL1/L939,L3739,L937
RTPANEL2/L940,L3940,L939
$     LEFT TAIL BOOM PANEL
LTPANEL1/L39109,L3739,L37109
LTPANEL2/L40109,L3940,L39109

$     TAIL ROTOR FRAME
GETY/QB4/2,7

GRID4
$     RIGHT TAIL ROTOR FRAME
RTRFR1/L4550,L4750,L4647,L4546
RTRFR2/L4849,L4950,L4550,L4548
RTRFR3/L5051,L5153,L4753,L4750
$     LEFT TAIL ROTOR FRAME
LTRFR1/L145150,L147150,L146147,L145146
LTRFR2/L148149,L149150,L145150,L145148
LTRFR3/L150151,L151153,L147153,L147150

GETY/TB3/2,7

GRID3
$     RIGHT TAIL ROTOR FRAME
RTRFR4/L5458,L5558,L5455
RTRFR5/L5658,L5556,L5558
RTRFR6/L5758,L5657,L5658
RTPFR7/L5457,L5758,L5458
RTRFR8/L5354,L5455,L5355
RTRFR9/L5253,L5254,L5354
RTRFR10/L5257,L5457,L5254
RTRFR11/L5152,L5253,L5153
RTRFR12/L4951,L5051,L4950
$     LEFT TAIL ROTOR FRAME
LTRFR4/L154158,L155158,L154155
LTRFR5/L156158,L155156,L155158
LTRFR6/L157158,L156157,L156158
LTRFR7/L154157,L157158,L154158
LTRFR8/L153154,L154155,L153155
LTRFR9/L152153,L152154,L153154
LTRFR10/L152157,L154157,L152154
LTRFR11/L151152,L152153,L151153
LTRFR12/L149151,L150151,L149150
```

```
LETY/BEAM2/9,10/SLINE,10
$     RIGHT SKID TUBE
L1011/10,11,5/5
L1112/11,12,5/5
L1213/12,13,5/5
$     LEFT SKID TUBE
L110111/110,111,5/105
L111112/111,112,5/105
L112113/112,113,5/105

$     SKID BEAMS
LETY/BEAM2/9,15/SLINE,10
L628/6,28,5/5
L1128/11,28,5/10
L106128/106,128,5/105
L111128/111,128,5/110
L829/8,29,5/7
L1229/12,29,5/11
L108129/108,129,5/107
L112129/112,129,5/111
L6106/6,106,5/5
L8108/8,108,5/107

$     ENG DRIVE SHAFT BEARING
LETY/BEAM2/3,19/SLINE,10
L2425/24,25,5/200
L24125/24,125,5/200

$      MAIN FRAME CROSS BRACKETS
LETY/BEAM2/3,19/SLINE,10
L26126/26,126,5/201
L27127/27,127,5/202
L33133/33,133,5/201
L34134/34,134,5/202

$    MR BEARING BRACKETS
LETY/BEAM2/2,20/SLINE,10
L1718/17,18,5/203
L18117/18,117,5/203
L2223/22,23,5/202
L23122/23,122,5/202

$    FWD TAIL BOOM BRACKET
LETY/BEAM2/3,18/SLINE,10
L3565/35,135,5/204
L65135/65,135,5/204

$     AFT TAIL BOOM BRACKET
LETY/BEAM2/3,17/SLINE,10
L3666/36,66,5/204
L66136/66,136,5/204
```

```
$    TAIL BOOM
LETY/BEAM2/8,8/SLINE,10
L6566/65,66,5/1
L3766/37,66,5/1
L3738/37,38,5/1
L3839/38,39,5/1
L3940B/39,40,5/1
L4041/40,41,5/1
L4142/41,42,5/1
L4263/42,63,5/1
L6364/63,64,5/1

$    TAIL BOOM TIE RODS
LETY/BEAM2/8,9/SLINE,10
L941/9,41,5/1
L41109/41,109,5/1

$    HORIZONTAL STAB
$LETY/BEAM2/3,16/SLINE,10
L4287/42,87,5/41
L4387/43,87,5/41
L4344/43,44,5/206
L42187/42,187,5/41
L143187/143,187,5/41
L143144/143,144,5/207

$   HORIZONTAL STAB MOUNT
LETY/BEAM2/2,25/SLINE,10
L4287/42,87,5/40
L42187/42,187,5/40

$    TAIL FRAME BRACKETS
LETY/BEAM2/2,21/SLINE,10
L4563/45,63,5/204
L63145/63,145,5/204
L5064/50,64,5/204
L64150/64,150,5/204

$    CIRC TAIL FRAME SUPPORTS
LETY/BEAM2/2,12/SLINE,10
L51151/51,151,5/1
L52152/52,152,5/1
L53153/53,153,5/1
L54154/54,154,5/1

$    TAIL ROTOR DRIVE SHAFT
LETY/BEAM2/6,11/SLINE,10
L58158/58,158,5/1
L5862/58,62,5/1
```

```
$    MAIN ROTOR DRIVE SHAFT
LETY/BEAM2/6,13/SLINE,10
L2332/23,32,5/1
L1823/18,23,5/1
L1830/18,30,5/1
L3031/30,31,5/1

$   MR HUB ARMS
LETY/BEAM2/2,22/SLINE,10
L3175/31,75,5/18
L3178/31,78,5/18
L3181/31,81,5/18
L3184/31,84,5/18

$   MR BLADE GRIPS
LETY/BEAM2/2,23/SLINE,10
L7576/75,76,5/18
L7879/78,79,5/18
L8182/81,82,5/18
L8485/84,85,5/18

$   MR BLADES
LETY/BEAM2/7,24/SLINE,10
L7677/76,77,5/208
L7980/79,80,5/208
L8283/82,83,5/208
L8586/85,86,5/208

$    NOTES
$WT OF ENGINE = 4.5 LBS
$WT OF BALLAST = 2438 GRAMS
$WT OF BATTERY = 643 GRAMS
$WT OF FUEL TANK = 852 GRAMS
$WT OF ENGINE BLOCK = 0.6 LBS
$WT OF ACCELEROMETER = 6.4 GRAMS
$WT OF MR BLADE = 237 GRAMS
$WT OF TAIL ROTOR = 130 GRAMS
$WT OF TAIL ROTOR FRAME = 194 GRAMS
$WT OF TAIL BOOM = 3.0 LBS
$WT OF MUFFLETS = 0.8 LBS
$WT OF SKIDS = 1.68 LBS
$WT OF NOSE = 6.96 LBS
$WT OF ENGINE AND MR SYS = 18.05 LBS

END
```

C. LOADBC "SRC" FILE

```
MASS

MASSP
23/.01814
62/0.0007423

MASSG
$    BATTERY
NDECK3/1.91E-4,1.91E-4,1.91E-4,1.91E-4
$    BALLAST
NDECK8/0.92E-3,0.92E-3,0.92E-3,0.92E-3
$    ENGINE
EDECK3/1.2E-3,1.2E-3,1.2E-3,1.2E-3
$    FUEL TANK
EDECK6/2.24E-3,2.24E-3,2.24E-3,2.24E-3

END
```

D. COMM "BATCH" FILE

```
$@server$dkb200:[000000.app.gifts]flg92.com
$ set def [.bruiser]
$ DEL MOD1.*;*
$ BEAMCS
MOD1
OLB/BCS
QUIT
$ BULKM
MOD1
OLB/BBM
QUIT
$ BULKF
MOD1
$ LOADBC
MOD1
OLB/LBC
QUIT
$ OPTIM
MOD1
2/5/16/23/37/42/58/62//
$ ADSTIF
MOD1
Y
$ ELSTFF
MOD1
$ SUBS
MOD1
10,1
10
6
150
```

APPENDIX B. FREQUENCY RESPONSE FUNCTIONS: VERTICAL

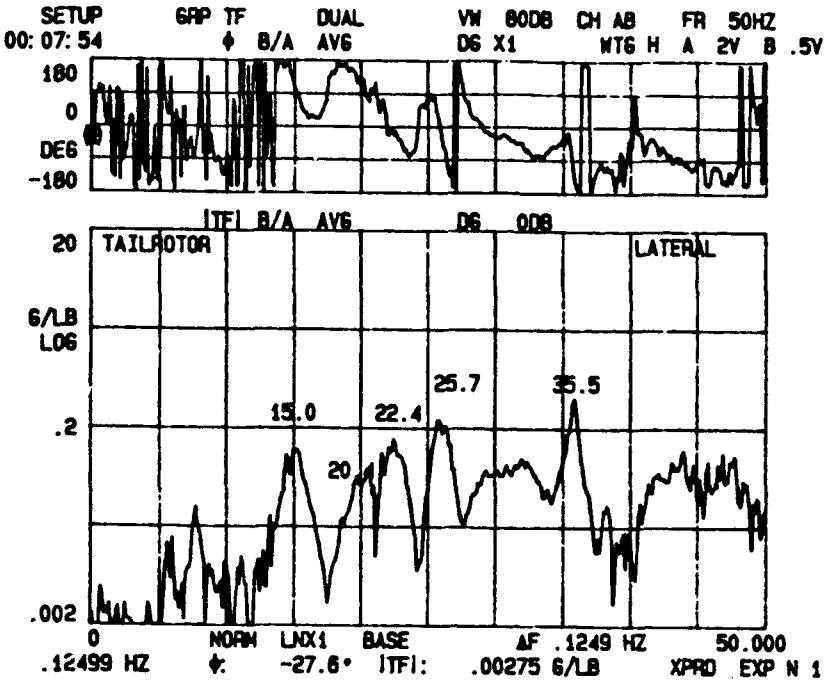

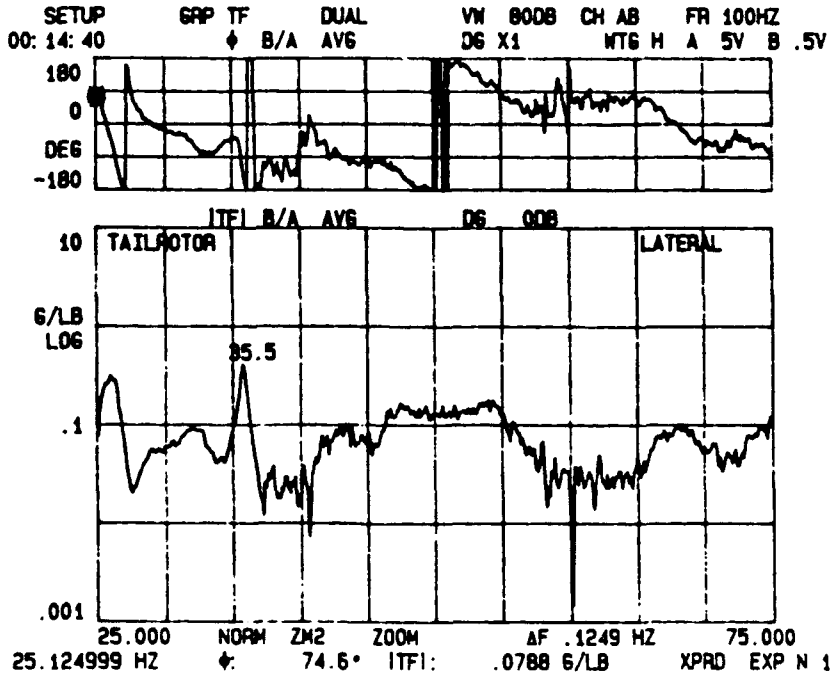

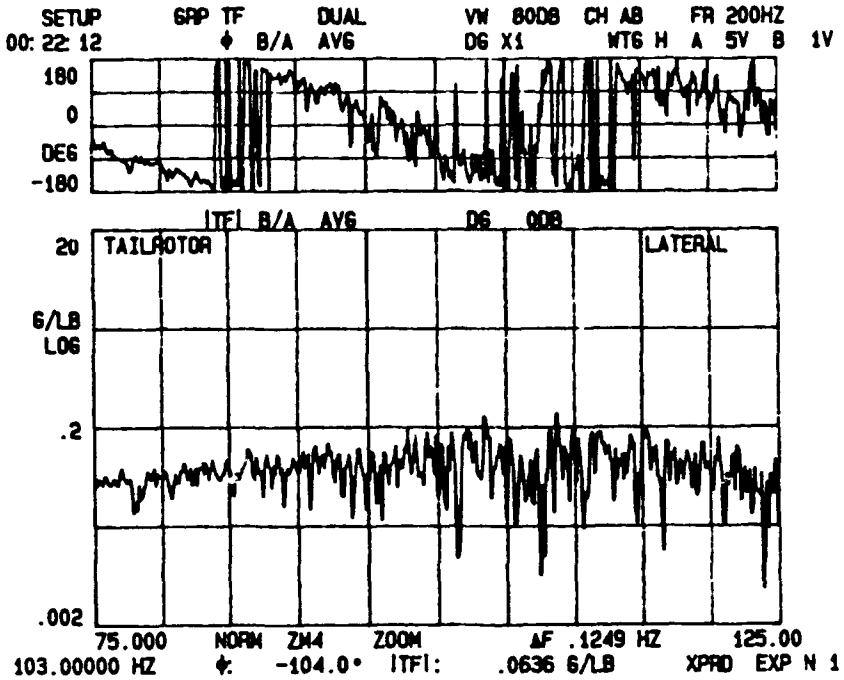
SETUP
00: 22: 12
GRP TF
DUAL
VW 800B CH AB
FR 200HZ
B/A AVG
DG X1
WTG H A 5V B 1V
180
0
DEG
-180
|TF| B/A AVG
DG 00B
20
TAILROTOR
LATERAL
G/LB
LOG
.2
.002
75.000
NORM ZM4 ZOOM
ΔF .1249 HZ
125.00
103.00000 HZ
-104.0°
|TF|: .0636 G/LB
XPRD EXP N 1

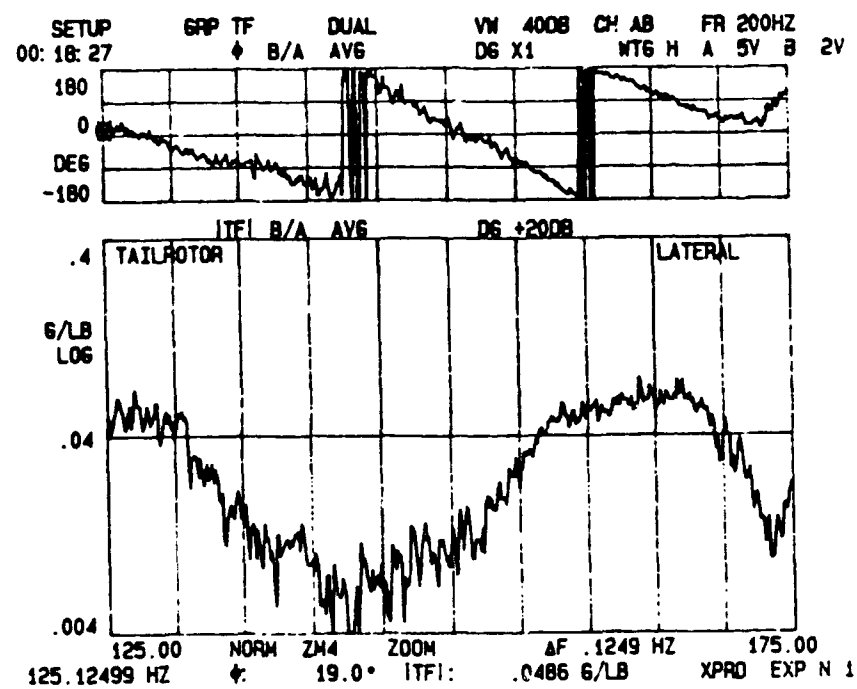
SETUP
00: 18: 27
GRP TF
DUAL
VW 400B CH AB
FR 200HZ
B/A AVG
DG X1
WTG H A 5V B 2V
180
0
DEG
-180
|TF| B/A AVG
DG +20DB
.4
TAILROTOR
LATERAL
G/LB
LOG
.04
.004
125.00
NORM ZM4 ZOOM
ΔF .1249 HZ
175.00
125.12499 HZ
19.0°
|TF|: .0486 G/LB
XPRD EXP N 1

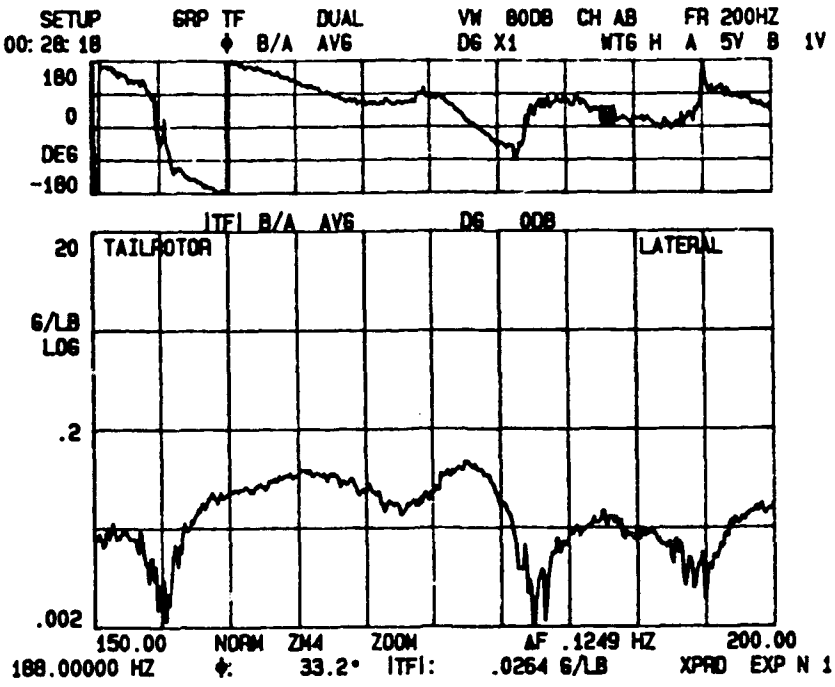
SETUP
GRP TF
DUAL
VW 80DB
CH AB
FR 200HZ
00: 26: 18
Φ B/A AVG
DG X1
WTG H A 5V B 1V
180
0
DEG
-180
|TF| B/A AVG
DG 0DB
20
TAILROTOR
LATERAL
G/LB
LOG
.2
.002
150.00
NORM ZM4
ZOOM
ΔF .1249 HZ
200.00
188.00000 HZ
Φ: 33.2°
|TF|: .0264 G/LB
XPRD EXP N 1

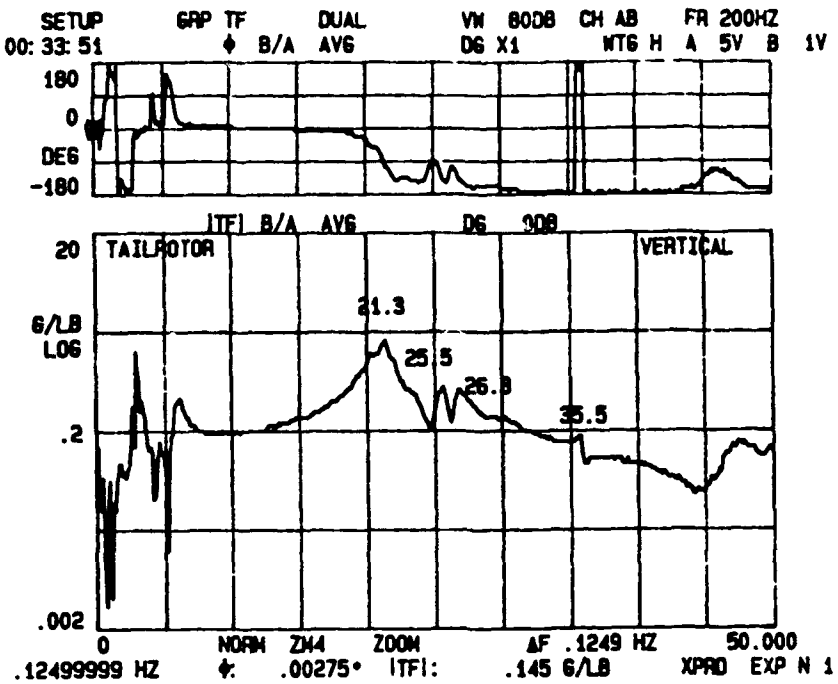
SETUP
00: 33: 51
GRP TF
DUAL
B/A AVG
VW 800B CH AB
DG X1
FR 200HZ
MTG H A 5V B 1V
180
0
DEG
-180
|TF| B/A AVG
DG 00B
20
TAILROTOR
VERTICAL
21.3
25.5
26.3
35.5
G/LB
LOG
.2
.002
0
NORM ZM4 ZOOM
ΔF .1249 HZ
50.000
.12499999 HZ
φ: .00275°
|TF|: .145 G/LB
XPRD EXP N 1

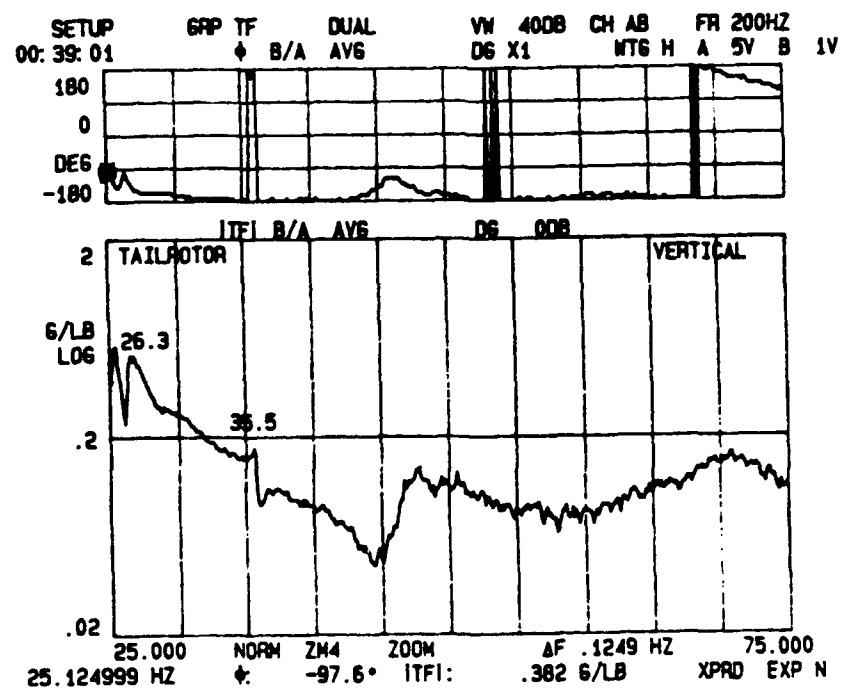
SETUP
00: 39: 01
GRP TF
DUAL
B/A AVG
VW 400B CH AB
DG X1
FR 200HZ
MTG H A 5V B 1V
180
0
DEG
-180
|TF| B/A AVG
DG 00B
2
TAILROTOR
VERTICAL
26.3
35.5
G/LB
LOG
.2
.02
25.000
NORM ZM4 ZOOM
ΔF .1249 HZ
75.000
25.124999 HZ
φ: -97.6°
|TF|: .382 G/LB
XPRD EXP N 1

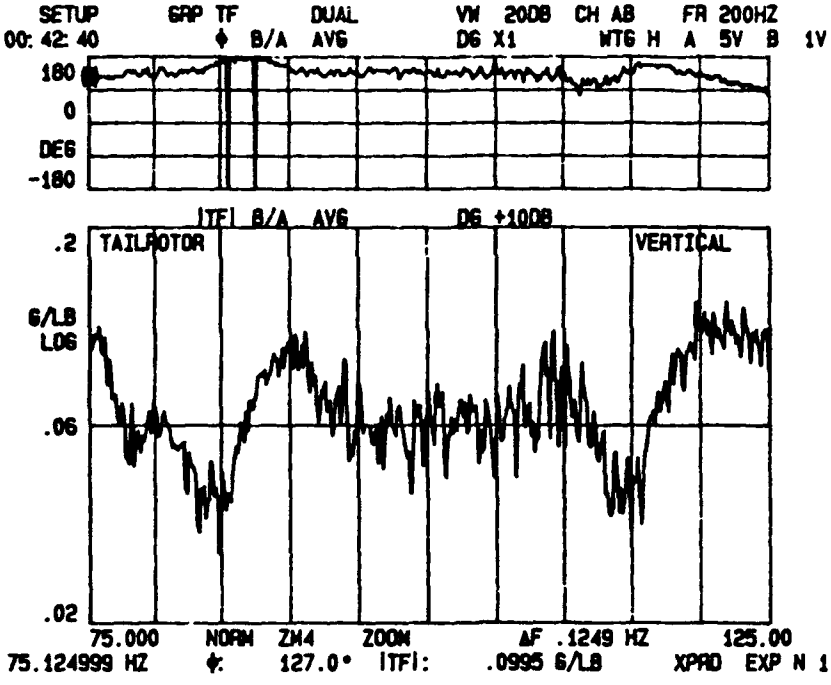
SETUP GRP TF DUAL VW 2008 CH AB FR 200HZ
00: 42: 40 ϕ B/A AVG DG X1 WTG H A 5V B 1V
180
0
DEG
-180
|TF| B/A AVG DG +1008
.2
TAILROTOR
VERTICAL
G/LB
LOG
.06
.02
75.000 NORM ZM4 ZOOM ΔF .1249 HZ 125.00
75.124999 HZ ϕ: 127.0° |TF|: .0995 G/LB XPRD EXP N 1

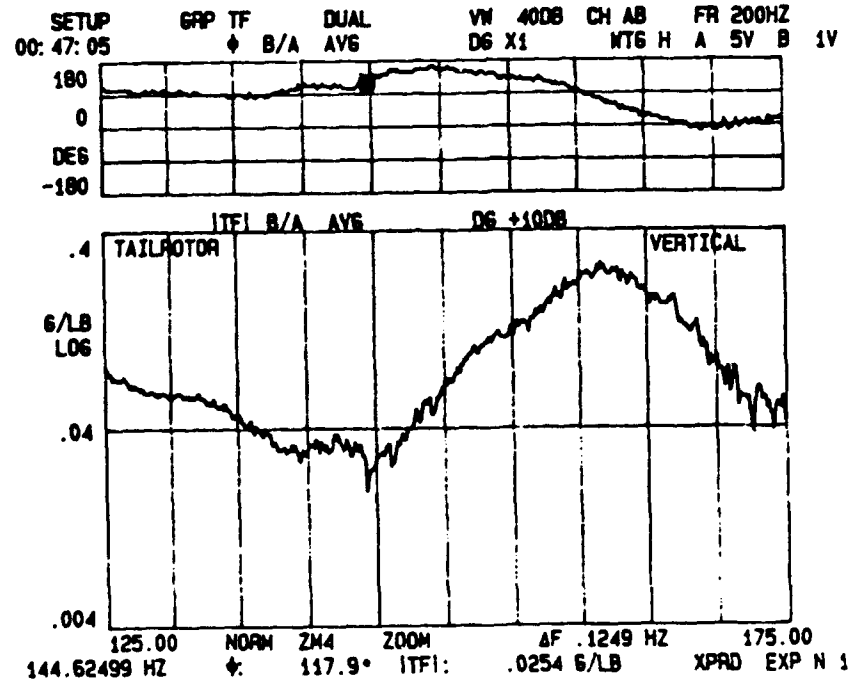
SETUP GRP TF DUAL VW 4008 CH AB FR 200HZ
00: 47: 05 ϕ B/A AVG DG X1 WTG H A 5V B 1V
180
0
DEG
-180
|TF| B/A AVG DG +1008
.4
TAILROTOR
VERTICAL
G/LB
LOG
.04
.004
125.00 NORM ZM4 ZOOM ΔF .1249 HZ 175.00
144.62499 HZ ϕ: 117.9° |TF|: .0254 G/LB XPRD EXP N 1

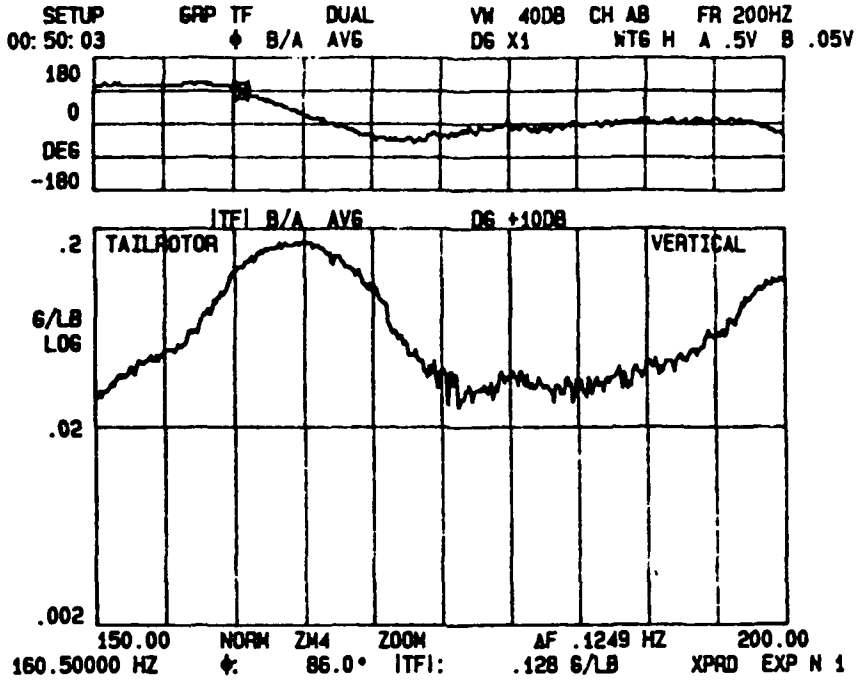
SETUP
00: 50: 03
GRP TF
DUAL
VW 40DB CH AB
FR 200HZ
DG X1
WTG H A .5V B .05V
180
0
DEG
-180
|TF| B/A AVG
DG +10DB
.2
TAILROTOR
VERTICAL
6/LB
LOG
.02
.002
150.00
NORM ZM4 ZOOM
AF .1249 HZ
200.00
160.50000 HZ
86.0°
|TF|:
.128 6/LB
XPRD EXP N 1

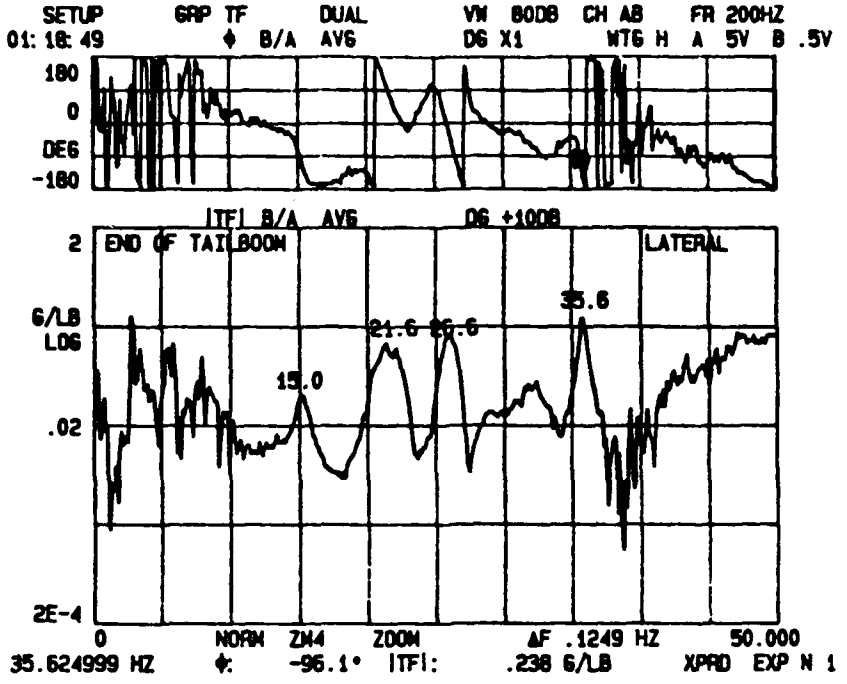
SETUP GRP TF DUAL VW 80DB CH AB FR 200HZ
01: 18: 49 ϕ B/A AVG DG X1 WTG H A 5V B .5V
180
0
DEG
-180
|TF| B/A AVG DG +10DB
2
END OF TAILBOOM
LATERAL
G/LB
LOG
15.0
21.6
26.6
35.6
.02
2E-4
0
NORM ZM4 ZOOM ΔF .1249 HZ 50.000
35.624999 HZ ϕ: -96.1° |TF|: .238 G/LB XPRD EXP N 1

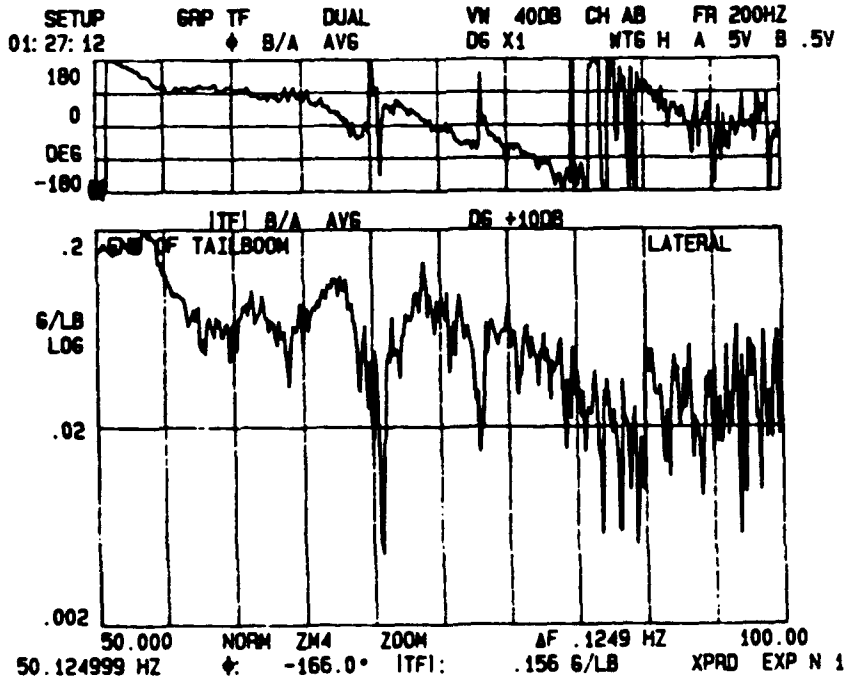
SETUP GRP TF DUAL VW 40DB CH AB FR 200HZ
01: 27: 12 ϕ B/A AVG DG X1 WTG H A 5V B .5V
180
0
DEG
-180
|TF| B/A AVG DG +10DB
.2
END OF TAILBOOM
LATERAL
G/LB
LOG
.02
.002
50.000 NORM ZM4 ZOOM ΔF .1249 HZ 100.00
50.124999 HZ ϕ: -166.0° |TF|: .156 G/LB XPRD EXP N 1

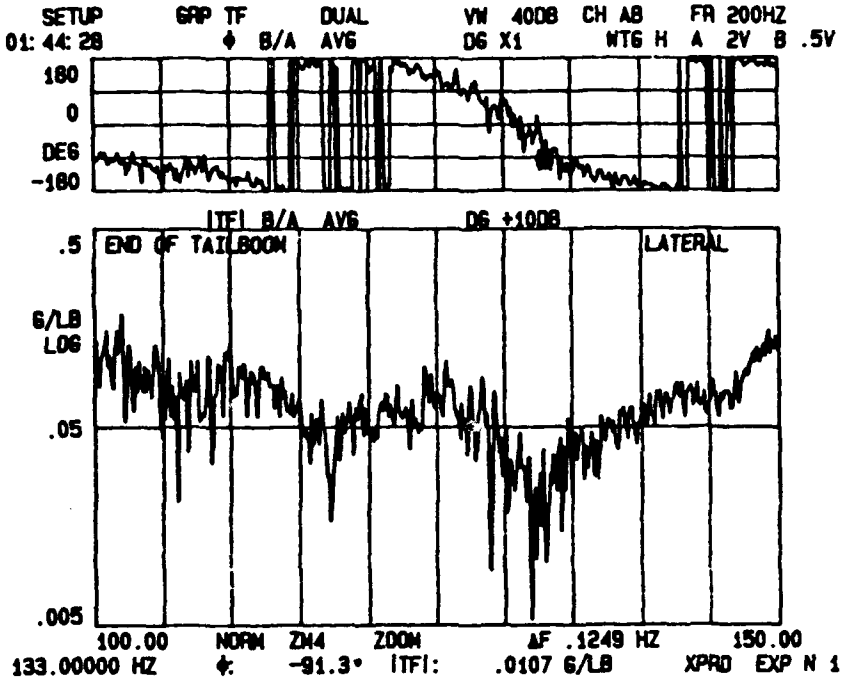
SETUP
01: 44: 28
GRP TF
Φ B/A
DUAL
AVG
VW 400B
DG X1
CH AB
WTG H
FR 200HZ
A 2V B .5V
180
0
DEG
-180
|TF| B/A AVG
DG +100B
.5
END OF TAILBOOM
LATERAL
G/LB
LOG
.05
.005
100.00
NORM ZM4
ZOOM
ΔF .1249 HZ
150.00
133.00000 HZ
Φ: -91.3°
|TF|: .0107 G/LB
XPRD EXP N 1

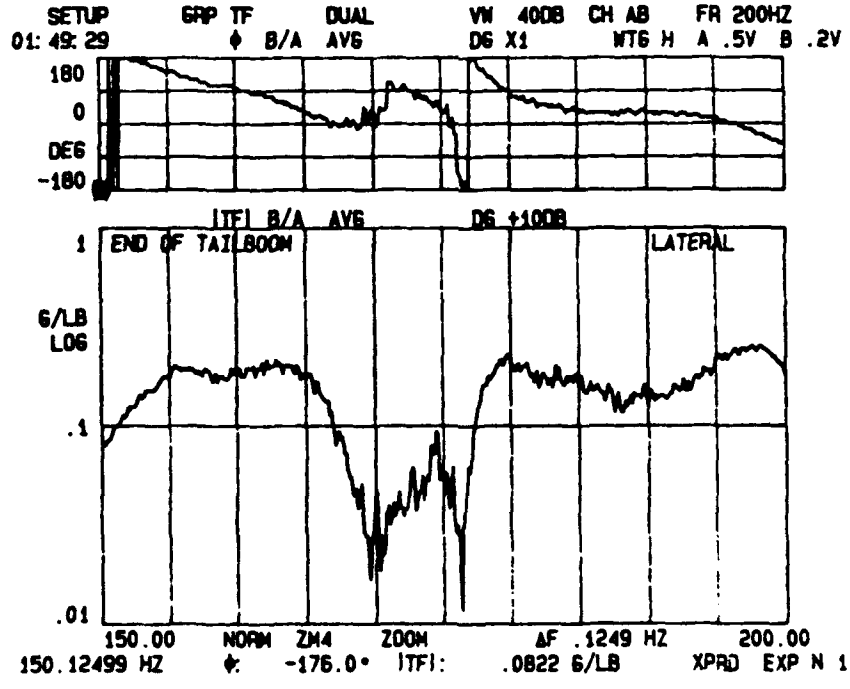
SETUP
01: 49: 29
GRP TF
Φ B/A
DUAL
AVG
VW 400B
DG X1
CH AB
WTG H
FR 200HZ
A .5V B .2V
180
0
DEG
-180
|TF| B/A AVG
DG +100B
1
END OF TAILBOOM
LATERAL
G/LB
LOG
.1
.01
150.00
NORM ZM4
ZOOM
ΔF .1249 HZ
200.00
150.12499 HZ
Φ: -176.0°
|TF|: .0822 G/LB
XPRD EXP N 1

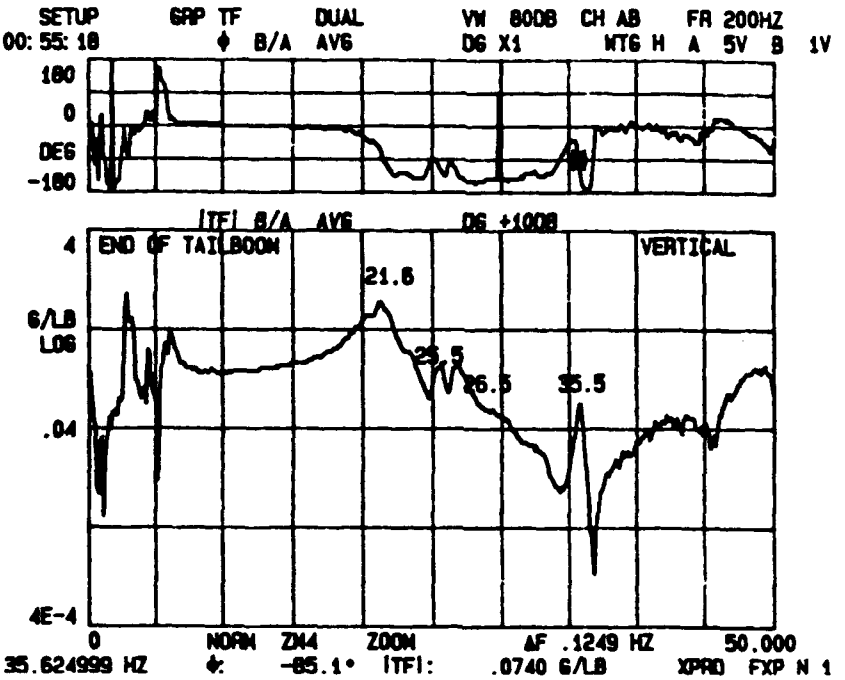
SETUP GRP TF DUAL VW 800B CH AB FR 200HZ
00: 55: 18 ϕ B/A AVG DG X1 MTG H A 5V B 1V
180
0
DEG
-180
|TF| B/A AVG DG +100B
4
END OF TAILBOOM
VERTICAL
21.6
26.5
26.5
35.5
G/LB
LOG
.04
4E-4
0
NORM ZM4 ZOOM ΔF .1249 HZ 50.000
35.624999 HZ ϕ: -85.1° |TF|: .0740 G/LB XPRD FXP N 1

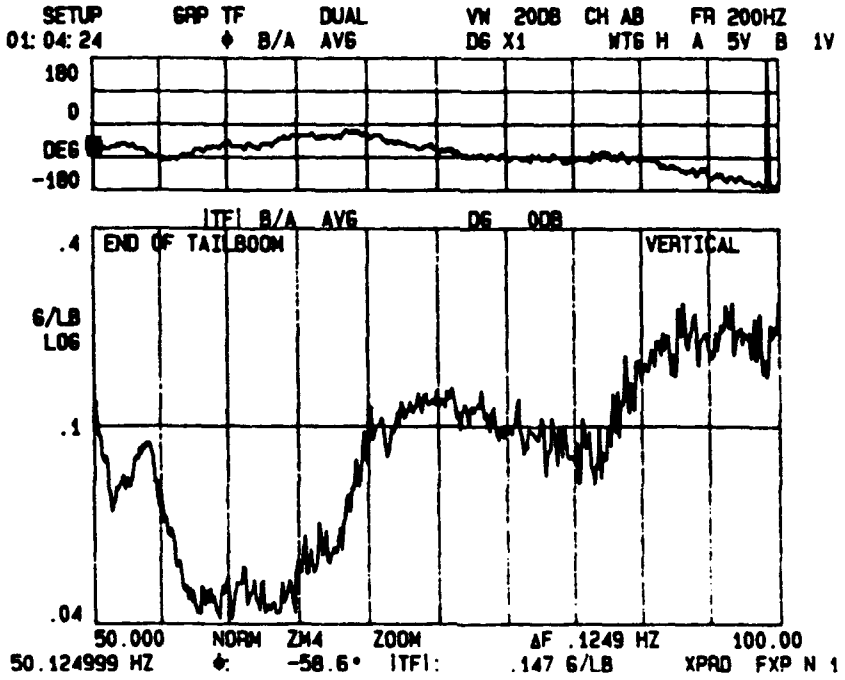
SETUP GRP TF DUAL VW 200B CH AB FR 200HZ
01: 04: 24 ϕ B/A AVG DG X1 MTG H A 5V B 1V
180
0
DEG
-180
|TF| B/A AVG DG 00B
.4
END OF TAILBOOM
VERTICAL
G/LB
LOG
.1
.04
50.000 NORM ZM4 ZOOM ΔF .1249 HZ 100.00
50.124999 HZ ϕ: -58.6° |TF|: .147 G/LB XPRD FXP N 1

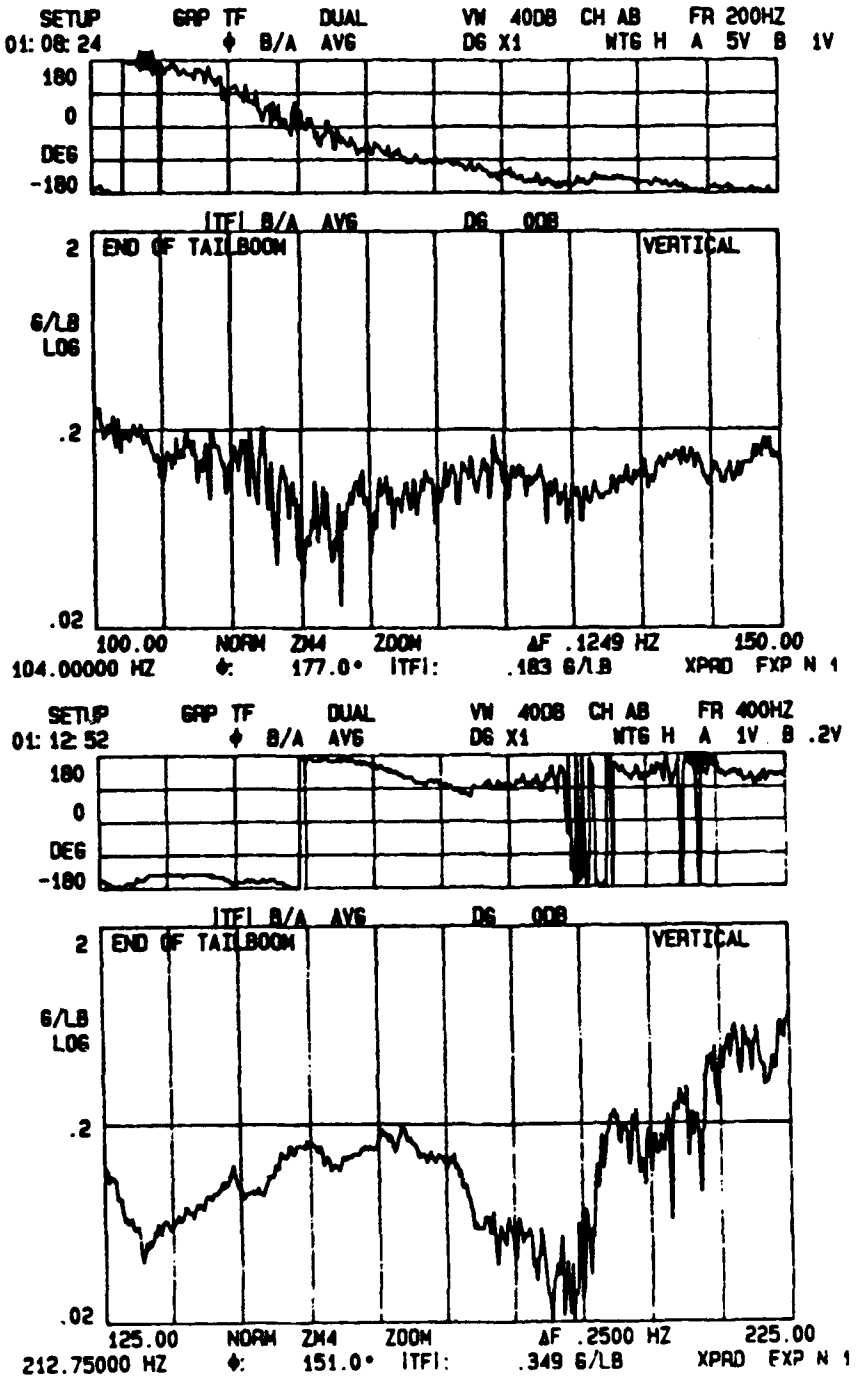
SETUP GRP TF DUAL VW 400B CH AB FR 200HZ
01: 08: 24 ϕ B/A AVG DG X1 WTG H A 5V B 1V
180
0
DEG
-180
|TF| B/A AVG DG 00B
2
END OF TAILBOOM
VERTICAL
G/LB
LOG
.2
.02
100.00 NORM ZM4 ZOOM ΔF .1249 HZ 150.00
104.00000 HZ ϕ: 177.0° |TF|: .183 G/LB XPRD FXP N 1
SETUP GRP TF DUAL VW 400B CH AB FR 400HZ
01: 12: 52 ϕ B/A AVG DG X1 WTG H A 1V B .2V
180
0
DEG
-180
|TF| B/A AVG DG 00B
2
END OF TAILBOOM
VERTICAL
G/LB
LOG
.2
.02
125.00 NORM ZM4 ZOOM ΔF .2500 HZ 225.00
212.75000 HZ ϕ: 151.0° |TF|: .349 G/LB XPRD FXP N 1

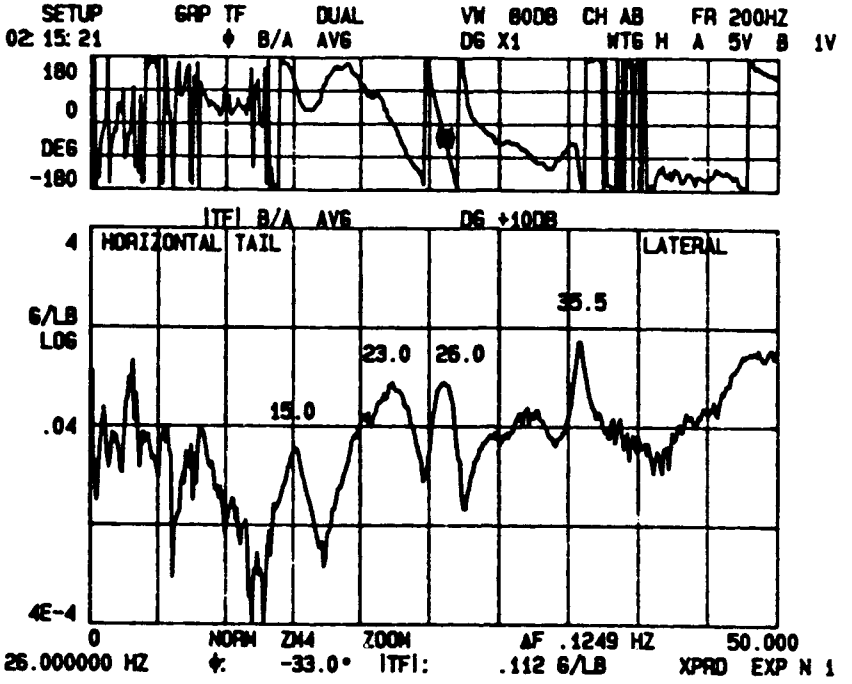
SETUP GRP TF DUAL VW 800B CH AB FR 200HZ
02: 15: 21 ϕ B/A AVG DG X1 WTG H A 5V B 1V
180
0
DEG
-180
|TF| B/A AVG DG +10DB
4
HORIZONTAL TAIL
LATERAL
G/LB
LOG
35.5
23.0
26.0
15.0
.04
4E-4
0 NORM ZM4 ZOOM ΔF .1249 HZ 50.000
26.000000 HZ ϕ: -33.0° |TF|: .112 G/LB XPRD EXP N 1

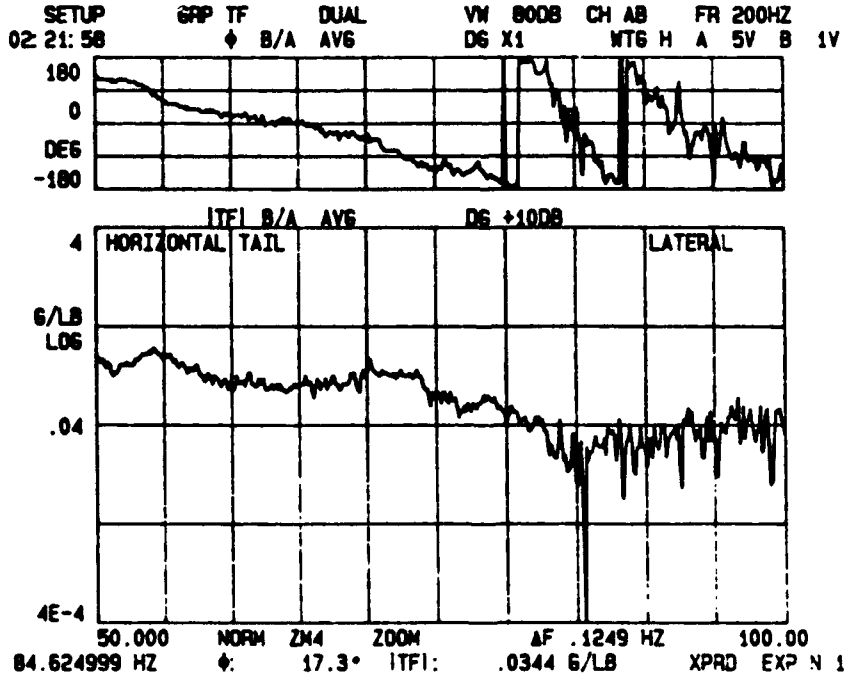
SETUP GRP TF DUAL VW 800B CH AB FR 200HZ
02: 21: 58 ϕ B/A AVG DG X1 WTG H A 5V B 1V
180
0
DEG
-180
|TF| B/A AVG DG +10DB
4
HORIZONTAL TAIL
LATERAL
G/LB
LOG
.04
4E-4
50.000 NORM ZM4 ZOOM ΔF .1249 HZ 100.00
84.624999 HZ ϕ: 17.3° |TF|: .0344 G/LB XPRD EXP N 1

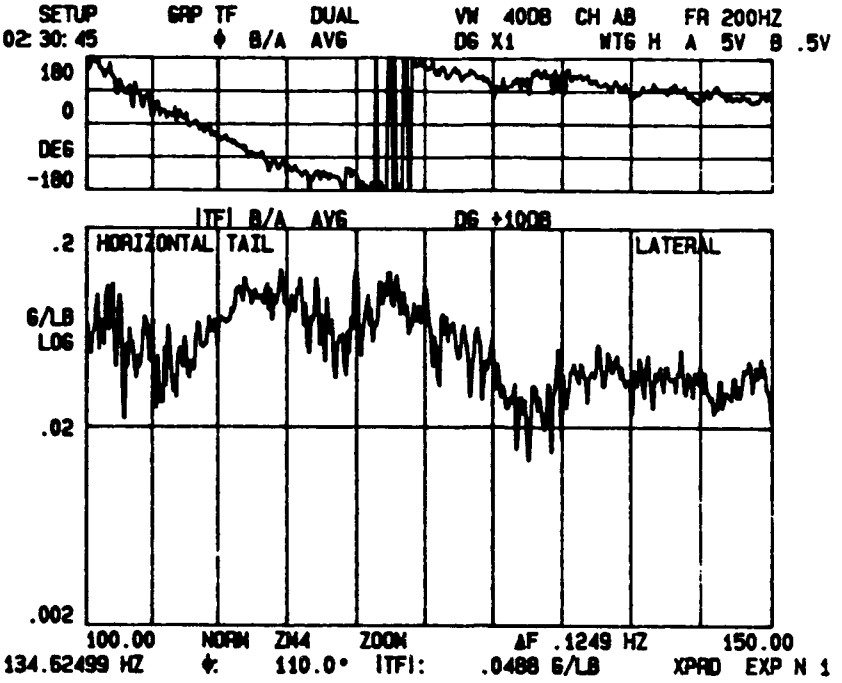
SETUP GRP TF DUAL VW 400B CH AB FR 200HZ
02: 30: 45 ϕ B/A AVG DG X1 WTG H A 5V B .5V
180
0
DEG
-180
|TF| B/A AVG DG +100B
.2
HORIZONTAL TAIL
LATERAL
G/LB
LOG
.02
.002
100.00 NORM ZM4 ZOOM ΔF .1249 HZ 150.00
134.62499 HZ ϕ: 110.0° |TF|: .0488 G/LB XPRD EXP N 1

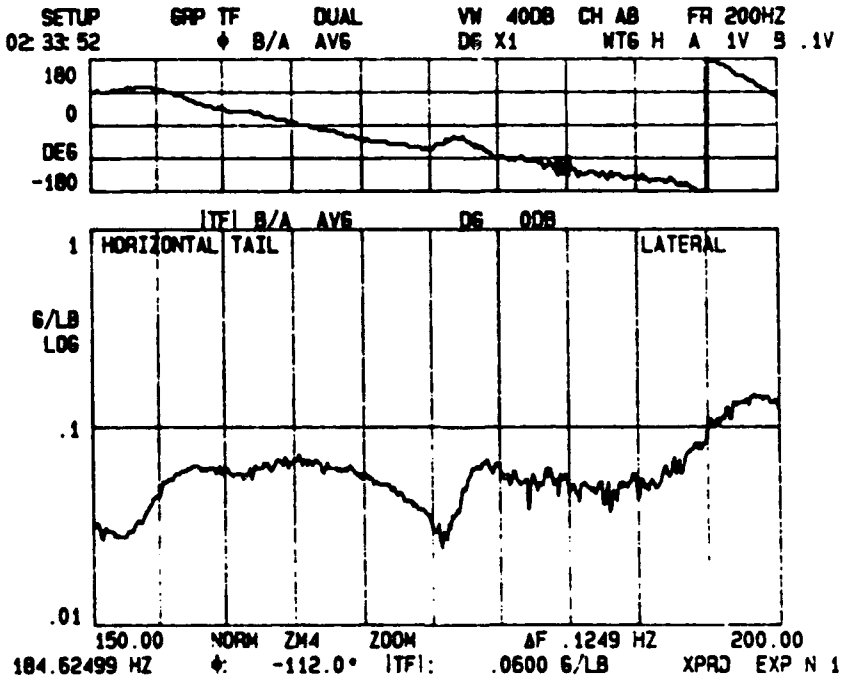
SETUP GRP TF DUAL VW 400B CH AB FR 200HZ
02: 33: 52 ϕ B/A AVG DG X1 WTG H A 1V B .1V
180
0
DEG
-180
|TF| B/A AVG DG 00B
1
HORIZONTAL TAIL
LATERAL
G/LB
LOG
.1
.01
150.00 NORM ZM4 ZOOM ΔF .1249 HZ 200.00
184.62499 HZ ϕ: -112.0° |TF|: .0600 G/LB XPRD EXP N 1

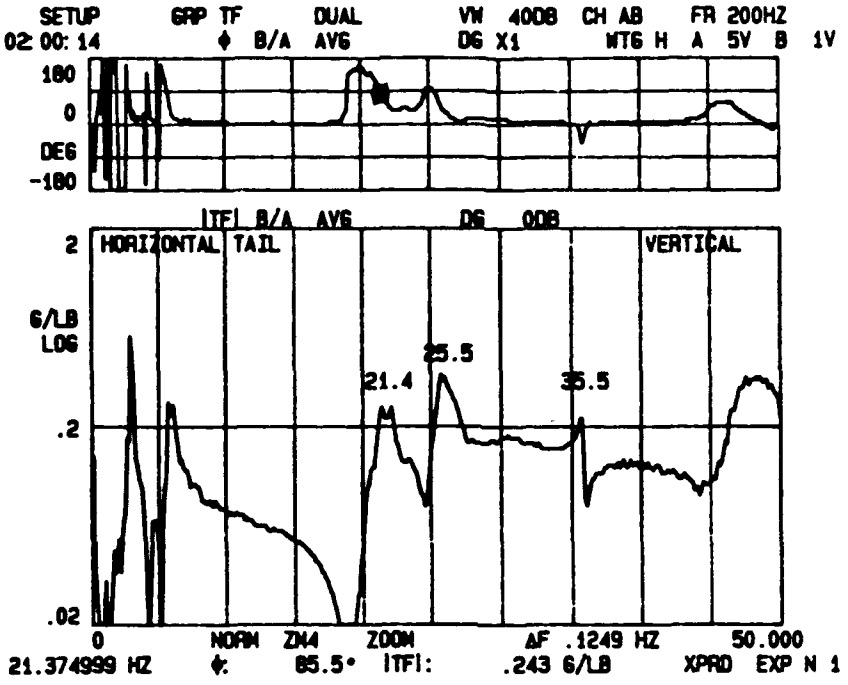
SETUP GRP TF DUAL VW 400B CH AB FR 200HZ
02: 00: 14 ϕ B/A AVG DG X1 WTG H A 5V B 1V
180
0
DEG
-180
|TF| B/A AVG DG 00B
2
HORIZONTAL TAIL
VERTICAL
G/LB
LOG
21.4
25.5
35.5
.2
.02
0
NORM ZM4 ZOOM ΔF .1249 HZ 50.000
21.374999 HZ ϕ: 85.5° |TF|: .243 G/LB XPRD EXP N 1

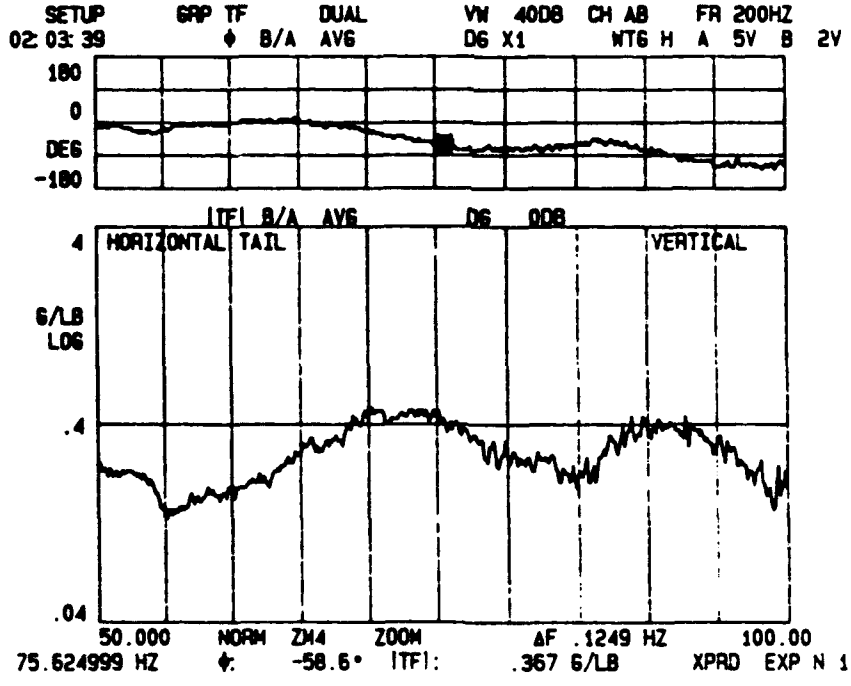
SETUP GRP TF DUAL VW 400B CH AB FR 200HZ
02: 03: 39 ϕ B/A AVG DG X1 WTG H A 5V B 2V
180
0
DEG
-180
|TF| B/A AVG DG 00B
4
HORIZONTAL TAIL
VERTICAL
G/LB
LOG
.4
.04
50.000 NORM ZM4 ZOOM ΔF .1249 HZ 100.00
75.624999 HZ ϕ: -58.6° |TF|: .367 G/LB XPRD EXP N 1

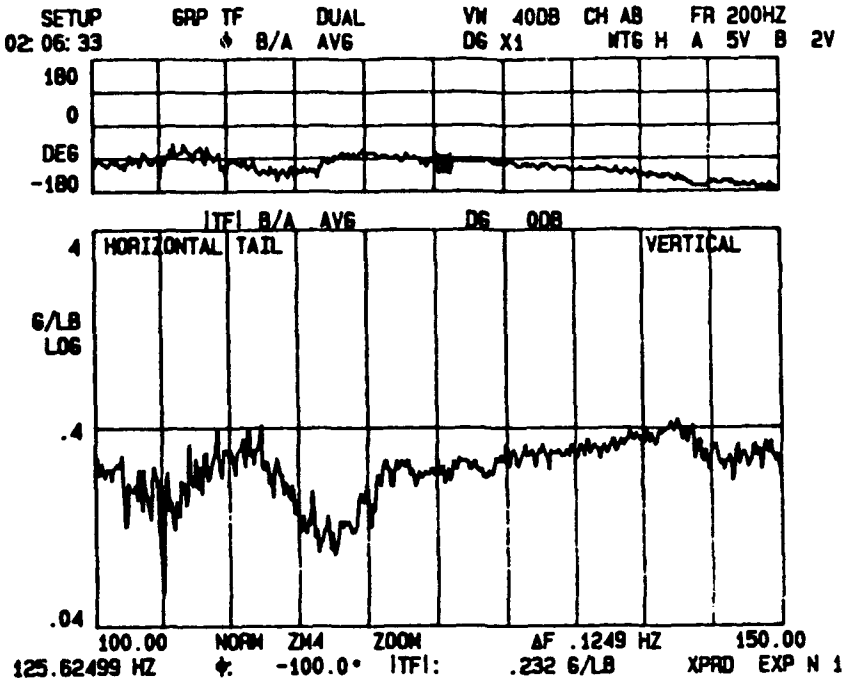
SETUP
02: 06: 33
GRP TF
DUAL
VW 400B CH AB
FR 200HZ
DG X1
WTG H A 5V B 2V
180
0
DEG
-180
|TF| B/A AVG
DG 00B
4
HORIZONTAL TAIL
VERTICAL
G/LB
LOG
.4
.04
100.00
NORM ZM4
ZOOM
ΔF .1249 HZ
150.00
125.62499 HZ
-100.0°
|TF|:
.232 G/LB
XPRD EXP N 1

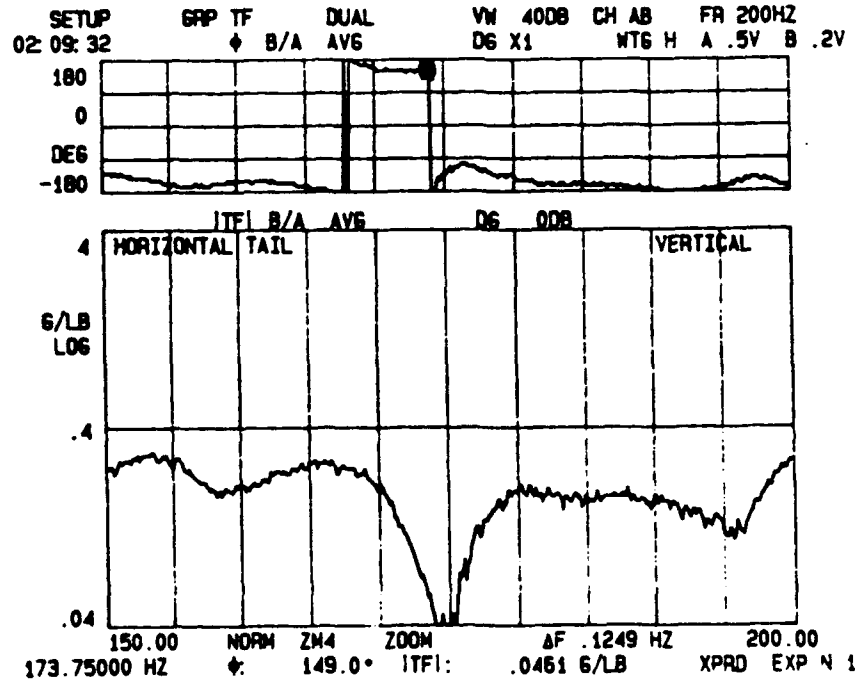
SETUP
02: 09: 32
GRP TF
DUAL
VW 400B CH AB
FR 200HZ
DG X1
WTG H A .5V B .2V
180
0
DEG
-180
|TF| B/A AVG
DG 00B
4
HORIZONTAL TAIL
VERTICAL
G/LB
LOG
.4
.04
150.00
NORM ZM4
ZOOM
ΔF .1249 HZ
200.00
173.75000 HZ
149.0°
|TF|:
.0461 G/LB
XPRD EXP N 1

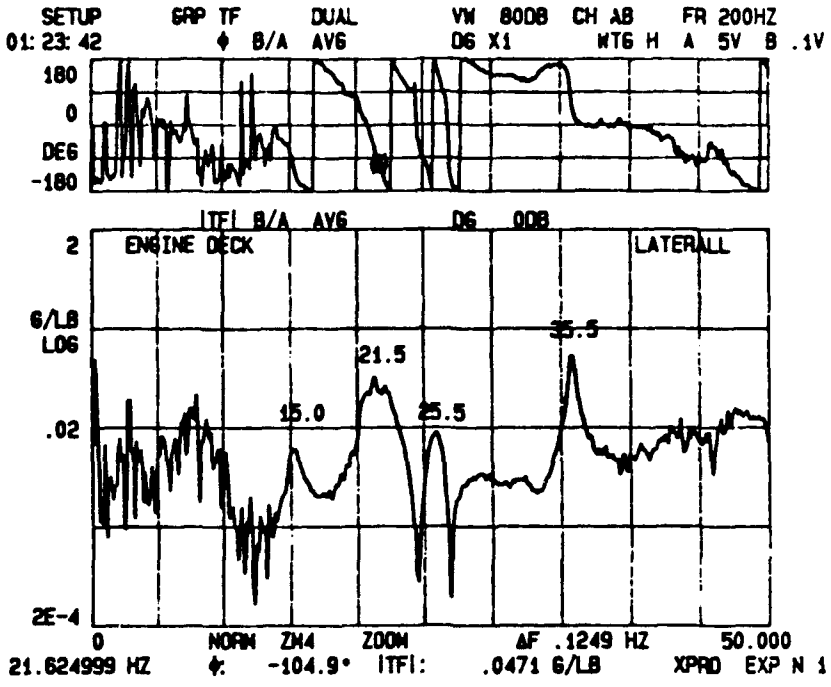
SETUP GRP TF DUAL VW 800B CH AB FR 200HZ
01: 23: 42 ϕ B/A AVG DG X1 WTG H A 5V B .1V
180
0
DEG
-180
ITFI B/A AVG DG 00B
2
ENGINE DECK
LATERALL
G/LB
LOG
21.5
35.5
15.0
25.5
.02
2E-4
0 NORM ZM4 ZOOM ΔF .1249 HZ 50.000
21.624999 HZ ϕ: -104.9° ITFI: .0471 G/LB XPRD EXP N 1

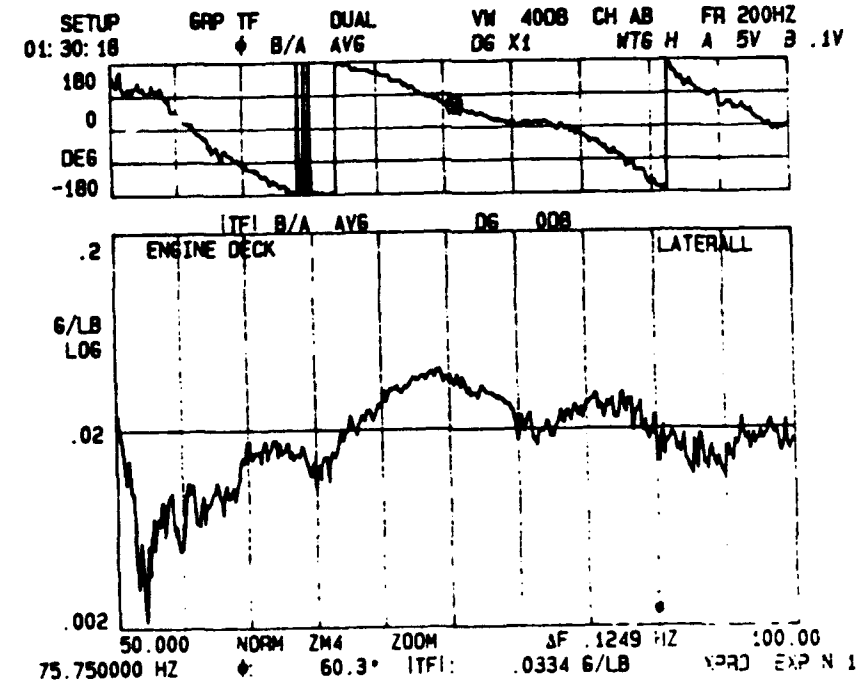
SETUP GRP TF DUAL VW 400B CH AB FR 200HZ
01: 30: 18 ϕ B/A AVG DG X1 WTG H A 5V B .1V
180
0
DEG
-180
ITFI B/A AVG DG 00B
.2
ENGINE DECK
LATERALL
G/LB
LOG
.02
.002
50.000 NORM ZM4 ZOOM ΔF .1249 HZ 100.00
75.750000 HZ ϕ: 60.3° ITFI: .0334 G/LB XPRD EXP N 1

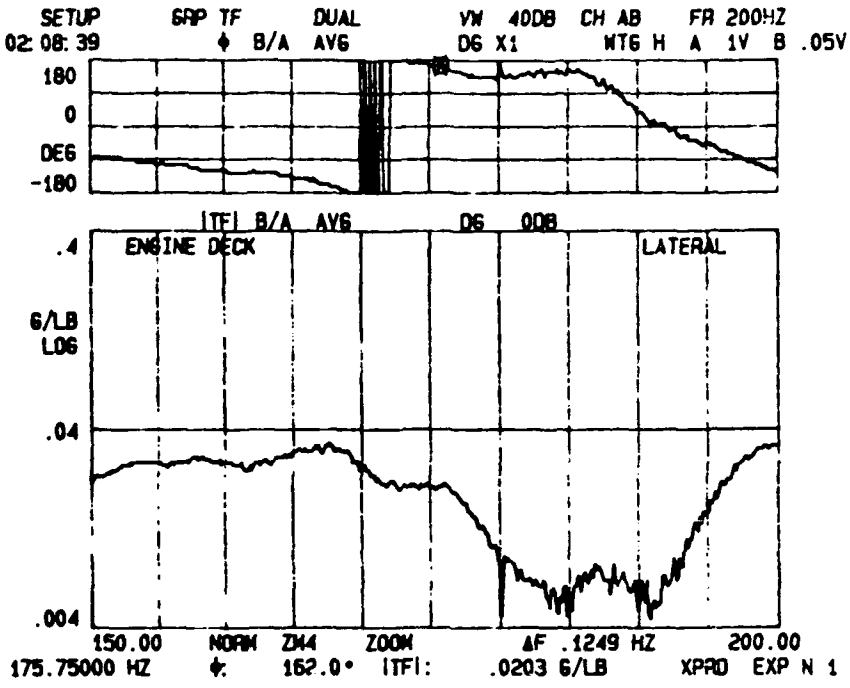
SETUP GRP TF DUAL VW 400B CH AB FR 200HZ
02: 08: 39 ϕ B/A AVG DG X1 WTG H A 1V B .05V
180
0
DEG
-180
|TF| B/A AVG DG 008
.4
ENGINE DECK
LATERAL
G/LB
LOG
.04
.004
150.00 NORM ZM4 ZOOM ΔF .1249 HZ 200.00
175.75000 HZ ϕ: 162.0° |TF|: .0203 G/LB XPRO EXP N 1

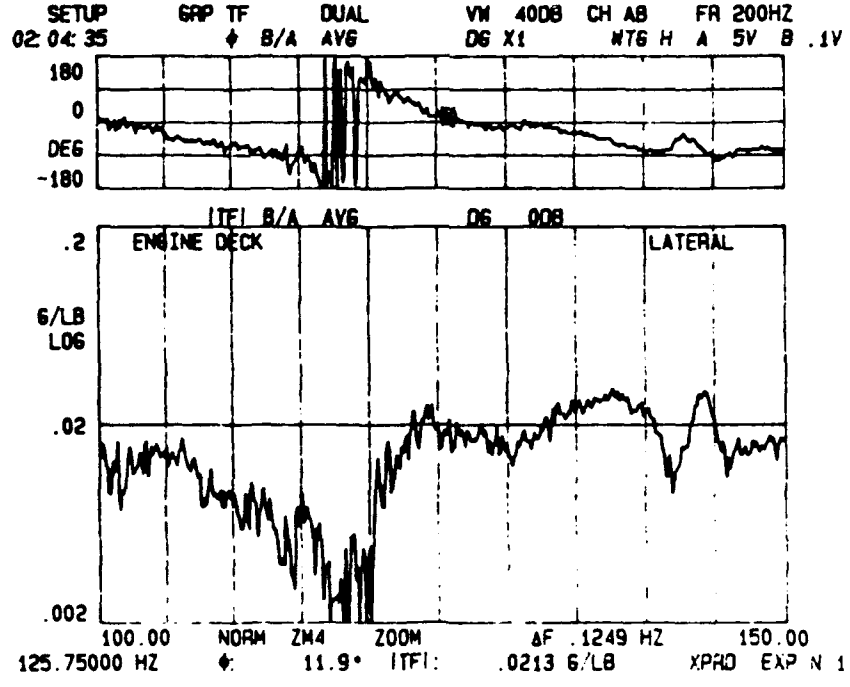
SETUP GRP TF DUAL VW 400B CH AB FR 200HZ
02: 04: 35 ϕ B/A AVG DG X1 WTG H A 5V B .1V
180
0
DEG
-180
|TF| B/A AVG DG 008
.2
ENGINE DECK
LATERAL
G/LB
LOG
.02
.002
100.00 NORM ZM4 ZOOM ΔF .1249 HZ 150.00
125.75000 HZ ϕ: 11.9° |TF|: .0213 G/LB XPRO EXP N 1

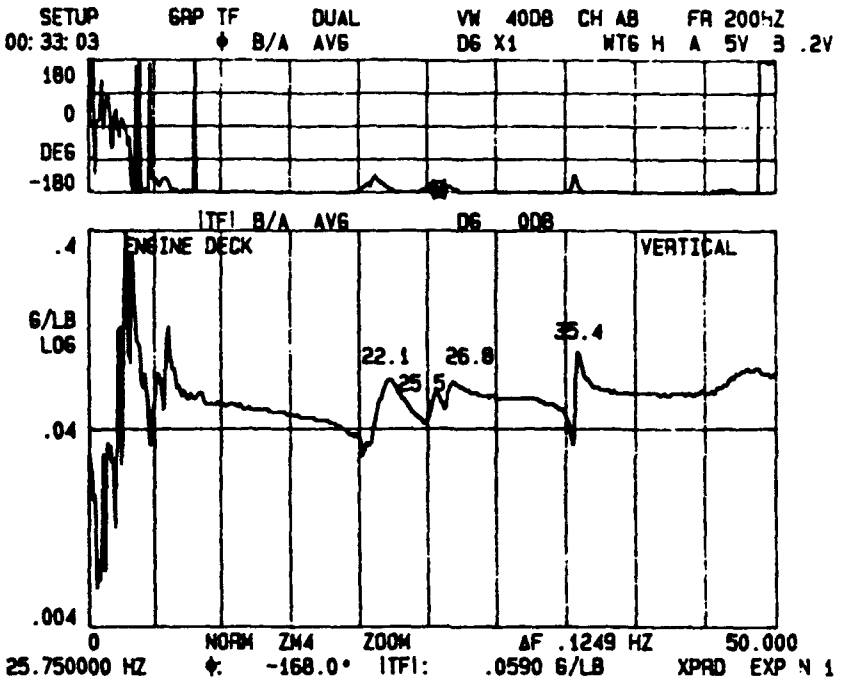
SETUP
00: 33: 03
GRP TF
B/A
AVG
DUAL
VW 400B
D6 X1
CH AB
WTG H
FR 200HZ
A 5V
B .2V
180
0
DEG
-180
|TF| B/A AVG
D6 00B
ENGINE DECK
VERTICAL
.4
G/LB
LOG
.04
.004
22.1
25.5
26.8
35.4
0
NORM
ZM4
ZOOM
ΔF .1249 HZ
50.000
25.750000 HZ
-168.0°
|TF|:
.0590 G/LB
XPRD
EXP N 1

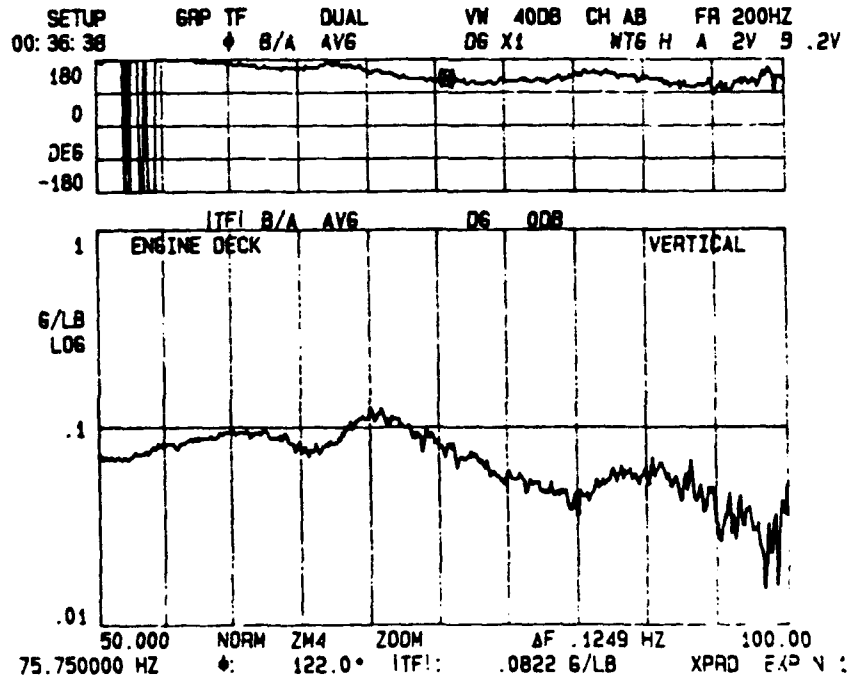
SETUP
00: 36: 38
GRP TF
B/A
AVG
DUAL
VW 400B
D6 X1
CH AB
WTG H
FR 200HZ
A 2V
B .2V
180
0
DEG
-180
|TF| B/A AVG
D6 00B
ENGINE DECK
VERTICAL
1
G/LB
LOG
.1
.01
50.000
NORM
ZM4
ZOOM
ΔF .1249 HZ
100.00
75.750000 HZ
122.0°
|TF|:
.0822 G/LB
XPRD

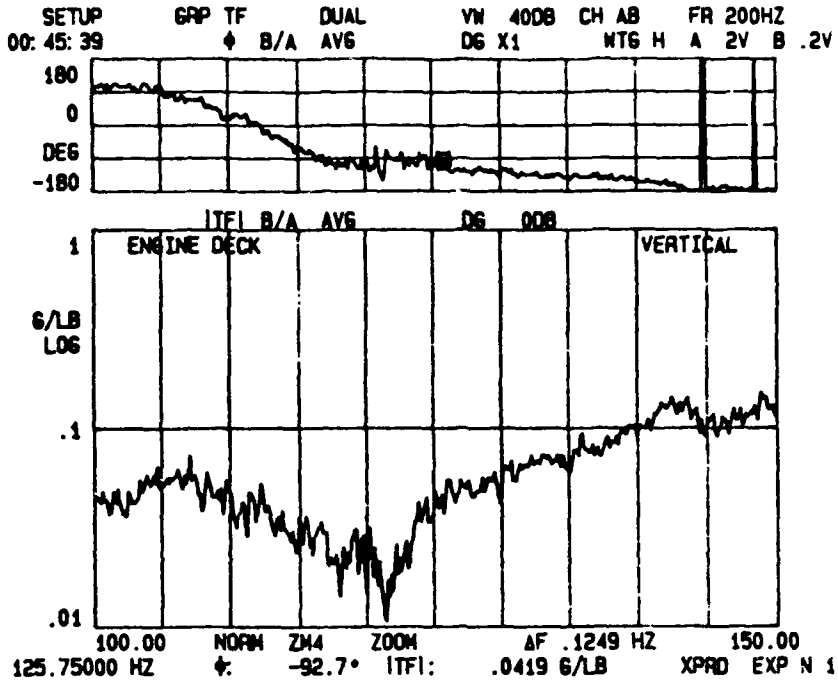
SETUP GRP TF DUAL VW 400B CH AB FR 200HZ
00: 45: 39 ϕ B/A AVG DG X1 WTG H A 2V B .2V
180
0
DEG
-180
|TF| B/A AVG DG 00B
1
ENGINE DECK
VERTICAL
G/LB
LOG
.1
.01
100.00 NORM ZM4 ZOOM ΔF .1249 HZ 150.00
125.75000 HZ ϕ: -92.7° |TF|: .0419 G/LB XPRD EXP N 1

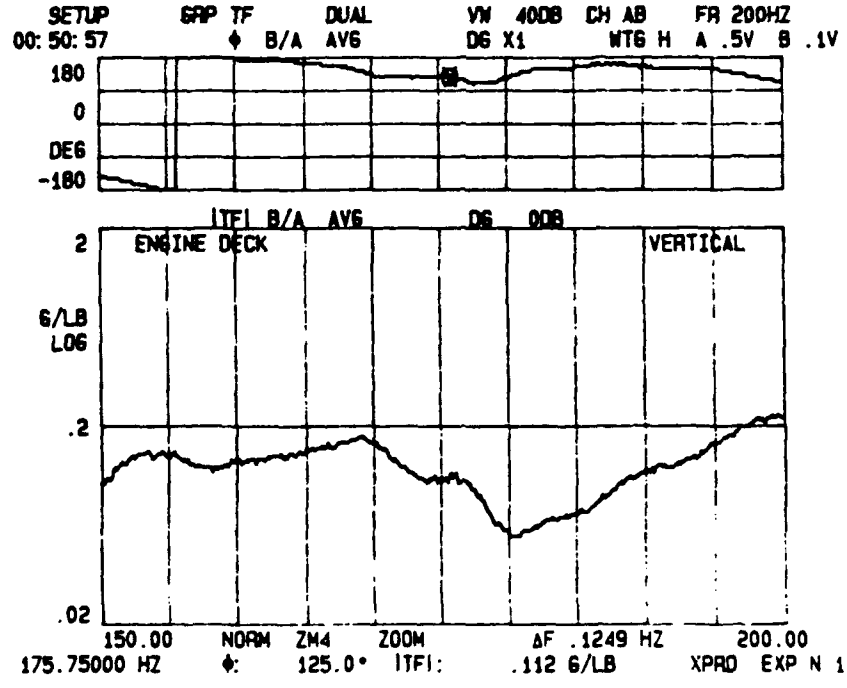
SETUP GRP TF DUAL VW 400B CH AB FR 200HZ
00: 50: 57 ϕ B/A AVG DG X1 WTG H A .5V B .1V
180
0
DEG
-180
|TF| B/A AVG DG 00B
2
ENGINE DECK
VERTICAL
G/LB
LOG
.2
.02
150.00 NORM ZM4 ZOOM ΔF .1249 HZ 200.00
175.75000 HZ ϕ: 125.0° |TF|: .112 G/LB XPRD EXP N 1

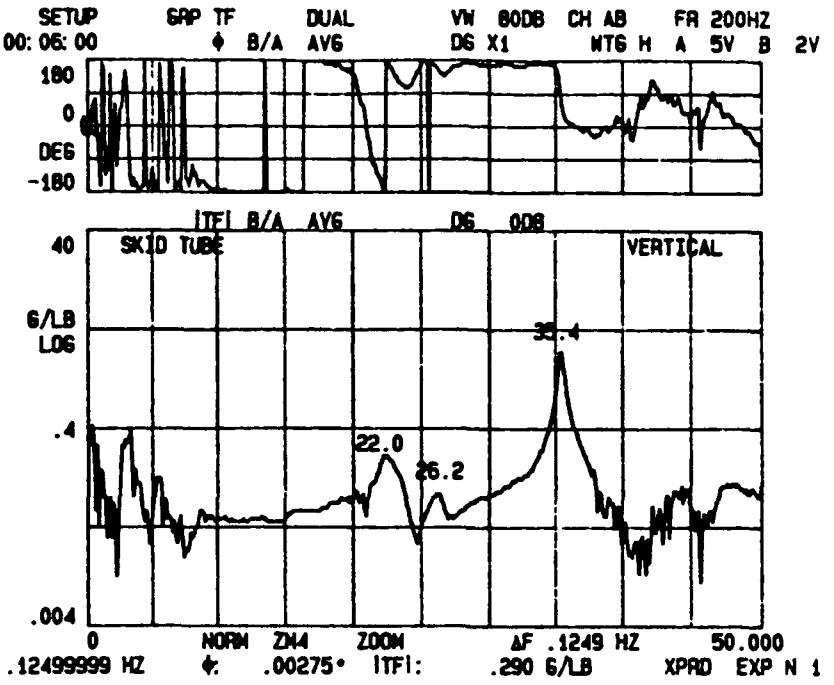
SETUP GRP TF DUAL VW 80DB CH AB FR 200HZ
00: 06: 00 ϕ B/A AVG DG X1 MTG H A 5V B 2V
180
0
DEG
-180
|TF| B/A AVG DG 0DB
40
SKID TUBE
VERTICAL
G/LB
LOG
35.4
.4
22.0
26.2
.004
0 NORM ZM4 ZOOM ΔF .1249 HZ 50.000
.12499999 HZ ϕ: .00275° |TF|: .290 G/LB XPRD EXP N 1

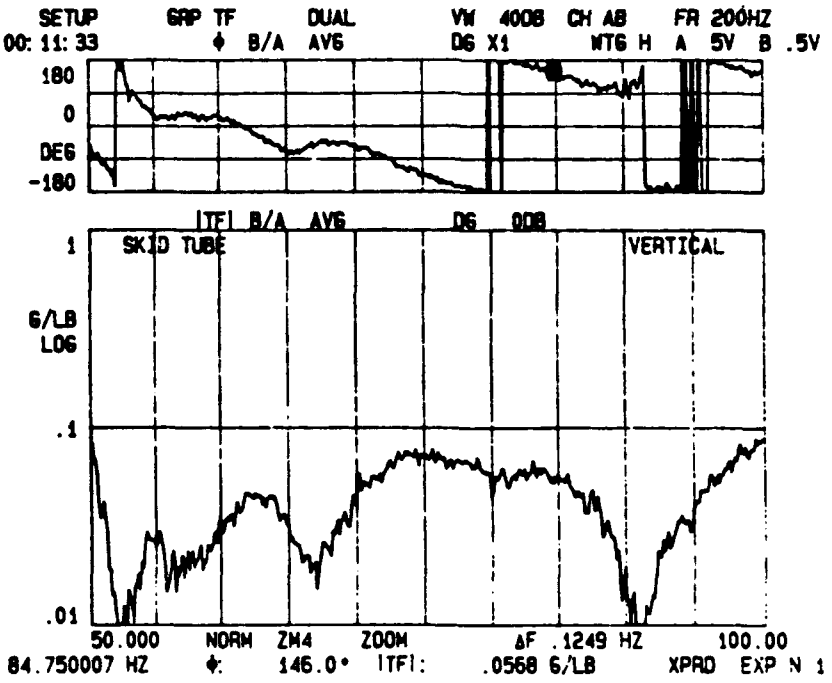
SETUP GRP TF DUAL VW 40DB CH AB FR 200HZ
00: 11: 33 ϕ B/A AVG DG X1 MTG H A 5V B .5V
180
0
DEG
-180
|TF| B/A AVG DG 0DB
1
SKID TUBE
VERTICAL
G/LB
LOG
.1
.01
50.000 NORM ZM4 ZOOM ΔF .1249 HZ 100.00
84.750007 HZ ϕ: 146.0° |TF|: .0568 G/LB XPRD EXP N 1

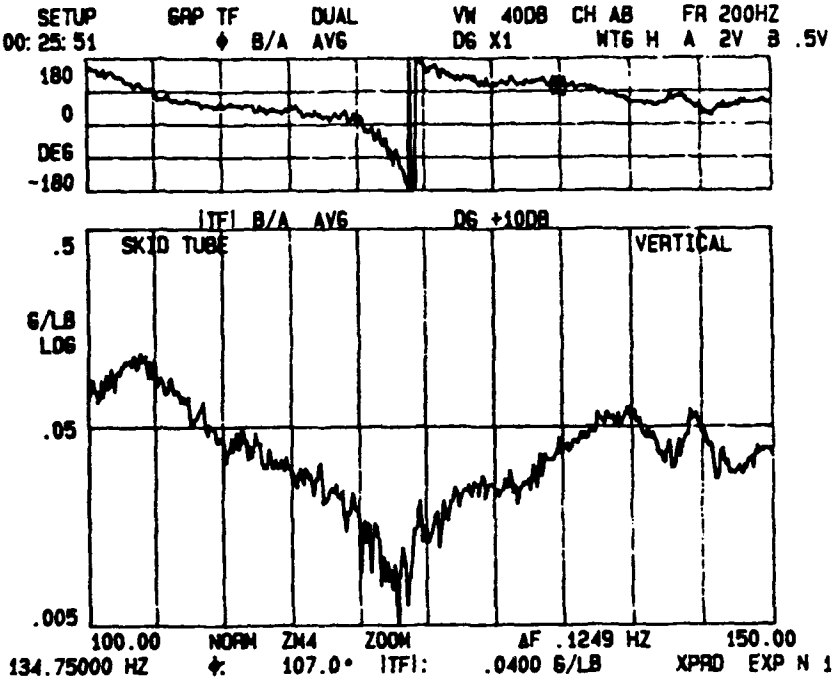
SETUP GRP TF DUAL VW 400B CH AB FR 200HZ
00: 25: 51 ϕ B/A AVG DG X1 WTG H A 2V B .5V
180
0
DEG
-180
|TF| B/A AVG DG +10DB
.5
SKID TUBE
VERTICAL
G/LB
LOG
.05
.005
100.00 NORM ZM4 ZOOM ΔF .1249 HZ 150.00
134.75000 HZ ϕ: 107.0° |TF|: .0400 G/LB XPRD EXP N 1

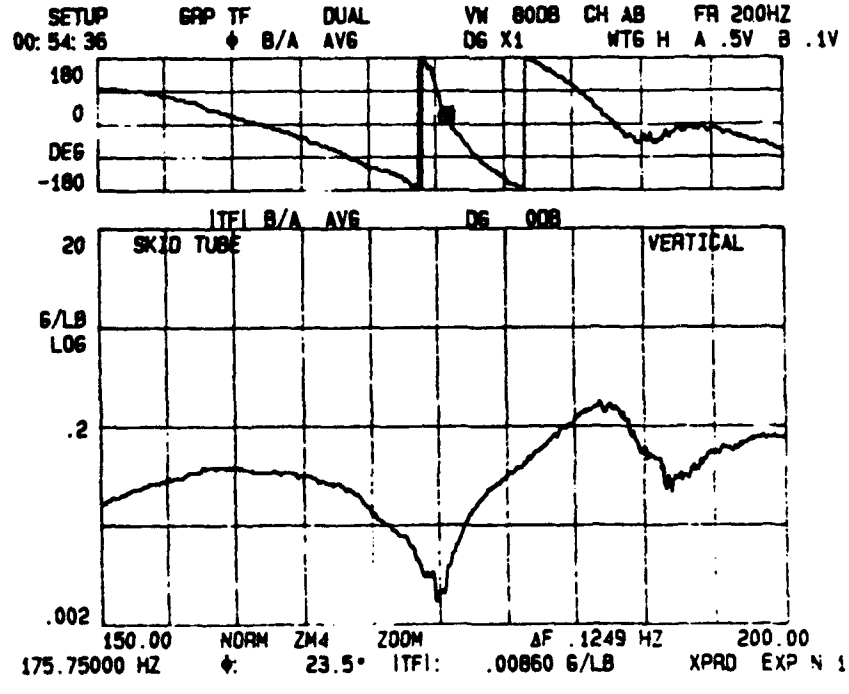
SETUP GRP TF DUAL VW 800B CH AB FR 200HZ
00: 54: 36 ϕ B/A AVG DG X1 WTG H A .5V B .1V
180
0
DEG
-180
|TF| B/A AVG DG 0DB
20
SKID TUBE
VERTICAL
G/LB
LOG
.2
.002
150.00 NORM ZM4 ZOOM ΔF .1249 HZ 200.00
175.75000 HZ ϕ: 23.5° |TF|: .00860 G/LB XPRD EXP N 1

APPENDIX C. FREQUENCY RESPONSE FUNCTIONS: LATERAL

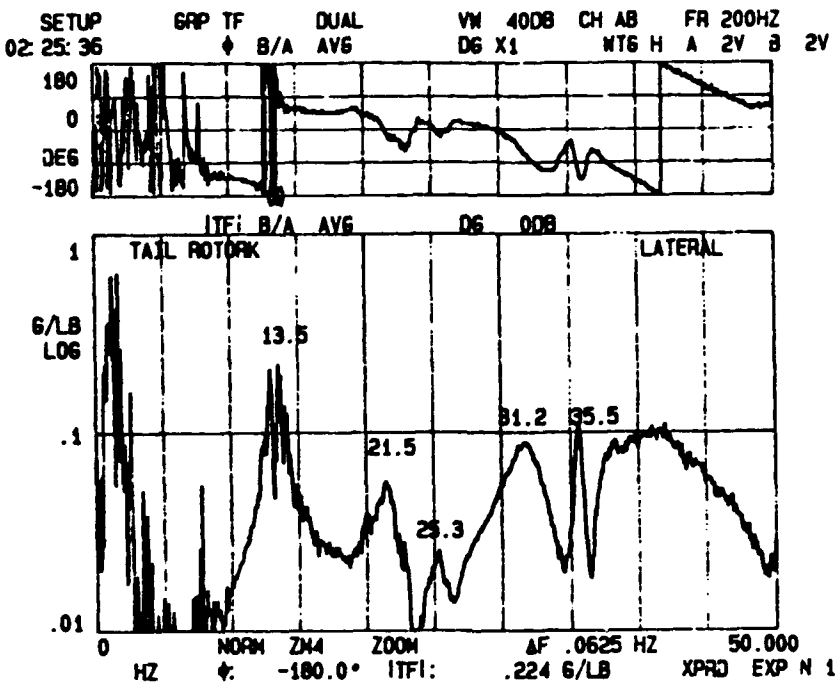

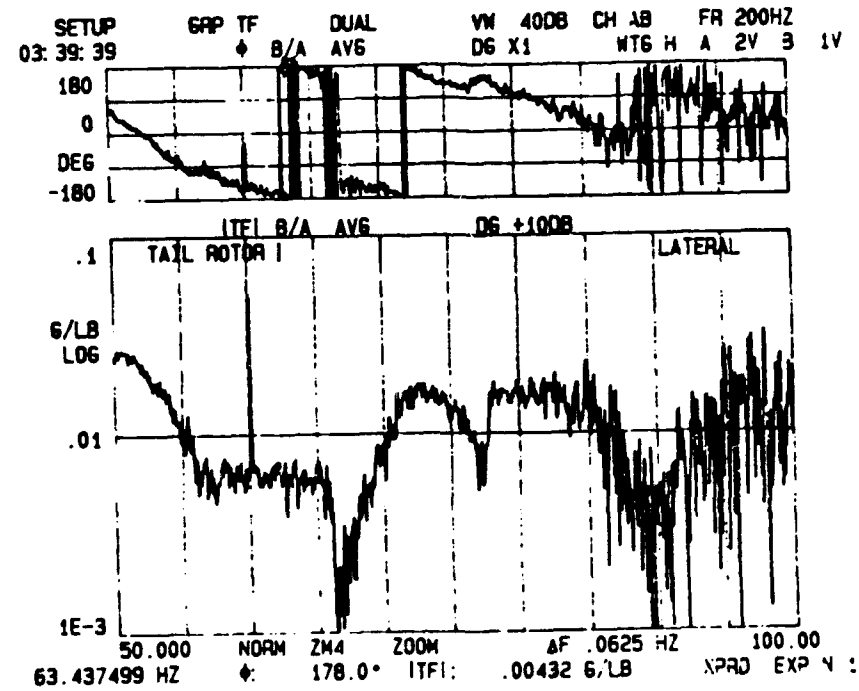

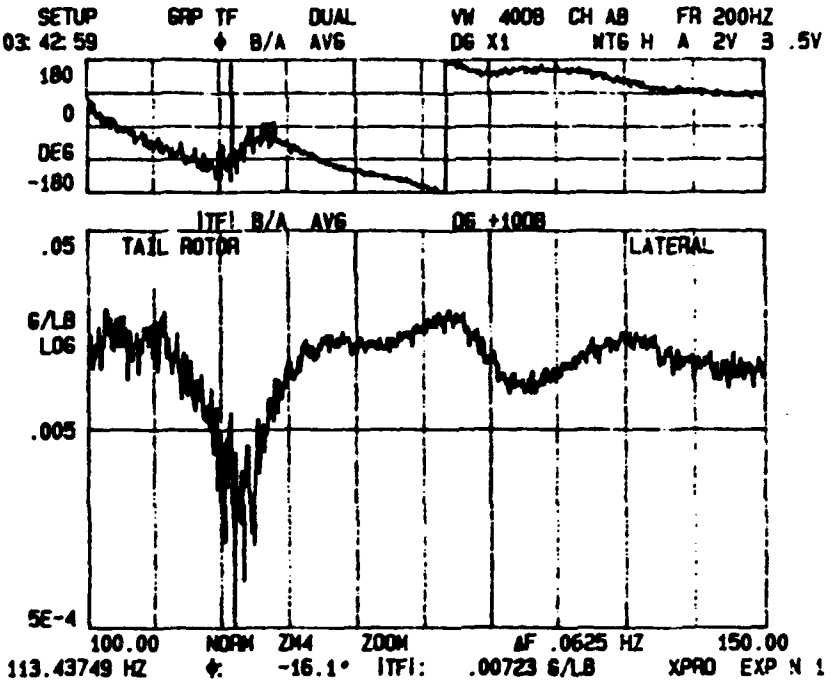
SETUP GRP TF DUAL VW 400B CH AB FR 200HZ
03: 42: 59 ϕ B/A AVG DG X1 WTG H A 2V B .5V
180
0
DEG
-180
|TF| B/A AVG DG +100B
.05
TAIL ROTOR
LATERAL
G/LB
LOG
.005
5E-4
100.00 NORM ZM4 ZOOM ΔF .0625 HZ 150.00
113.43749 HZ ϕ: -16.1° |TF|: .00723 G/LB XPRO EXP N 1

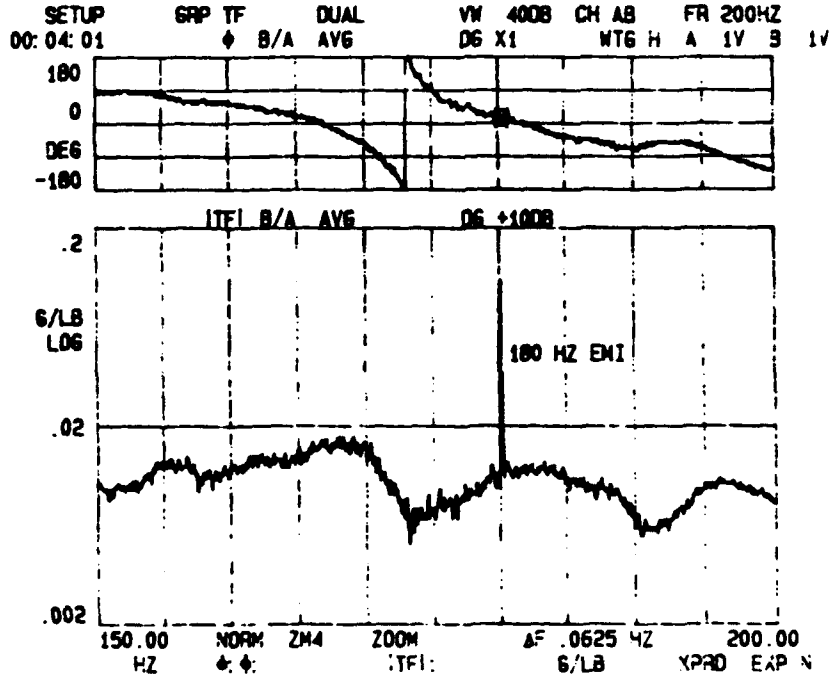
SETUP GRP TF DUAL VW 400B CH AB FR 200HZ
00: 04: 01 ϕ B/A AVG DG X1 WTG H A 1V B 1V
180
0
DEG
-180
|TF| B/A AVG DG +100B
.2
G/LB
LOG
180 HZ EMI
.02
.002
150.00 NORM ZM4 ZOOM ΔF .0625 HZ 200.00
HZ ϕ: ϕ: |TF|: G/LB XPRO EXP N

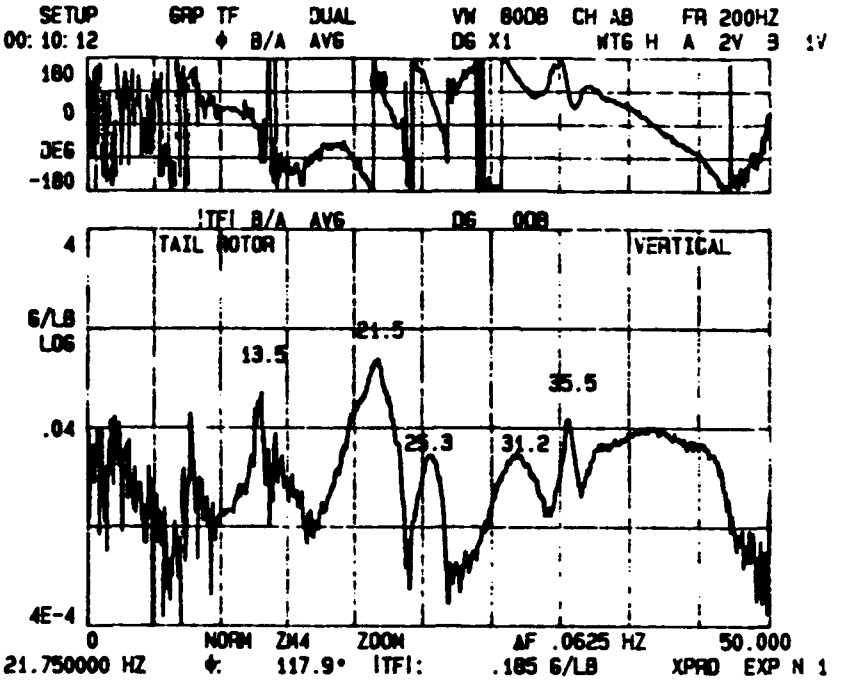
SETUP GRP TF DUAL VW 8008 CH AB FR 200HZ
00: 10: 12 ϕ B/A AVG DG X1 WTG H A 2V 3 1V
180
0
DEG
-180
ITFI B/A AVG DG 008
4
TAIL ROTOR
VERTICAL
G/LB
LOG
13.5
21.5
35.5
25.3
31.2
.04
4E-4
0 NORM ZM4 ZOOM ΔF .0625 HZ 50.000
21.750000 HZ ϕ: 117.9° ITFI: .185 G/LB XPRD EXP N 1

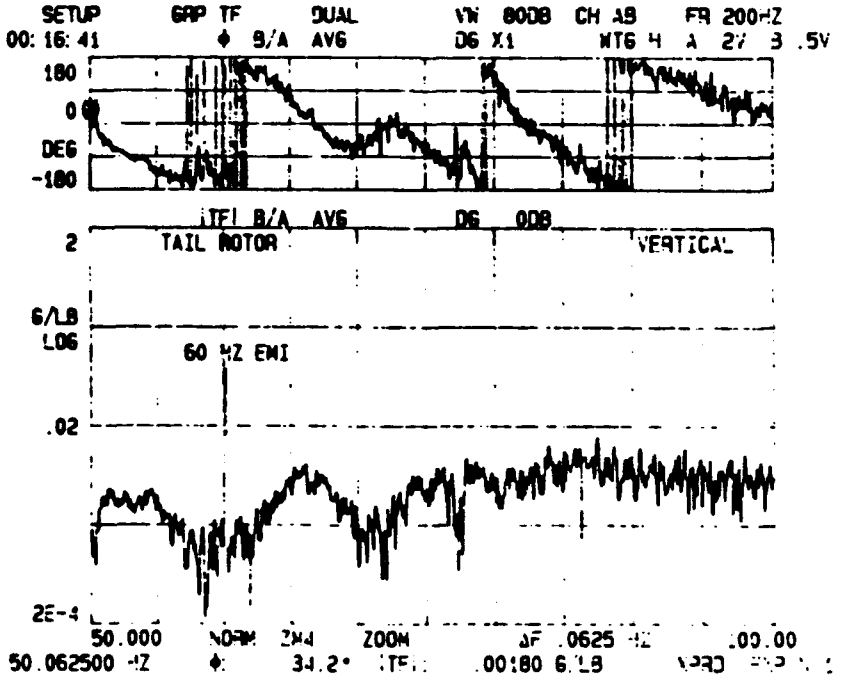
SETUP GRP TF DUAL VW 8008 CH AB FR 200HZ
00: 16: 41 ϕ B/A AVG DG X1 WTG H A 2V 3 .5V
180
0
DEG
-180
ITFI B/A AVG DG 008
2
TAIL ROTOR
VERTICAL
G/LB
LOG
60 HZ EMI
.02
2E-4
50.000 NORM ZM4 ZOOM ΔF .0625 HZ 100.00
50.062500 HZ ϕ: 34.2° ITFI: .00180 G/LB XPRD EXP N 1

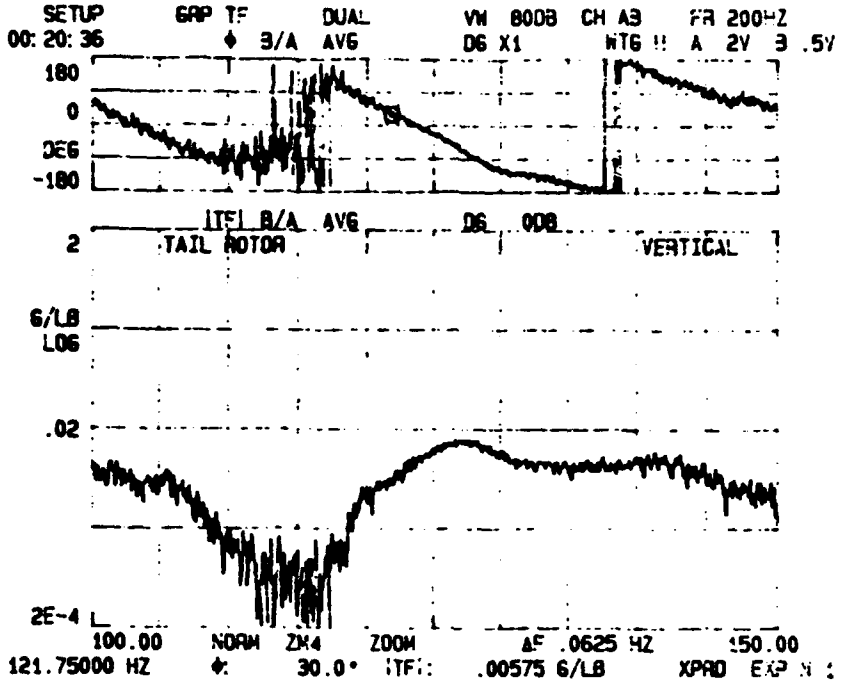
SETUP GRP TF DUAL VW 8008 CH AB FR 200HZ
00: 20: 36 ♦ B/A AVG DG X1 WTG A 2V B .5V
180
0
DEG
-180
TF: B/A AVG DG 008
2
TAIL ROTOR
VERTICAL
G/LB
LOG
.02
2E-4
100.00 NORM ZM4 ZOOM ΔF .0625 HZ 150.00
121.75000 HZ ♦: 30.0° TF: .00575 G/LB XPRO EXP

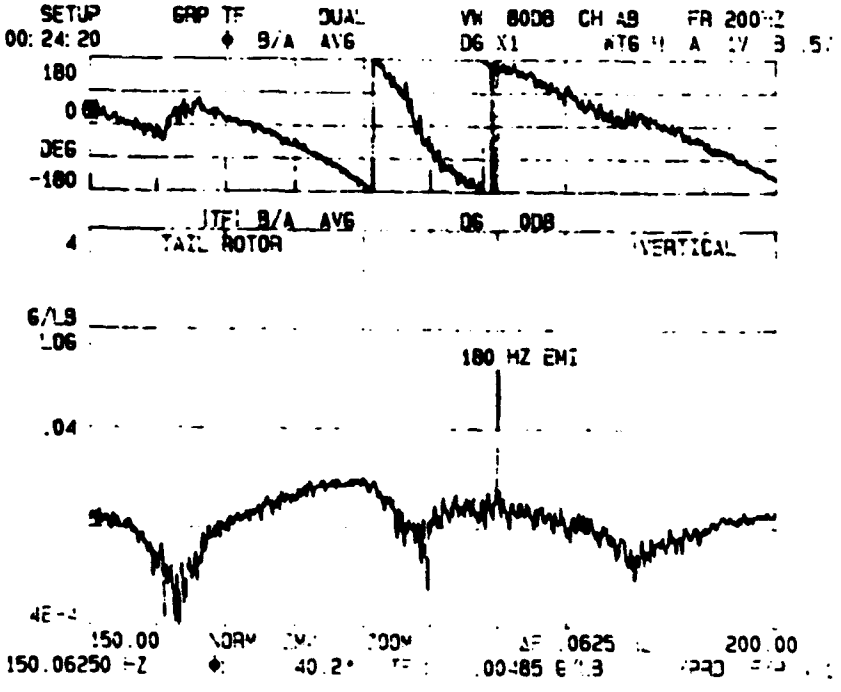
SETUP GRP TF DUAL VW 8008 CH AB FR 200HZ
00: 24: 20 ♦ B/A AVG DG X1 WTG A 2V B .5V
180
0
DEG
-180
TF: B/A AVG DG 008
4
TAIL ROTOR
VERTICAL
G/LB
LOG
180 HZ EMI
.04
4E-4
150.00 NORM ZM4 ZOOM ΔF .0625 200.00
150.06250 HZ ♦: 40.2° TF: .00485 G/LB XPRO EXP

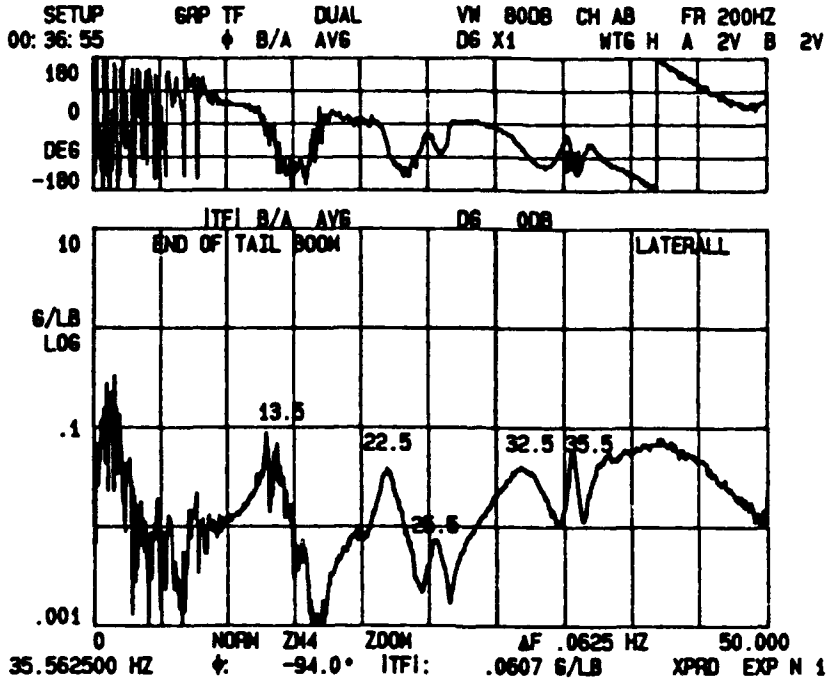
SETUP
00: 36: 55
GRP TF
DUAL
VW 800B CH AB
FR 200HZ
ϕ B/A AVG
DG X1
WTG H A 2V B 2V
180
0
DEG
-180
|TF| B/A AVG
DG 00B
END OF TAIL BOOM
LATERALL
10
G/LB
LOG
.1
.001
13.5
22.5
32.5
35.5
26.6
0
NORM ZM4
ZOOM
ΔF .0625 HZ
50.000
35.562500 HZ
ϕ: -94.0°
|TF|: .0607 G/LB
XPRD EXP N 1

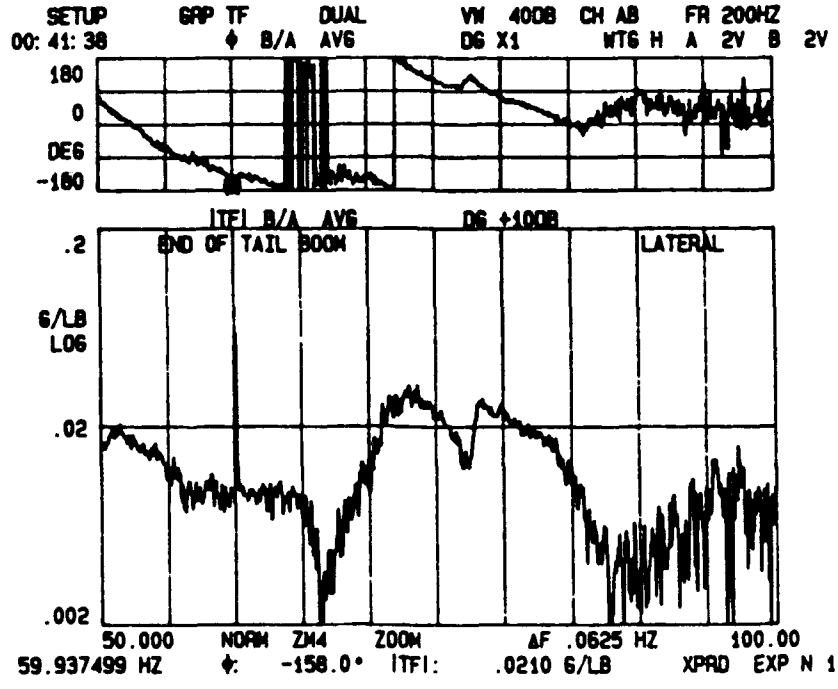
SETUP
00: 41: 38
GRP TF
DUAL
VW 400B CH AB
FR 200HZ
ϕ B/A AVG
DG X1
WTG H A 2V B 2V
180
0
DEG
-180
|TF| B/A AVG
DG +10DB
END OF TAIL BOOM
LATERAL
.2
G/LB
LOG
.02
.002
50.000
NORM ZM4
ZOOM
ΔF .0625 HZ
100.00
59.937499 HZ
ϕ: -158.0°
|TF|: .0210 G/LB
XPRD EXP N 1

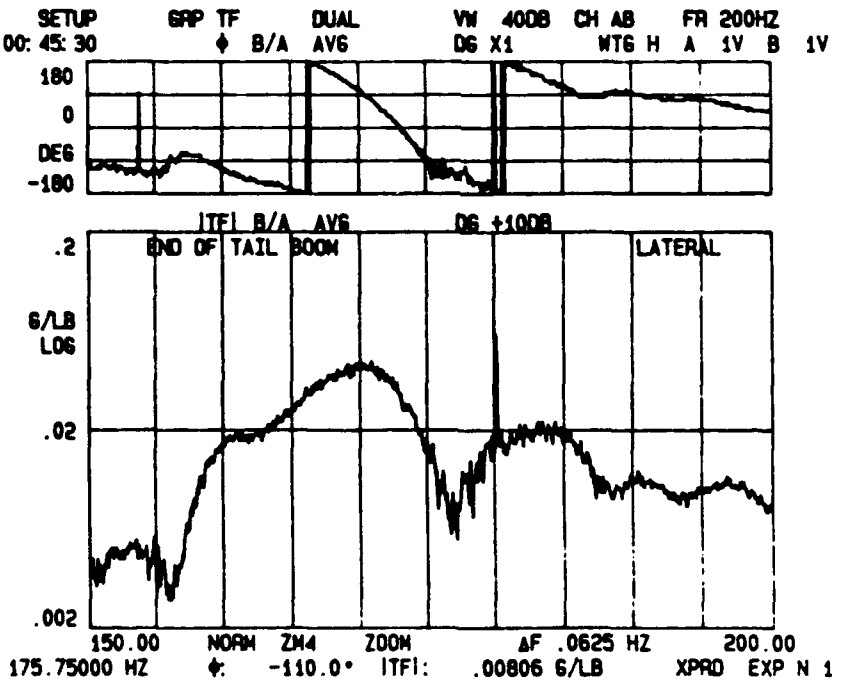
SETUP
00: 45: 30
GRP TF
φ B/A
DUAL
AVG
VW 400B
DG X1
CH AB
WTG H
FR 200HZ
A 1V B 1V
180
0
DEG
-180
|TF| B/A AVG
DG +100B
.2
END OF TAIL BOOM
LATERAL
G/LB
LOG
.02
.002
150.00
NORM ZM4
ZOOM
ΔF .0625 HZ
200.00
175.75000 HZ
φ: -110.0°
|TF|: .00806 G/LB
XPRD EXP N 1

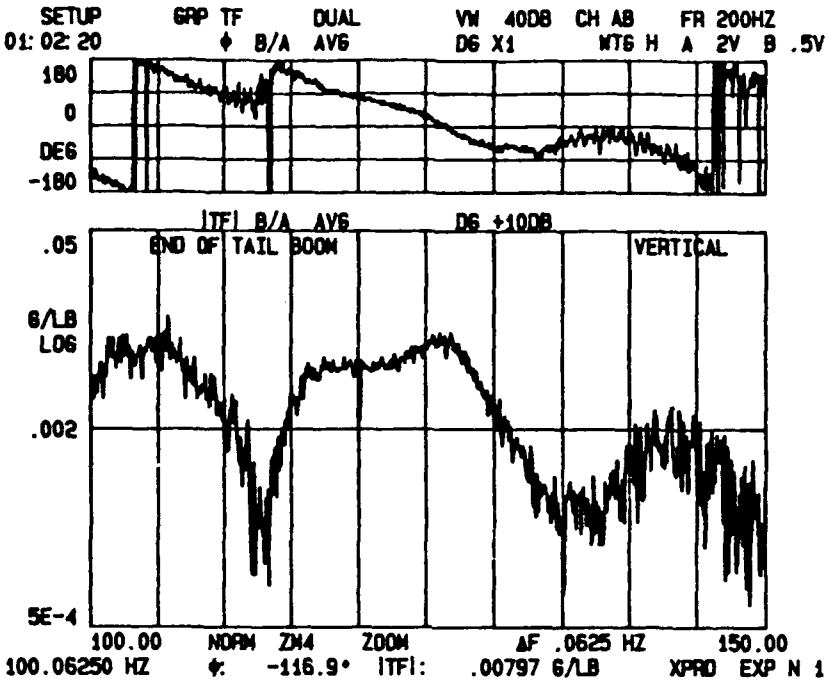
SETUP GRP TF DUAL VW 40DB CH AB FR 200HZ
01: 02: 20 ϕ B/A AVG DG X1 WTG H A 2V B .5V
180
0
DEG
-180
|TF| B/A AVG DG +10DB
.05
END OF TAIL BOOM
VERTICAL
G/LB
LOG
.002
5E-4
100.00 NORM ZM4 ZOOM ΔF .0625 HZ 150.00
100.06250 HZ ϕ: -116.9° |TF|: .00797 G/LB XPRD EXP N 1

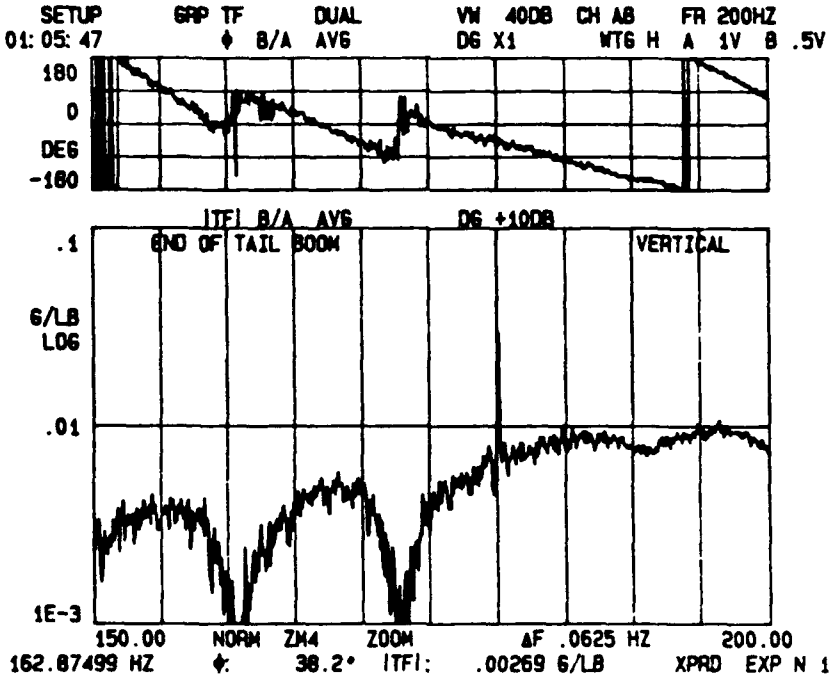
SETUP GRP TF DUAL VW 40DB CH AB FR 200HZ
01: 05: 47 ϕ B/A AVG DG X1 WTG H A 1V B .5V
180
0
DEG
-180
|TF| B/A AVG DG +10DB
.1
END OF TAIL BOOM
VERTICAL
G/LB
LOG
.01
1E-3
150.00 NORM ZM4 ZOOM ΔF .0625 HZ 200.00
162.87499 HZ ϕ: 38.2° |TF|: .00269 G/LB XPRD EXP N 1

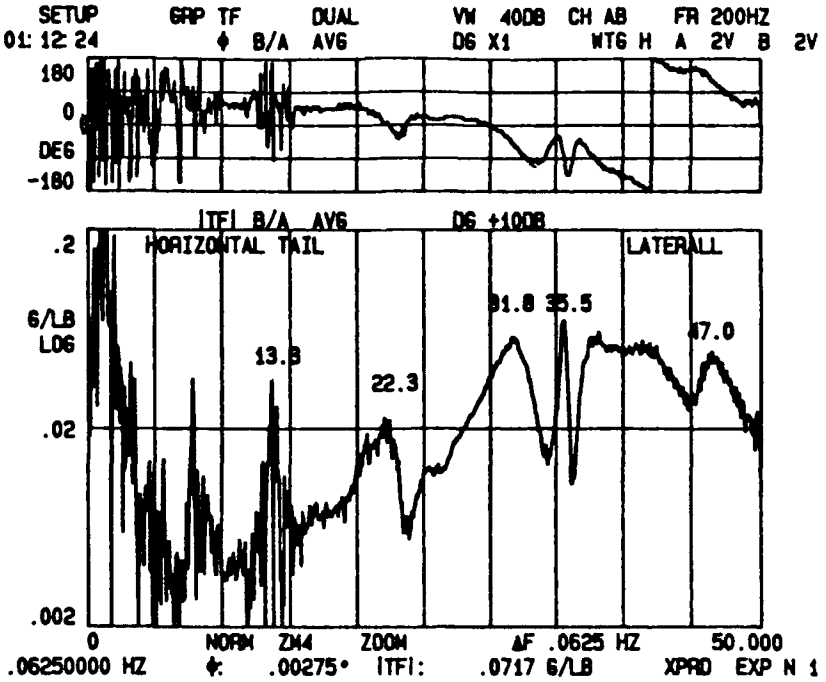
SETUP GRP TF DUAL VW 400B CH AB FR 200HZ
01: 12: 24 ϕ B/A AVG DG X1 WTG H A 2V B 2V
180
0
DEG
-180
|TF| B/A AVG DG +100B
HORIZONTAL TAIL
LATERALL
.2
G/LB
LOG
.02
.002
13.8
22.3
31.8
35.5
47.0
0 NORM ZM4 ZOOM ΔF .0625 HZ 50.000
.06250000 HZ ϕ: .00275° |TF|: .0717 G/LB XPRD EXP N 1

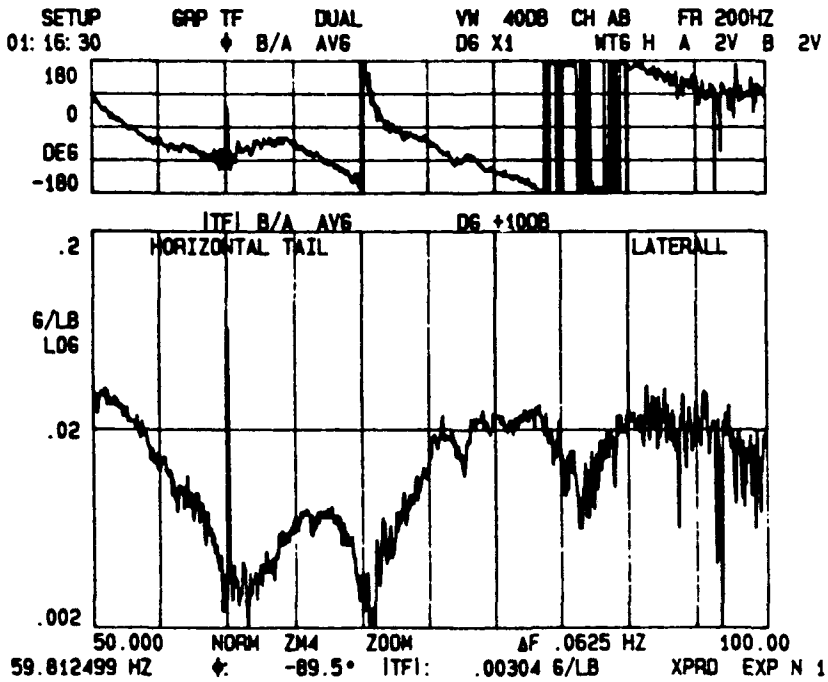
SETUP GRP TF DUAL VW 400B CH AB FR 200HZ
01: 16: 30 ϕ B/A AVG DG X1 WTG H A 2V B 2V
180
0
DEG
-180
|TF| B/A AVG DG +100B
HORIZONTAL TAIL
LATERALL
.2
G/LB
LOG
.02
.002
50.000 NORM ZM4 ZOOM ΔF .0625 HZ 100.00
59.812499 HZ ϕ: -89.5° |TF|: .00304 G/LB XPRD EXP N 1

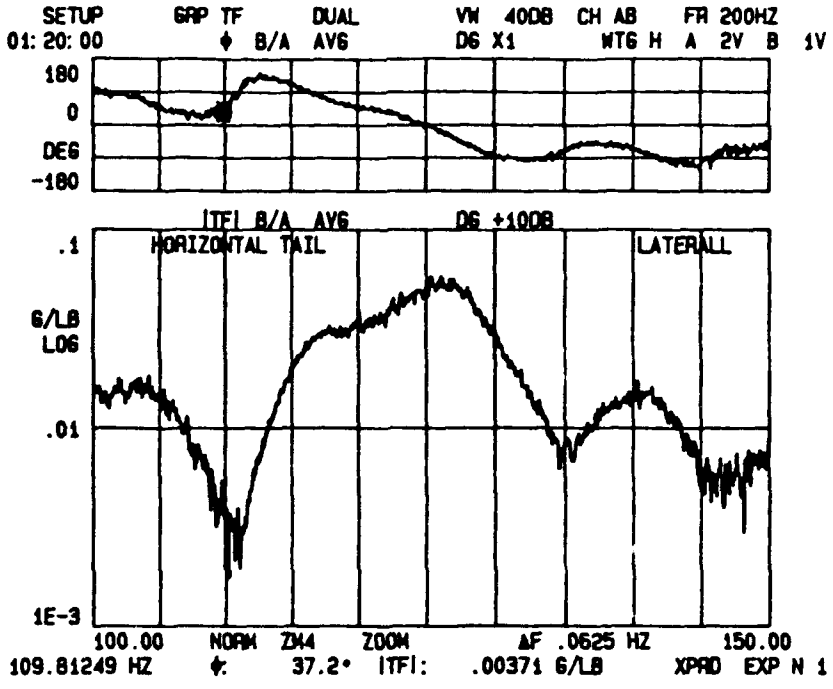
SETUP GRP TF DUAL VW 400B CH AB FR 200HZ
01: 20: 00 ϕ B/A AVG DG X1 WTG H A 2V B 1V
180
0
DEG
-180
|TF| B/A AVG DG +100B
.1
HORIZONTAL TAIL
LATERALL
G/LB
LOG
.01
1E-3
100.00 NORM ZM4 ZOOM ΔF .0625 HZ 150.00
109.81249 HZ ϕ: 37.2° |TF|: .00371 G/LB XPRD EXP N 1

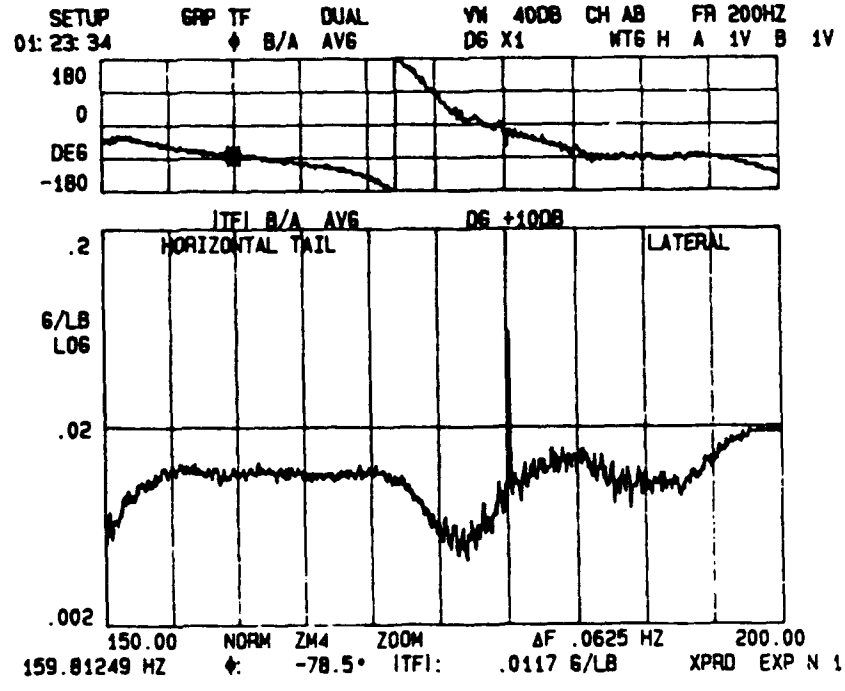
SETUP GRP TF DUAL VW 400B CH AB FR 200HZ
01: 23: 34 ϕ B/A AVG DG X1 WTG H A 1V B 1V
180
0
DEG
-180
|TF| B/A AVG DG +100B
.2
HORIZONTAL TAIL
LATERAL
G/LB
LOG
.02
.002
150.00 NORM ZM4 ZOOM ΔF .0625 HZ 200.00
159.81249 HZ ϕ: -78.5° |TF|: .0117 G/LB XPRD EXP N 1

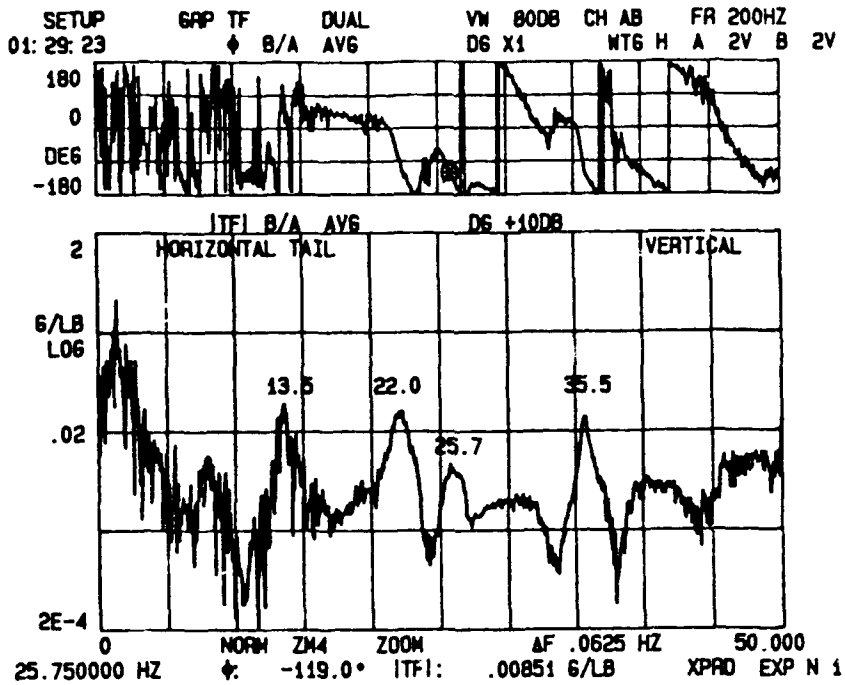
SETUP
01: 29: 23
GRP TF
∠ B/A
DUAL
AVG
VW 80DB
DG X1
CH AB
WTG H
FR 200HZ
A 2V
B 2V
180
0
DEG
-180
|TF| B/A AVG
DG +10DB
HORIZONTAL TAIL
VERTICAL
2
G/LB
LOG
13.5
22.0
25.7
35.5
.02
2E-4
0
NORM
ZM4
ZOOM
ΔF .0625 HZ
50.000
25.750000 HZ
∠: -119.0°
|TF|: .00851 G/LB
XPRD EXP N 1

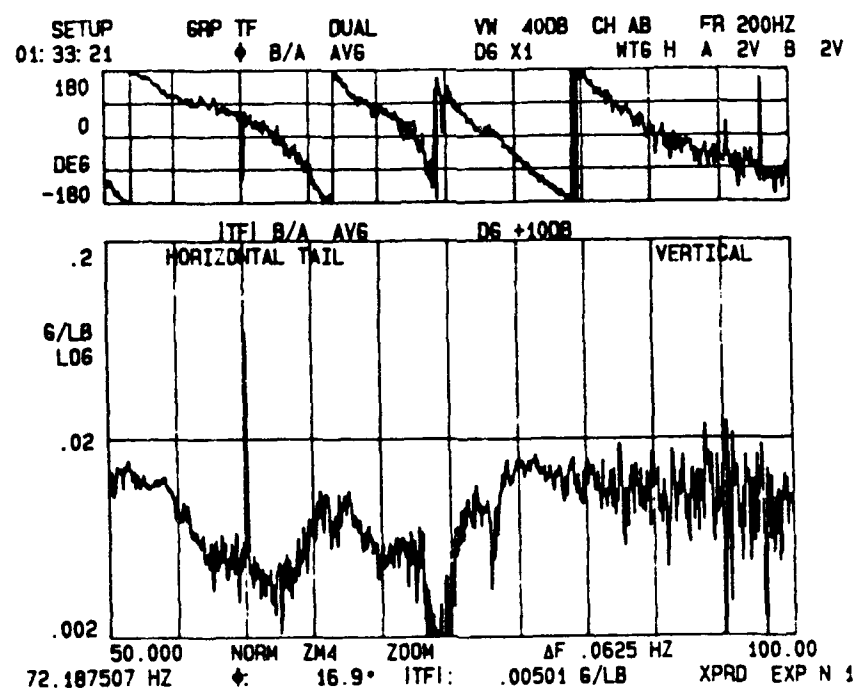
SETUP
01: 33: 21
GRP TF
∠ B/A
DUAL
AVG
VW 40DB
DG X1
CH AB
WTG H
FR 200HZ
A 2V
B 2V
180
0
DEG
-180
|TF| B/A AVG
DG +10DB
HORIZONTAL TAIL
VERTICAL
.2
G/LB
LOG
.02
.002
50.000
NORM
ZM4
ZOOM
ΔF .0625 HZ
100.00
72.187507 HZ
∠: 16.9°
|TF|: .00501 G/LB
XPRD EXP N 1

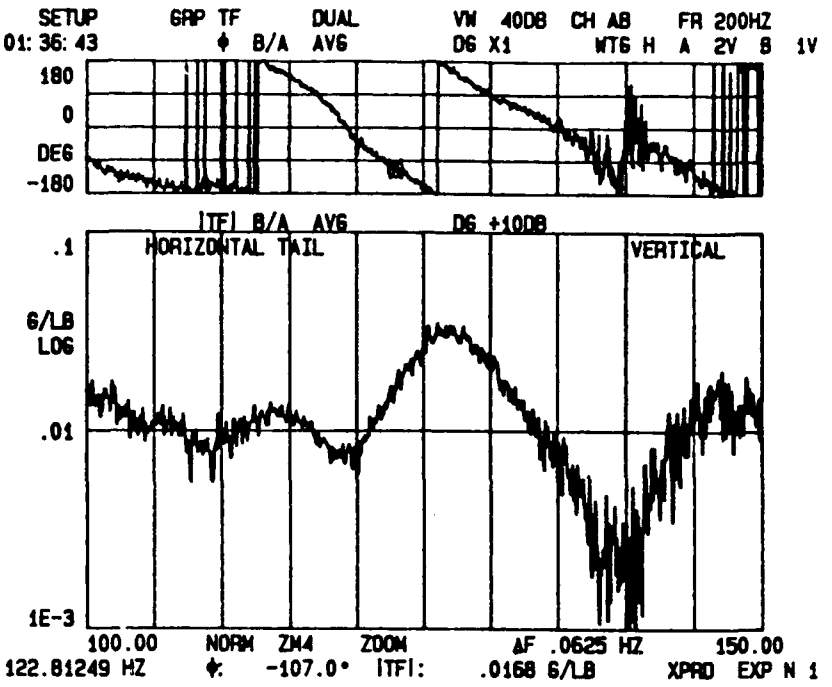
SETUP GRP TF DUAL VW 40DB CH AB FR 200HZ
01: 36: 43 ϕ B/A AVG DG X1 WTG H A 2V B 1V
180
0
DEG
-180
|TF| B/A AVG DG +10DB
HORIZONTAL TAIL
VERTICAL
.1
G/LB
LOG
.01
1E-3
100.00 NORM ZM4 ZOOM ΔF .0625 HZ 150.00
122.81249 HZ ϕ: -107.0° |TF|: .0168 G/LB XPRD EXP N 1

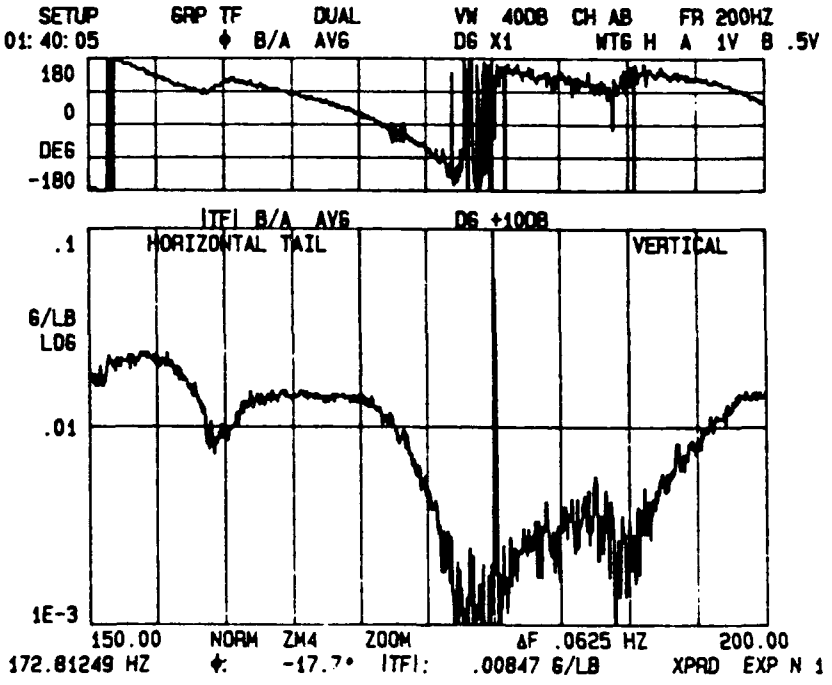
SETUP GRP TF DUAL VW 40DB CH AB FR 200HZ
01: 40: 05 ϕ B/A AVG DG X1 WTG H A 1V B .5V
180
0
DEG
-180
|TF| B/A AVG DG +10DB
HORIZONTAL TAIL
VERTICAL
.1
G/LB
LOG
.01
1E-3
150.00 NORM ZM4 ZOOM ΔF .0625 HZ 200.00
172.81249 HZ ϕ: -17.7° |TF|: .00847 G/LB XPRD EXP N 1

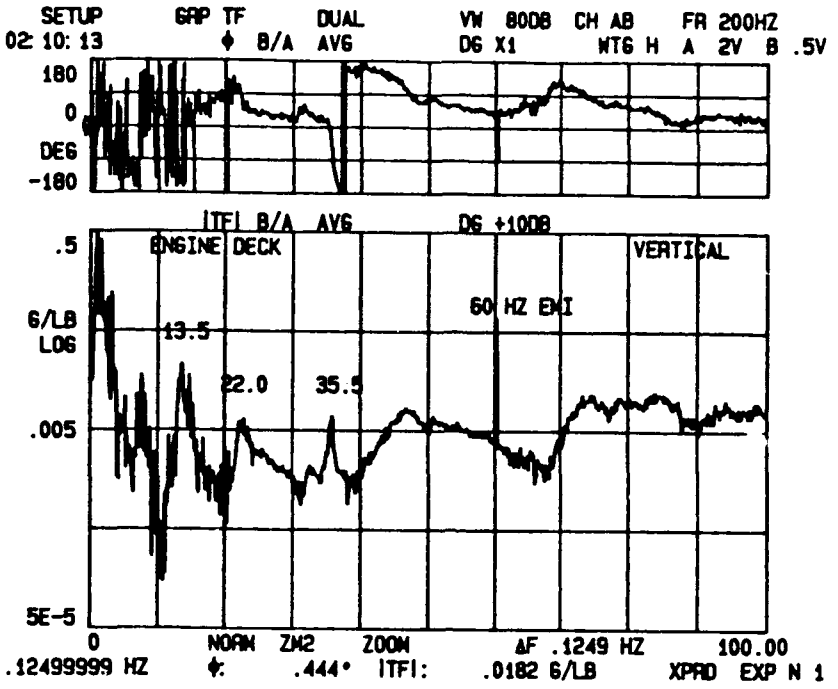
SETUP
02: 10: 13
GRP TF
DUAL
VW 800B CH AB
FR 200HZ
φ B/A AVG
DG X1
WTG H A 2V B .5V
180
0
DEG
-180
|TF| B/A AVG
DG +100B
.5
ENGINE DECK
VERTICAL
60 HZ EMI
G/LB
LOG
13.5
22.0
35.5
.005
5E-5
0
NORM ZM2 ZOOM
ΔF .1249 HZ
100.00
.12499999 HZ
φ: .444°
|TF|: .0182 G/LB
XPRD EXP N 1

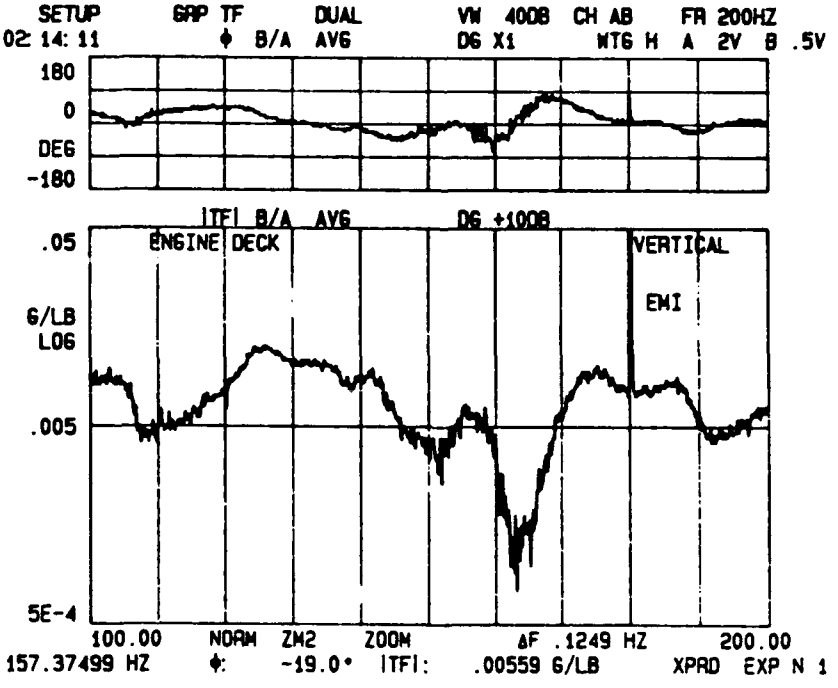
SETUP
02: 14: 11
GRP TF
DUAL
VW 400B CH AB
FR 200HZ
φ B/A AVG
DG X1
WTG H A 2V B .5V
180
0
DEG
-180
|TF| B/A AVG
DG +100B
.05
ENGINE DECK
VERTICAL
EMI
G/LB
LOG
.005
5E-4
100.00
NORM ZM2 ZOOM
ΔF .1249 HZ
200.00
157.37499 HZ
φ: -19.0°
|TF|: .00559 G/LB
XPRD EXP N 1

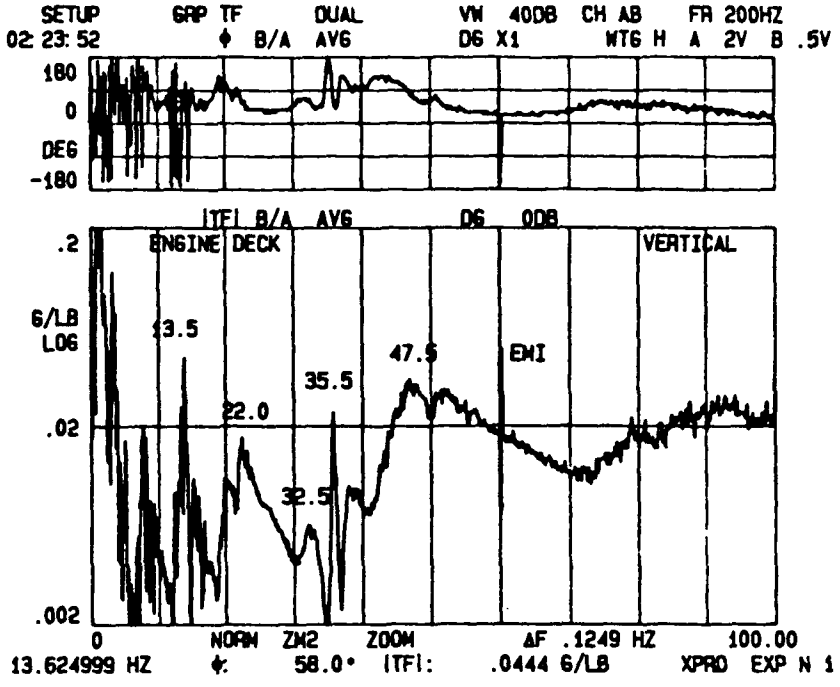
SETUP
02: 23: 52
GRP TF
ϕ B/A
DUAL
AVG
VW 400B
D6 X1
CH AB
WT6 H
FR 200HZ
A 2V B .5V
180
0
DE6
-180
|TF| B/A AVG
D6 00B
.2
ENGINE DECK
VERTICAL
6/LB
LOG
13.5
22.0
35.5
47.5
EMI
.02
32.5
.002
0
NORM ZM2
ZOOM
ΔF .1249 HZ
100.00
13.624999 HZ
ϕ: 58.0°
|TF|: .0444 G/LB
XPRD EXP N 1

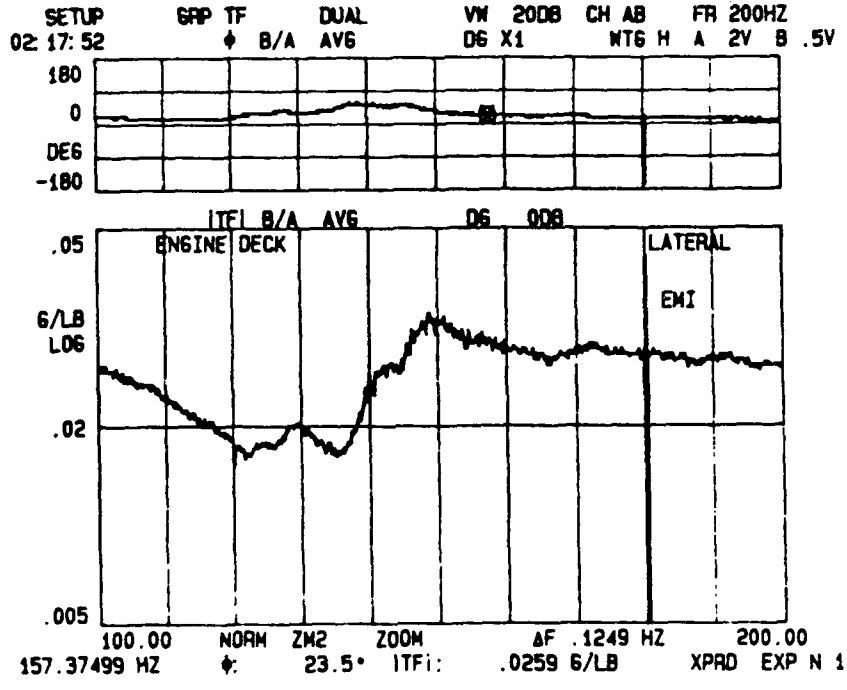
SETUP
02: 17: 52
GRP TF
ϕ B/A
DUAL
AVG
VW 200B
D6 X1
CH AB
WT6 H
FR 200HZ
A 2V B .5V
180
0
DE6
-180
|TF| B/A AVG
D6 00B
.05
ENGINE DECK
LATERAL
EMI
6/LB
LOG
.02
.005
100.00
NORM ZM2
ZOOM
ΔF .1249 HZ
200.00
157.37499 HZ
ϕ: 23.5°
|TF|: .0259 G/LB
XPRD EXP N 1

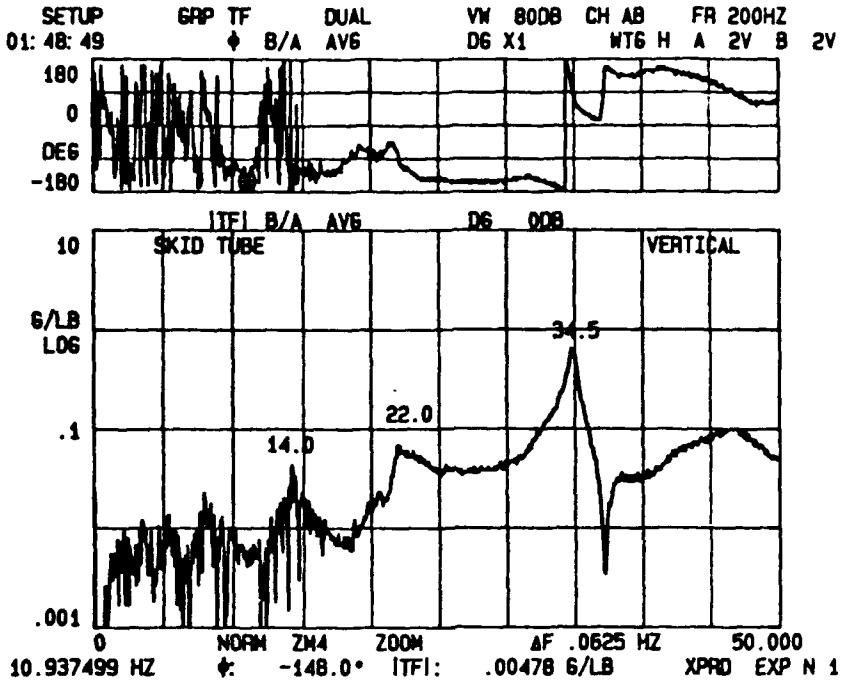
SETUP
01: 48: 49
GRP TF
φ B/A
DUAL
AVG
VW 800B
DG X1
CH AB
WTG H
FR 200HZ
A 2V B 2V
180
0
DEG
-180
|TF| B/A AVG
DG 00B
10
SKID TUBE
VERTICAL
G/LB
LOG
34.5
22.0
14.0
.1
.001
0
NORM ZM4 ZOOM
ΔF .0625 HZ
50.000
10.937499 HZ
φ: -148.0°
|TF|: .00478 G/LB
XPRD EXP N 1

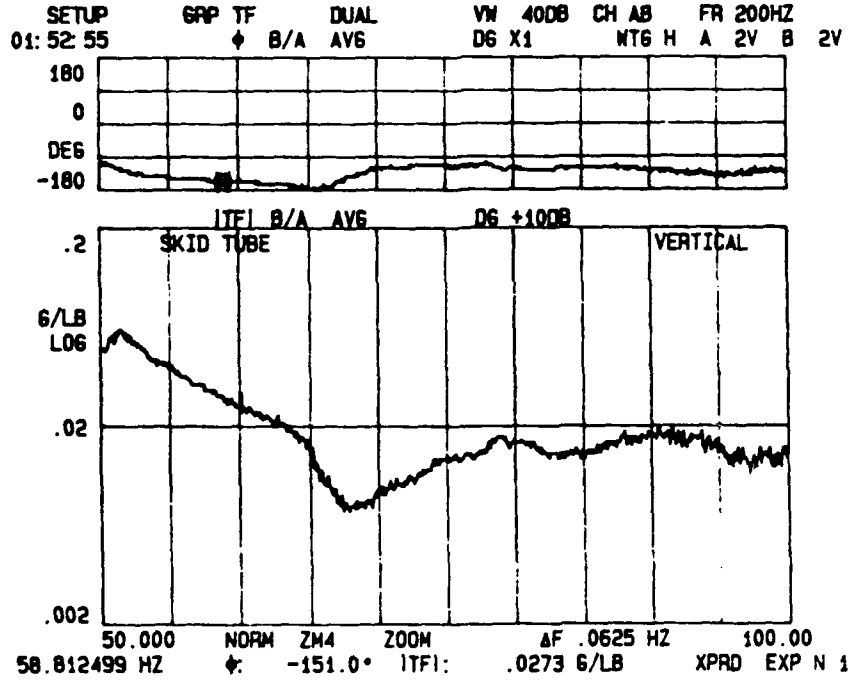
SETUP
01: 52: 55
GRP TF
φ B/A
DUAL
AVG
VW 400B
DG X1
CH AB
WTG H
FR 200HZ
A 2V B 2V
180
0
DEG
-180
|TF| B/A AVG
DG +10DB
.2
SKID TUBE
VERTICAL
G/LB
LOG
.02
.002
50.000
NORM ZM4 ZOOM
ΔF .0625 HZ
100.00
58.812499 HZ
φ: -151.0°
|TF|: .0273 G/LB
XPRD EXP N 1

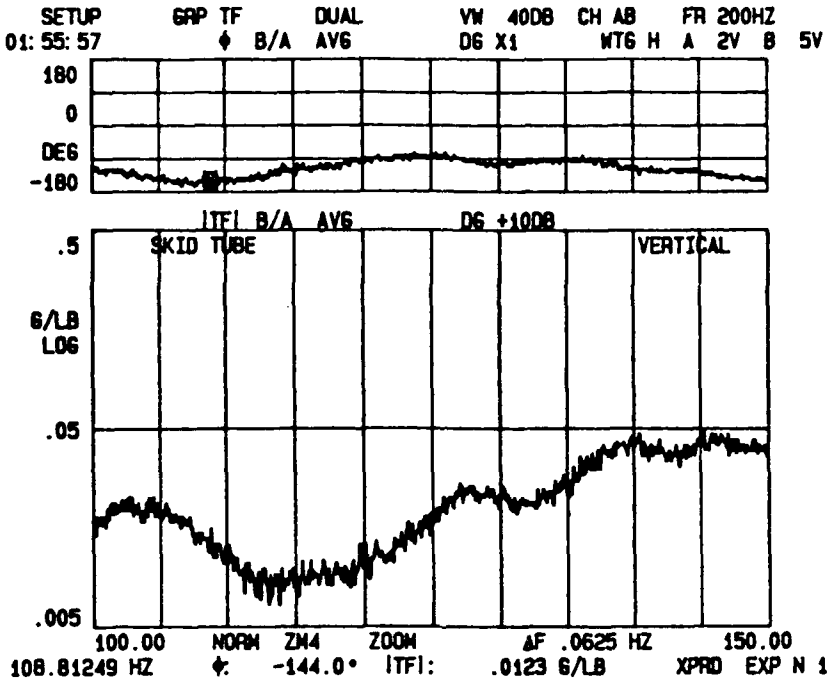
SETUP GRP TF DUAL VW 40DB CH AB FR 200HZ
01: 55: 57 ∅ B/A AVG DG X1 WTG H A 2V B 5V
180
0
DEG
-180
|TF| B/A AVG DG +10DB
.5
SKID TUBE
VERTICAL
G/LB
LOG
.05
.005
100.00 NORM ZM4 ZOOM ΔF .0625 HZ 150.00
108.81249 HZ ∅: -144.0° |TF|: .0123 G/LB XPRD EXP N 1

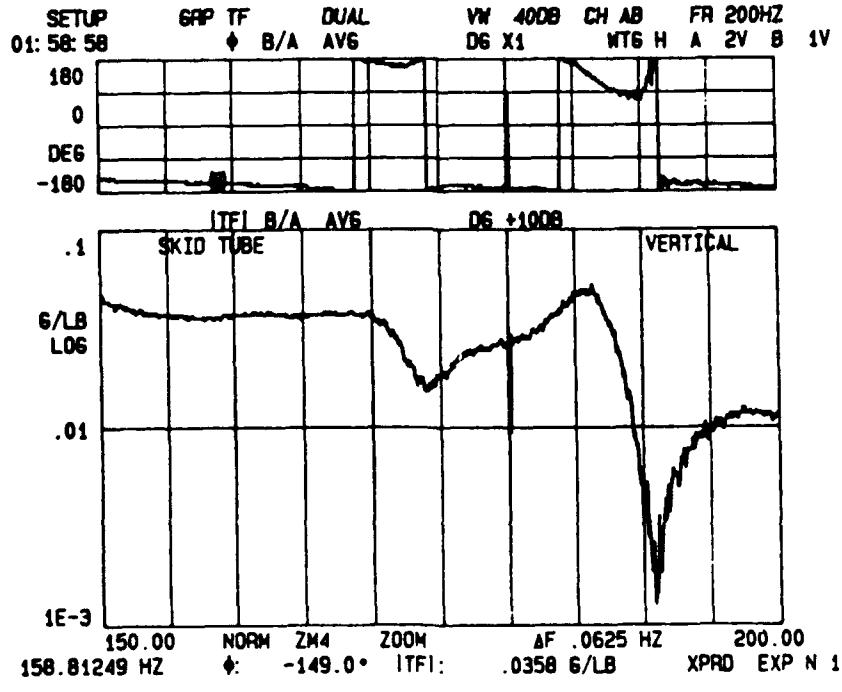
SETUP GRP TF DUAL VW 40DB CH AB FR 200HZ
01: 58: 58 ∅ B/A AVG DG X1 WTG H A 2V B 1V
180
0
DEG
-180
|TF| B/A AVG DG +10DB
.1
SKID TUBE
VERTICAL
G/LB
LOG
.01
1E-3
150.00 NORM ZM4 ZOOM ΔF .0625 HZ 200.00
158.81249 HZ ∅: -149.0° |TF|: .0358 G/LB XPRD EXP N 1

LIST OF REFERENCES

1. Gupta, B.P. and Wood, E.R., "Low Vibration Design of AAH for Mission Proficiency Requirements." paper presented at the American Helicopter Society Northeast Region National Specialists' Meeting of Helicopter Vibration - Technology for the Jet Smooth Ride, Hartford, Connecticut, November 1981.

2. Staple, A.E., "An Evaluation of Active Control of Structural Response as a Means of Reducing Helicopter Vibration," paper presented at the 15th European Rotorcraft Forum, Amsterdam, Netherlands, September 1989.

3. Wood, E.R., Powers, R.W., Cline, J.H. , and Hammond, C.E., "On Developing and Flight Testing a Higher Harmonic Control System," Journal of the American Helicopter Society, January 1985.

4. Department of The Army Aeronautical Design Standard (ADS)-27, *Requirements for Rotorcraft Vibration Specifications, Modeling and Testing,* U.S. Army Systems Command, November 1986.

5. Welsh, W.A., Von Hardenberg, P. C., Von Hardenberg, P.W, Staple, A.E., "Test and Evaluation of Fuselage Vibration Utilizing Active Control of Structural Response (ACSR) Optimized to ADS-27," paper presented at the American Helicopter Societies 46th Annual Forum, 21-23 May 1990.

6. Webb, C.D., *Initial Design Study of Existing Flight Control System of RPH and Feasibility Study of Implementing HHC on the SH-60B,* Master's Thesis, Naval Postgraduate School, Monterey, California, September 1990.

7. CASA/GIFTS Inc., *User's Reference Manual*, not dated.

8. Wood, E.R., "An Introduction to Helicopter Dynamics," Lecture notes from Department of Aeronautics and Astronautics of the Naval Postgraduate School, Monterey, California, not dated.

9. Prouty, R.W., "Vibration Criteria: Finding Discomfort Levels," *Rotor & Wing International*, v.26, no.3, pp.94-96, March 1992.

10. Hintze, C.J., *Construction and Use of a Radio Controlled Model Helicopter for Research,* Master's Thesis, Naval Postgraduate School, Monterey, California, March 1985.

11. Cotten, R.P., *Hover Performance of a Remotely Piloted Helicopter*, Master's Thesis, Naval Postgraduate School, Monterey, California, December 1986.

12. Sarigul-Klijn, M.M., Kolar, R., Wood, E.R., and Straub, F.L., "On Chaos Methods Applied to Higher Harmonic Control." paper presented at American Helicopter Society's 46th Annual Forum, Washington, D.C., May 1990.

13. Scott, J.G., *Establishment of a Remotely Piloted Helicopter Flight Test Program for Higher Harmonic Control Research*, Master's Thesis, Naval Postgraduate School, Monterey, California, June 1990.

14. McGovern, J.H., *Flight Operations for Higher Harmonic Control Research*, Master's Thesis, Naval Postgraduate School, Monterey, California, March 1991.

15. Wood, E.R., Higman, J., and Kolar, R., "Higher Harmonic Control Promises Improved Dynamic Interface Operations," AGARD Proceedings of the 78th Flight Mechanics Panel, Seville, Spain, May 1991.

16. Ransford, K.M., *Baseline Vibration Measurements of Remotely Piloted Helicopters for Higher Harmonic Control Research*, Master's Thesis, Naval Postgraduate School, Monterey, California, December 1991.

17. Wilcoxon Research, *Vibration Generating System Operating Guide: Model F7/F4 Shaker, Model Z7 Transducer Base*, April 1985.

18. Wilcoxon Research, *Instruction Book, Power Amplifier Models: PA7C, PA7CM-1 & PA7CM-4*, not dated.

19. Scientific Atlanta, Spectral Dynamics Division, *SD380 Operators Manual*, not dated.

20. Bruel & Kjaer, *Modal Analysis of Large Structures - Multiple Exciter Systems*, not dated.

21. Ewins, D. J., *Modal Testing: Theory and Practice*, Research Studies Press LTD., 1984.

22. Den Hartog, J. P., *Mechanical Vibrations*,p 459, McGraw-Hill Book Company, Inc., 1947

23. Beer, F. P. and Johnston, E. R., *Mechanics of Materials*, McGraw Hill Inc., 1981.

24. Timoshenko, S., *Vibration Problems in Engineering*, pp. 325-343, D. Van Nostrand Company, Inc., 1955.

25. NACA Technical Note 3459, *Simplified Procedures for the Rapid Estimation of Bending Frequencies of Rotating Beams*, by R. T. Yntema, June 1955.

INITIAL DISTRIBUTION LIST

		No. of Copies
1.	Defense Technical Information Center Cameron Station Alexandria, Virginia 22304-6145	2
2.	Library, Code 52 Naval Postgraduate School Monterey, California 93943-5000	2
3.	Chairman, Code AA/Co Department of Aeronautics and Astronautics Naval Postgraduate School Monterey, California 93943-5000	2
4.	Professor E. Roberts Wood, Code AA/Wd Department of Aeronautics and Astronautics Naval Postgraduate School Monterey, California 93943-5000	2
5.	Professor Ramesh Kolar, Code AA/Ko Department of Aeronautics and Astronautics Naval Postgraduate School Monterey, California 93943-5000	2
6.	Lieutenant Commander William T. Trainer 12000 Wayland Street Oakton, Virginia 22124	2